

# Manual for the Assessment of Load-Bearing Unreinforced Masonry Structures



Thomas E. Boothby  
Huriye Sezer Atamtürktür  
Ece Erdogmus  
Department of Architectural Engineering  
The Pennsylvania State University  
104 Engineering Unit A  
University Park, PA 16802  
(814) 863-2082  
tebarc@engr.psu.edu

prepared for

US Department of the Interior  
National Park Service  
National Center for Preservation Technology and Training

5 May 2006

## TABLE OF CONTENTS

List of Figures	- 3 -
List of Tables	- 7 -
1 Introduction	- 8 -
2 Arch Assessment	- 9 -
2.1 Elastic Methods	- 12 -
2.2 Rigid-Plastic Methods	- 13 -
2.3 Application of Elastic Analysis Methods	- 14 -
2.4 Application of Rigid-Plastic Analysis Methods	- 22 -
2.5 Non-linear Analysis Using Frame Analysis Programs	- 25 -
2.5.1 Linear Analysis	- 27 -
2.5.2 Non-Linear Analysis	- 30 -
3 Three-Dimensional Masonry Vault Assessment	- 37 -
3.1 Building a Model	- 37 -
3.2 Geometric Model	- 38 -
3.3 Solid Model	- 41 -
3.4 Element Types	- 43 -
3.4.1 Frame	- 43 -
3.4.2 Shell	- 44 -
3.4.3 Solid	- 44 -
3.5 Meshing	- 45 -
3.6 Material Properties	- 46 -
3.7 Loading	- 49 -
3.8 Boundary Conditions	- 49 -
3.9 Solution	- 50 -
3.10 Software Specific Suggestions	- 50 -
3.10.1 ANSYS	- 51 -
3.10.2 SAP	- 51 -
3.10.3 STAAD	- 52 -
3.11 Validating a Model	- 52 -
3.11.1 Validation by Dynamic Analysis	- 52 -
4 Case Study 1: Cathedral of Saint John the Divine; New York, NY	- 54 -
4.1 Building the FE model in ANSYS	- 55 -
4.2 Application of Experimental Modal Analysis	- 58 -
4.3 Validation of ANSYS Model Based on Dynamic Analysis	- 60 -
4.4 Static Analysis with ANSYS Model	- 61 -
4.5 Building the FE Model in SAP 9.0 Nonlinear	- 65 -
4.6 Validation of SAP 9.0 Model Based on Static Analysis	- 69 -
5 Case Study 2: National Cathedral; Washington, DC	- 70 -
5.1 General Information on ANSYS Model	- 70 -

5.2	Boundary Conditions	- 71 -
5.3	Material Properties	- 72 -
5.4	Model Validation	- 74 -
5.5	Building the FE Model in SAP 9.0 Nonlinear	- 82 -
6	Case Study 3: State Education Building; Albany, NY	- 84 -
6.1	Building the FE model in ANSYS	- 85 -
6.2	Application of Experimental Modal Analysis	- 89 -
6.3	Validation of ANSYS Model Based on Dynamic Analysis	- 90 -
6.4	Static Analysis with ANSYS Model	- 93 -
6.5	Building the FE Model in SAP 9.0 Nonlinear	- 94 -
6.6	Validation of SAP 9.0 Model Based on Static Analysis	- 95 -
7	Conclusions	- 95 -
8	Acknowledgements	- 97 -
9	References Cited	- 98 -

## List of Figures

Figure 1: View of Nave Vaults of the Cathedral of St. John the Divine, Showing Transverse Arches	- 9 -
Figure 2: Loading sequence for masonry arch: cracking allowed	- 11 -
Figure 3 Dimensionless Interaction Diagram of arch capacity	- 14 -
Figure 4: Arch Geometric Quantities	- 15 -
Figure 5: Semicircular arch	- 16 -
Figure 6: Segmental arch	- 17 -
Figure 7: Nodes and members for arch ring	- 17 -
Figure 8: Simple Arch for Analysis Example	- 18 -
Figure 9: Stress distribution: elastic, uncracked	- 20 -
Figure 10: Stress distribution: elastic, cracked	- 20 -
Figure 11: Stress distribution, inelastic, cracked	- 21 -
Figure 12: Maximum and Minimum Horizontal Thrust	- 22 -
Figure 13: Collapse Mechanism for Crown Loading	- 24 -
Figure 14: Arcade Arch Example	- 26 -
Figure 15: SAP Model of Arcade Arch	- 28 -
Figure 16: Live Load Pressure Resulting from Triforium Piers	- 29 -
Figure 17 Masonry Stress-Strain Law for Compression	- 31 -
Figure 18: Masonry Stress-Strain Law for tension	- 31 -
Figure 19: Pier for pushover analysis	- 32 -
Figure 20: Fiber hinge for pushover analysis	- 32 -
Figure 21: Pier pushover analysis load-displacement results	- 33 -
Figure 22: Frame Hinge Locations	- 34 -

Figure 23: Hinge Status at Various Load Factors	- 35 -
Figure 24: Bending Moment Diagram for Arcade Arch	- 36 -
Figure 25: Eccentricity Diagram for Arcade Arch	- 37 -
Figure 26: Arch profile related to 1/4 point rise. The three arches have the same span and rise, but are differentiated by the 1/4 point rise.	- 40 -
Figure 27: Geometric simplification of the center pier cross section with constant area.	- 41 -
Figure 28: Vault Rib Intersection at Springing	- 42 -
Figure 29: Model of Vault Rib Intersection	- 43 -
Figure 30: Nave Vaults of Cathedral of St. John the Divine	- 54 -
Figure 31: a) The AutoCAD drawing of the nave vaults b) the solid model in ANSYS	- 56 -
Figure 32: The quarter and full vault model of the Cathedral of St. John the Divine in ANSYS	- 57 -
Figure 33: The three-vault model of the Cathedral of St. John the Divine in ANSYS	- 57 -
Figure 34: The three excitation locations	- 59 -
Figure 35: The FRF and coherence graphs at the driving point #2 and #3	- 59 -
Figure 36: The comparison of the results obtained from experimental and analytical methods.	- 60 -
Figure 37: The final boundary conditions and the Nave of Cathedral of St. John the Divine, New York, NY, viewed from south	- 61 -
Figure 38: The quarter and full vault model of the Cathedral of St. John the Divine in ANSYS	- 64 -
Figure 39: The simplified geometric models of the masonry vaults of the Cathedral of St. John the Divine in AutoCAD	- 67 -
Figure 40: The SAP 9.0 model of the vaults of the Cathedral of St. John the Divine in AutoCAD	- 68 -
Figure 41: Full-vault model of National Cathedral Choir Bay	- 70 -
Figure 42: Three-vault model of the NC choir vaults	- 71 -
Figure 43: Initially Assumed Boundary Condition Set-1 for the NC.	- 72 -

Figure 44: Experimental Setup Column above the National Cathedral Vaults	- 75 -
Figure 45: Experimental Setup Row above the National Cathedral Vaults.	- 76 -
Figure 46: National Cathedral FRF plot for all the accelerometers in Column Setup	- 77 -
Figure 47: Phase Plot for Accelerometer 4 on Column Setup - Heel Drop at Point A	- 78 -
Figure 48: Accelerance FRF and Coherence Plots for Accelerometer 4 on Column Setup- Heel Drop at Point A	- 78 -
Figure 49: Imaginary Plot for the FRF for Column Heel Drop Excitation	- 79 -
Figure 50: Schematic for the deformed shape of the top ribs in the NC	- 80 -
Figure 51: Final Boundary Conditions for the NC Triple-Vault Model	- 81 -
Figure 52: The NC Triple Vault Model: UZ displacements plot- Mode 5 Entire model (left) and only top beams (right)	- 82 -
Figure 53: The AutoCAD drawings of National Cathedral.	- 83 -
Figure 54: The SAP model of a single choir vault.	- 83 -
Figure 55: Solution of SAP model for stress resultant.	- 84 -
Figure 56: The view of rib and dome construction.	- 85 -
Figure 57: View of the back of the domes.	- 85 -
Figure 58: FEM model of the single dome.	- 86 -
Figure 59: The composite nature of tile and mortar assembly.	- 87 -
Figure 60: The hydraulic displacement controlled testing of tile and mortar unit.	- 88 -
Figure 61: The dynamic testing plan.	- 89 -
Figure 62: The FRF and coherence plot at Point 15.	- 90 -
Figure 63: The calibrated boundary conditions.	- 91 -
Figure 64: The analytically obtained mode shapes.	- 92 -
Figure 65: The reaction forces at the validated support conditions.	- 93 -
Figure 66: The AutoCAD drawing of the State Education Building dome.	- 94 -

Figure 67: The solid model in SAP.

- 94 -

## List of Tables

Table 1: Internal Force and Eccentricity for Uniformly Distributed Load	- 19 -
Table 2: Internal Force and Eccentricity for Uniformly Distributed Load + Crown Load	- 21 -
Table 3: Virtual Work Summary for Crown Loading	- 25 -
Table 4: Nodal Coordinates For Arch Analysis	- 27 -
Table 5: Linear Axial Force and Bending Moment Results, Arcade Arch	- 30 -
Table 6: Material Properties used in Vault Models	- 58 -
Table 7: Sensitivity Analysis on Tile Mass Variation	- 63 -
Table 8: Sensitivity Analysis on Tile Stiffness Variation	- 63 -
Table 9: Sensitivity Analysis on Poisson's Ratio Variation	- 63 -
Table 10: Sensitivity Analysis on Mesh Refinement	- 64 -
Table 11: The Comparison of Reaction Forces for SAP 9.0 and ANSYS	- 69 -
Table 12: Material Properties for Analysis of National Cathedral Vault	- 73 -
Table 13: Test Results: Stone Used in National Cathedral Construction	- 73 -
Table 14: Assembly Material Properties	- 74 -
Table 15: Final Material Properties for National Cathedral Finite Element Model	- 80 -
Table 16: Natural frequencies for the NC three-vault model	- 82 -



# 1 Introduction

The assessment of unreinforced masonry structures is difficult to undertake in practice. A structural engineer is usually confronted with a standing, apparently competent, structure that seems to defy most of the rules of structural behavior, as incorporated in modern building codes. The engineer must then choose between reinforcing the structure according to a modern understanding of material strength and structural behavior or trying to make sense of the behavior and anticipated strength of the structure on a more fundamental level. A fundamental structural assessment, although it involves a considerable amount of effort in analysis and in furthering the understanding of masonry behavior, is the more rewarding. This course of action is consistent with the principles of historic preservation, as summarized in the *Secretary of the Interior's Standards for the Treatment of Historic Properties*. The following manual is intended to introduce a sympathetic structural engineer to some of the principles of unreinforced masonry and especially to provide some basic instructions in preparing a model of such a structure for analysis, using widely available, modern tools for structural analysis. In Section 2, the assessment of two dimensional arches is introduced. This section begins with an elaboration of the competing issues of code compliance and rational assessment as described in the introductory remarks above. Section 3 covers the assessment of three-dimensional masonry vaults using widely available structural analysis software. Case studies, illustrating the procedure recommended for the assessment of masonry structures are provided in Sections 4 through 6.

## 2 Arch Assessment

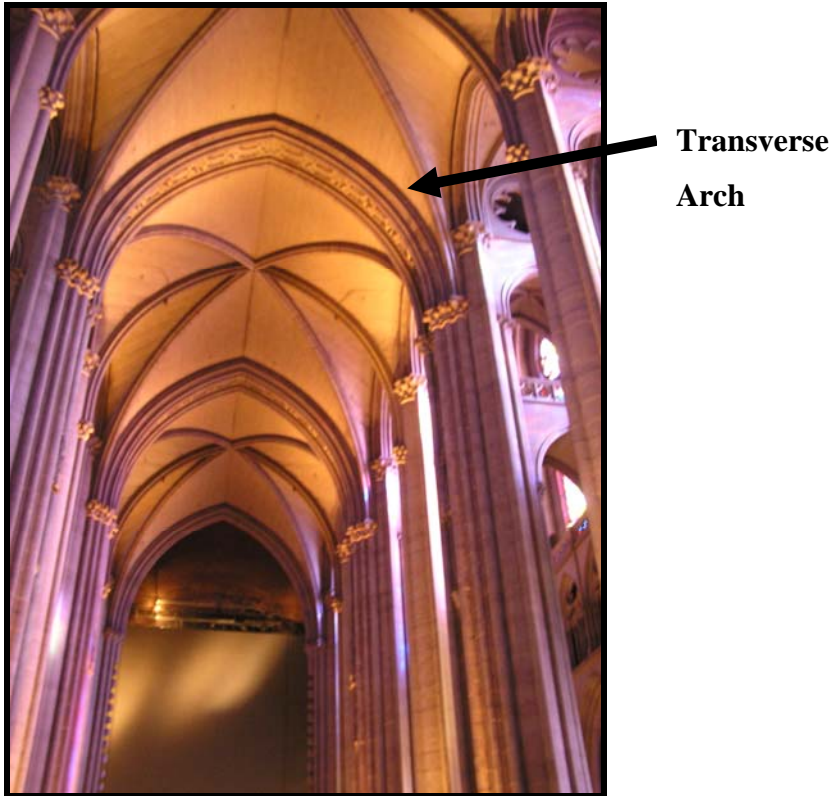


Figure 1: View of Nave Vaults of the Cathedral of St. John the Divine, Showing Transverse Arches

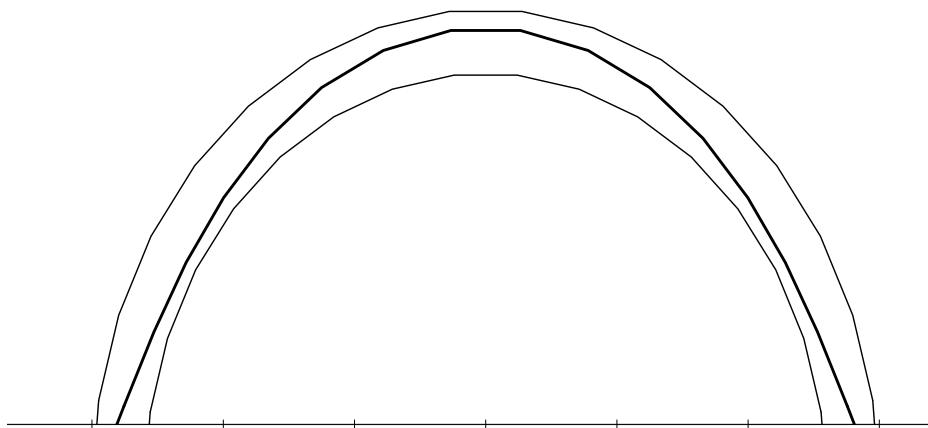
The assessment of plane arches although much simpler than the assessment of three-dimensional vaults; introduces the basis of the assessment of three-dimensional vaulted structures. This analysis may often be treated by hand methods, or by modifications of hand methods. The analysis of an arch provides an immediate example of the problem described in the Introduction, Section 1, above. A masonry arch, such as the transverse arches at St. John the Divine (see Figure 1), is subject to various combinations of bending and axial force. The application of model building codes, such as the International Building Code, requires adopting ACI 530: *Building Code Requirements for Masonry Structures* as a reference. This document uses a limit state the development of the first crack in the masonry to define the failure of unreinforced masonry.

To begin with, the mortar used in the construction of this building is in all likelihood a high lime content historic mortar a 1:2:9 portland cement:lime:sand ratio—which is considered

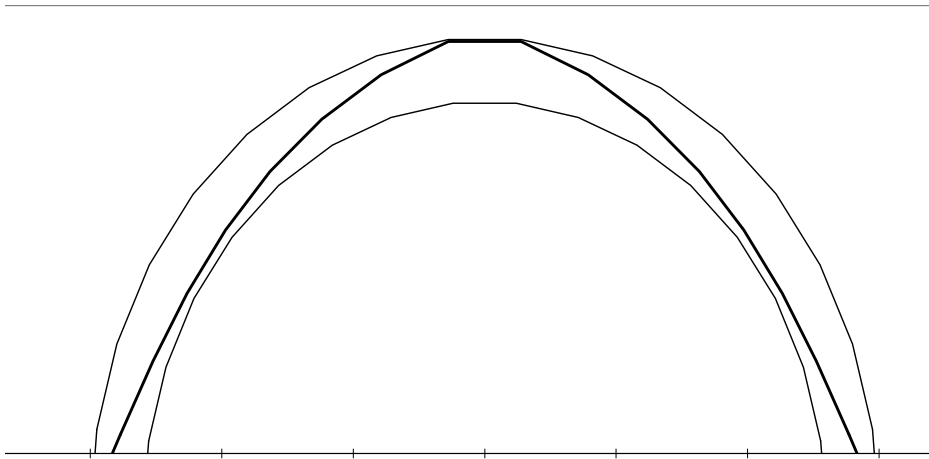
unsuitable for load-bearing masonry by any model building code. Even accepting that the mortar has a higher cement content, such as a 1:1:6 Type N mortar, the failure criterion in ACI 530 is 15 psi net tension. As will be shown for a simple arch in Section 2.3, tensile stresses of this magnitude, computed on the basis of elastic analysis, are encountered in practically any arch.

However, to understand the strength and durability of an arched unreinforced masonry structure, a willingness to re-examine the validity of the failure criterion of the development of the first crack is necessary. It is clear that masonry, even after cracking, can resist combinations of large axial force  $P$  and bending moment  $M$ , as long as the eccentricity of the axial thrust  $e = M/P$  remains less than  $1/2$  the depth of the masonry section. The sequence of loading shown in

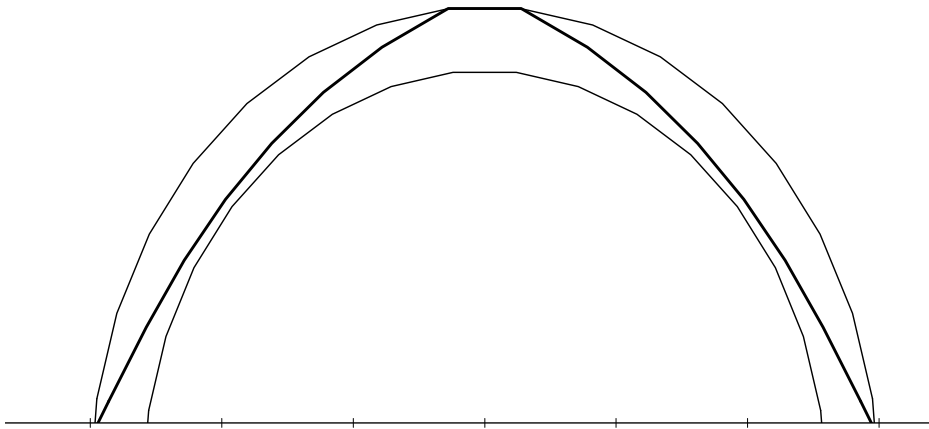
Figure 2 illustrates this. The eccentricity of the thrust can be represented by a thrust line, or pressure line, as shown in the figure. The initial state of the arch, when subjected to dead weight alone, may be compression only, represented by a thrust line in the middle  $1/3$  of the arch, or it may include a crack at the crown or haunches, represented by the eccentricity of the thrust line (Figure 2a). If a concentrated load is added to the crown, the eccentricity of the thrust will increase to a maximum value of half the depth of the arch (Figure 2b). This is well beyond the development of the initial crack at the crown of the arch. As the load increases further, the eccentricity at the crown will remain at a maximum value as the eccentricity at the supports increases. Even with the development of hinges at the supports (Figure 2c), the arch has been simply reduced to a three-hinged arch and is capable of taking further load. The arch fails only when sufficient load is applied to form four hinges, as in (Figure 2d). this theory of the arch, and some of its historical precedents, is elaborated by Heyman (1982, 1995).



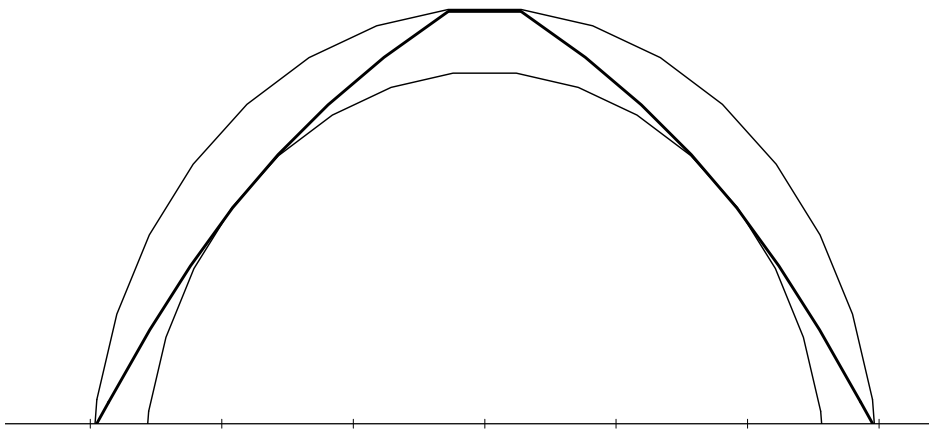
(a) self-weight only



(b) self-weight + crown load: hinge at crown



(c) self-weight + crown load: hinges at crown and supports



(d) self-weight + crown load: hinges at crown, supports, and haunches

Figure 2: Loading sequence for masonry arch: cracking allowed

The application of a rational theory of arch behavior, such as outlined above, permits a significantly greater assessed strength for the arch. This theory is elaborated in the following sections for the arch.

## **2.1 Elastic Methods**

Formulas for the analysis of the elastic arch have been presented in many analytical textbooks, and general arch solutions can be found, for instance, in Roark (1989). In this treatment, the arch is considered as a three degree statically indeterminate structure and, subject to various simplified loading conditions (uniformly distributed load, concentrated load at center, concentrated load at any point, etc.), values of three redundant quantities can be determined. These values further allow the determination of axial force, shear, and bending moment at any point within the arch. These methods require some simplification of the arch shape, usually to a segment of a circle and simplification of the loading that the arch is subjected to. The assumption that the response to axial force and bending moment is linear is a further simplification, which depends on the axial force being large enough with respect to the bending moment that the stress in the arch is compressive.

A frame analysis program can also be used to complete the elastic analysis of an arch. The centerline of the arch can be subdivided into a series of straight bars; ten bars are usually sufficient to capture the behavior of the arch. Material and section properties consistent with the material and geometry of the arch are entered for the bars. The loading on the arch is determined by finding the self-weight, dead load and live load that is distributed over the horizontally projected length of each of the bars. This system is analyzed using a frame analysis program for the loading conditions identified for the structure. The frame analysis output is examined in detail. Of particular interest are the member forces and moments, especially the axial force and bending moment. Due to the nature of the material resistance, namely that the material resists larger compressive stresses than tensile stresses, the arch can resist a very large axial force at low eccentricity and significant bending moment in the presence of axial force. It is necessary to apply a failure criterion, such as that shown in 2.2, to determine the capacity of the arch on the basis of the combinations of axial force and bending moment found by frame analysis. This procedure is described in detail in Section 2.3.

## 2.2 Rigid-Plastic Methods

A masonry arch lends itself easily to analysis by rigid-plastic methods. The arch ring is considered to resist compression, but not tension. The interaction diagram, shown in Figure 3, for axial force and bending moment results from this assumption. An increase in axial force generally increases the bending moment capacity of the arch. An upper limit on compressive stress may also be set, resulting in the interaction diagram shown as a dashed line in the figure. For an arch ring of width  $b$  and thickness  $d$ , the relationship between axial force ( $P$ ) and bending moment ( $M$ ), without a compression cap is:

$$M \leq P \frac{d}{2}$$

Given a maximum compressive stress of  $f_c$  and the further intermediate quantities

$$P_0 = bdf_c$$

$$M_0 = \frac{bd^2}{8} f_c = P_0 \frac{d}{4}$$

the relation becomes

$$\frac{1}{4} \left| \frac{M}{M_0} \right| - \left( \frac{P}{P_0} \right) + \left( \frac{P}{P_0} \right)^2 \leq 0$$

This is a 'yield condition' in the sense of plastic analysis. Combined with the equilibrium condition, that all internal and external forces are in equilibrium, and the mechanism condition, that the total virtual work is zero in a kinematically admissible mechanism, the three theorems of plasticity analysis can be invoked:

- Lower Bound: The structure is safe under a set of loads if the equilibrium and yield condition can be simultaneously satisfied at all points in the structure
- Upper Bound: The structure is unsafe under a set of loads for which the internal virtual work is zero in a kinematically admissible collapse mechanism
- Plastic Collapse: The structure is at the point of collapse under a set of loads for which the equilibrium, mechanism and yield condition are simultaneously satisfied.

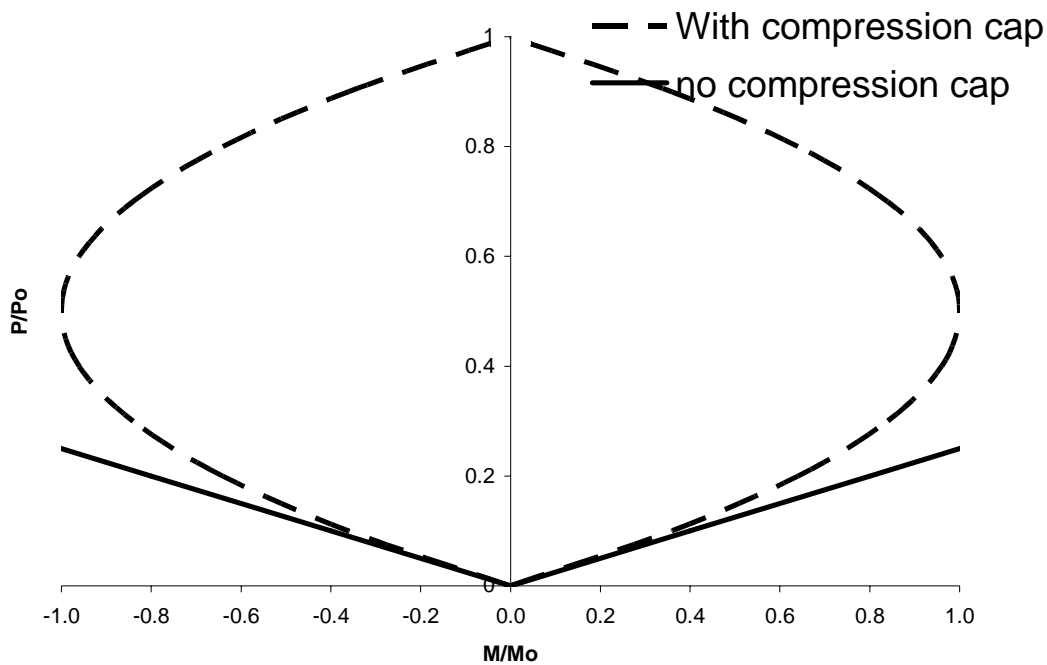


Figure 3 Dimensionless Interaction Diagram of arch capacity

A set of loads satisfying the equilibrium and yield conditions is safe, a set of loads satisfying the mechanism condition is unsafe, and a set of loads satisfying all three conditions is the actual collapse load. In this formulation, the assessment of an arch reduces to an assessment made by invoking either the lower bound or the upper bound theorem. Safety can be assured by satisfying the conditions of the lower bound theorem. The application of the upper bound theorem is necessarily accompanied by a search for a 'least upper bound.' The application of these principles to a simple arch will be illustrated in Section 2.4.

### 2.3 Application of Elastic Analysis Methods

This section describes the development of joint coordinates, member incidences, cross section properties, material properties, and support conditions for a masonry arch. These values are entered into a frame analysis program to complete an elastic analysis of the arch.

Survey data or measured drawings are used to establish the geometry of the arch ring. A series of nodes representing equal subdivisions of the arch are established along the centerline of

the arch. For segmental and semicircular arches, the location of the nodes can be established on the basis of equations for the coordinates of a circle. For multi-centered or amorphous arch shapes, this procedure may require the application of other geometric methods or graphically locating the centre of the arch ring at various angles.

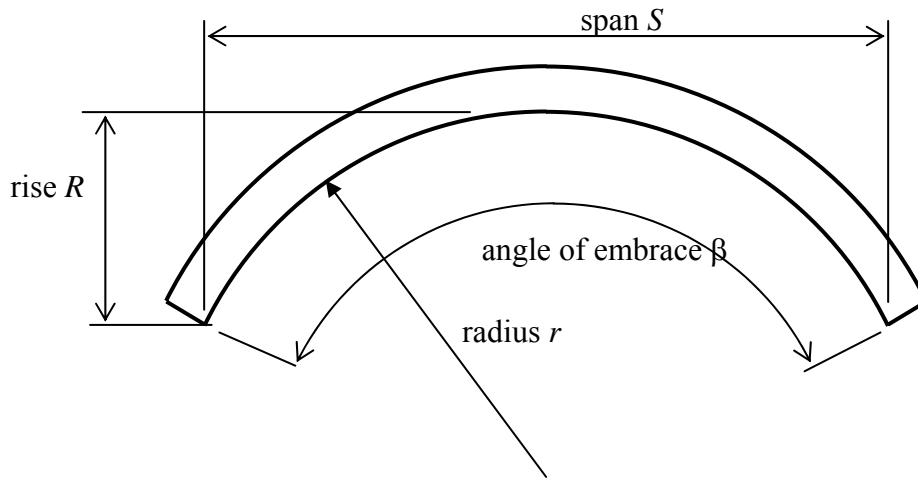


Figure 4: Arch Geometric Quantities

In order to determine the angle of embrace or intrados radius for a segmental or semicircular arch, the following relations between the intrados radius  $r$ , the rise  $R$ , the span  $S$ , and the angle of embrace  $\beta$  can be used. The quantities are defined in Figure 4.

$$R = r \left( 1 - \cos \left[ \frac{\beta}{2} \right] \right)$$

$$S = 2r \sin \left( \frac{\beta}{2} \right)$$

$$r = \frac{R^2 + \left( \frac{S}{2} \right)^2}{2R}$$

$$\beta = 2 \sin^{-1} \left( \frac{S}{2r} \right)$$

Following the establishment of the arch centerline, the arch ring is divided into segments. A semi-circular arch with intrados radius  $r$ , thickness  $t$  and midline radius  $r + t/2$  is shown in Figure 5. For this structure, divide the  $180^\circ$  angle of embrace into 10 equal segments of  $18^\circ$ . The nodal coordinates with respect to the centerline of the arch ring will be



$$x = (r + t/2)\cos \alpha$$

$$y = (r + t/2)\sin \alpha$$

A segmental arch with intrados radius  $r$ , thickness  $t$  and midline radius  $r + t/2$  is shown in Figure 6. For this structure, divide the angle of embrace  $\beta$  into 10 equal segments. The nodal coordinates are

$$x = (r + t/2)\cos \alpha$$

$$y = (r + t/2)\sin \alpha$$

The nodes are joined by straight members, shown in Figure 7, for which appropriate material and cross-sectional properties are computed. Member material properties for entry into the frame analysis program can be determined by analysis of the field data, finite element results, and consultation with literature on stone masonry construction. The cross sectional area and moment of inertia are based on the geometry of the arch. The fundamental material stiffness property used in the analysis is an effective modulus of elasticity representing the combined effect of masonry units, mortar, and joints. The resulting modulus of elasticity is significantly lower than the modulus of elasticity of the units alone, reflecting the general use of soft mortars in the construction of arches. Recommended values of modulus of elasticity are described in Section 3.6.

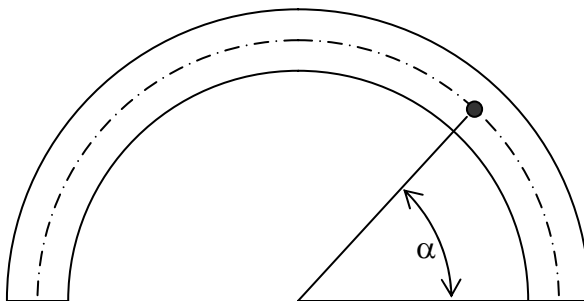


Figure 5: Semicircular arch

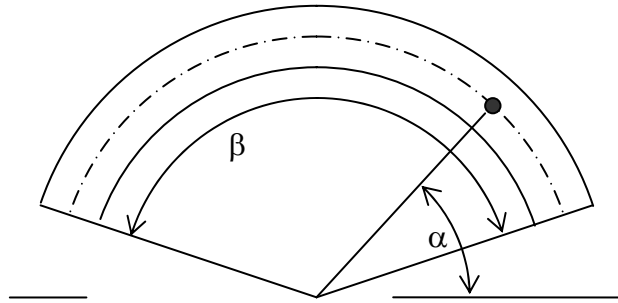


Figure 6: Segmental arch

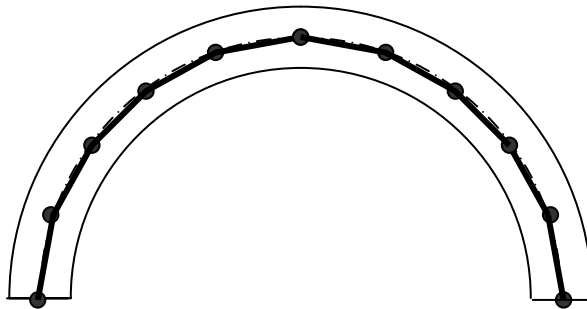


Figure 7: Nodes and members for arch ring

The arch may be fixed or pinned for in-plane rotation at its abutment or pier supports. In most cases, the use of fixed supports is simplest to implement in a frame analysis program and will give good results. However, for high span-rise ratios, fixing this support may give rise to much higher than necessary bending moments at the supports which would skew the strength results. In these cases, simply considering these supports as pinned may produce more realistic results. In practice, both support conditions can be attempted, and the more favorable result can be chosen. This is a consequence of the lower bound theorem of plasticity, described in Section 2.2, as either fixing or pinning the supports results in a statically admissible solution.

If the assessment of the support conditions determines that the supports are compliant in the horizontal direction, then a horizontal spring is added at the supports. The influence of support compliance is usually indicated by the presence of a vertical crack at the crown of the arch, showing that the supports of the arch have spread. The relaxation of rigid horizontal support for the arch ring has a significant impact on the assessed capacity of the arch ring.

As a general example of the procedures for analysis of an arch, consider a semicircular arch with an intrados radius of ten feet, ring thickness of two feet, and uniformly distributed load, including self-weight, of 2000 lbs/ft. This arch, shown in Figure 8, is also the arch used in Section 2.4 below. The arch is modeled using ten frame elements in SAP. For the given 2-foot arch ring depth and a 1-foot width, a cross-sectional area of 288 in<sup>2</sup> is input and a moment of inertia of 13800 in<sup>4</sup>. The program outputs values of axial force and bending moment, giving the eccentricities listed in Table 1 for the 2 k/ft uniformly distributed load. The horizontal component of the internal force, or the crown thrust, is found to be 12.1 k. These results are comparable to the lower bound analysis, given in Section 2.4.

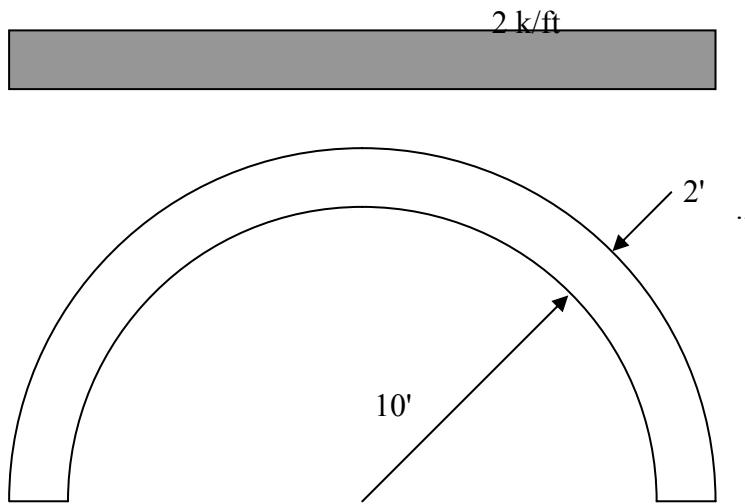


Figure 8: Simple Arch for Analysis Example

The eccentricity at the crown and at the supports is quite high, approaching half the thickness of the arch. This indicates that three hinges will form at these locations if the load is increased slightly. A concentrated load at the crown will increase the eccentricity at these locations very quickly. The further application of this type of loading can be investigated by adding crown loading to the existing model.

Table 1: Internal Force and Eccentricity for Uniformly Distributed Load

member	station (in)	axial force (k)	moment (in-k)	eccentricity (in)	maximum stress uncracked (psi)	minimum stress uncracked (psi)	elastic stress cracked psi	plastic stress cracked psi
1	0.0	-23.6	-271	11.5	154	-318	-2622	-1902
1	20.6	-23.1	-95	4.1	2	-163	-162	-122
1	41.3	-22.6	84	-3.7	-5	-152	-80	-60
2	0.0	-24.1	84	-3.5	-11	-157	-86	-65
2	20.7	-22.7	118	-5.2	24	-181	-73	-55
2	41.3	-21.4	167	-7.8	71	-220	-60	-45
3	0.0	-21.1	167	-7.9	72	-218	-59	-44
3	20.6	-19.4	101	-5.2	20	-155	-63	-47
3	41.3	-17.7	71	-4.0	0	-123	-61	-46
4	0.0	-16.7	71	-4.3	4	-120	-57	-43
4	20.7	-15.3	-25	1.6	-31	-75	-82	-61
4	41.3	-13.9	-64	4.6	7	-104	-104	-78
5	0.0	-13.0	-64	4.9	11	-101	-102	-77
5	20.6	-12.5	-129	10.4	69	-156	-434	-310
5	41.3	-12.0	-125	10.4	67	-150	-417	-316
6	0.0	-12.0	-125	10.4	67	-150	-417	-316
6	20.6	-12.5	-129	10.4	69	-156	-434	-310
6	41.3	-13.0	-64	4.9	11	-101	-102	-77
7	0.0	-13.9	-64	4.6	7	-104	-104	-78
7	20.7	-15.3	-25	1.6	-31	-75	-82	-61
7	41.3	-16.7	71	-4.3	4	-120	-57	-43
8	0.0	-17.7	71	-4.0	0	-123	-61	-46
8	20.6	-19.4	101	-5.2	20	-155	-63	-47
8	41.3	-21.1	167	-7.9	72	-218	-59	-44
9	0.0	-21.4	167	-7.8	71	-220	-60	-45
9	20.7	-22.7	118	-5.2	24	-181	-73	-55
9	41.3	-24.1	84	-3.5	-11	-157	-86	-65
10	0.0	-22.6	84	-3.7	-5	-152	-80	-60
10	20.6	-23.1	-95	4.1	2	-163	-162	-122
10	41.3	-23.6	-271	11.5	154	-318	-2622	-1902

Maximum tensile or compressive stress can be computed, based on the assumption that the cross section remains uncracked, with the stress distribution shown in Figure 9, or cracked, with the stress distribution shown in Figure 10. For the elastic, uncracked case, tension must remain below the permissible tension in the masonry material and governs the capacity of the section. On the other hand, where the section is allowed to crack, compressive stresses govern the capacity of the section. The imposition of the restriction against cracking of the arch seriously reduces the assessed capacity of an arch. Allowing cracking, while ensuring stability by the methods described in Section 2.4, results in much more rational assessments.

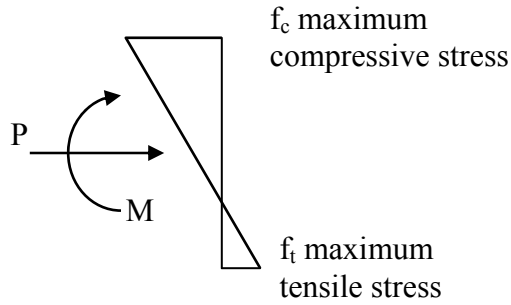


Figure 9: Stress distribution: elastic, uncracked

For the uncracked case, for an arch barrel of width  $b$ , and depth  $d$ ,

$$f_c = \frac{P}{bd} + \frac{6M}{bd^2}$$
$$f_t = \frac{P}{bd} - \frac{6M}{bd^2}$$

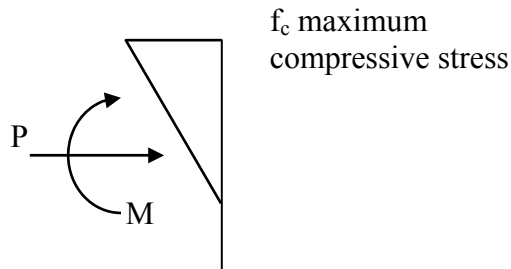


Figure 10: Stress distribution: elastic, cracked

For the cracked, elastic case, recognizing that the eccentricity of the axial thrust  $e = M/P$ , it can be found that

$$f_c = \frac{4P}{b(3d - 6e)}$$

Recognizing that the masonry material approaches an elastic limit, it is also possible to consider a maximum inelastic stress distribution, such as shown in Figure 11.

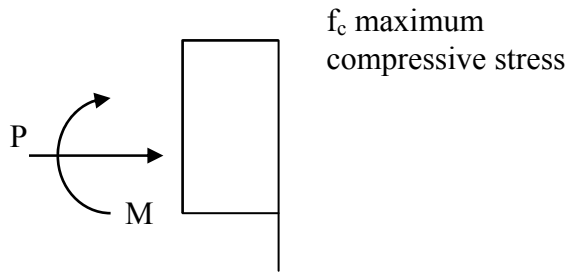


Figure 11: Stress distribution, inelastic, cracked

For the cracked, plastic case, recognizing that the eccentricity of the axial thrust  $e = M/P$ , it can be found that

$$f_c = \frac{P}{bd} \left( \frac{d}{d - 2e} \right)$$

The maximum tensile stress for the uncracked stress distribution and the maximum compressive stress for the cracked stress distribution are presented in Table 1. Adding a 14.0 kip crown load, as discussed in Section 2.4, gives the results shown in Table 2. The eccentricities at the crown and at the supports resulting from elastic analysis are too high for the material to resist. The redistribution of internal forces, as shown in the following sections, allows for this load to be resisted, but this effect cannot be predicted by elastic analysis.

Table 2: Internal Force and Eccentricity for Uniformly Distributed Load + Crown Load

member	station (in)	axial force (k)	moment (in-k)	eccentricity (in)
1	0	-31.533	-461.591	15
1	41.298	-30.47	108.285	-4
2	0	-33.269	108.285	-3
2	41.301	-30.484	294.027	-10
3	0	-30.601	294.027	-10
3	41.295	-27.16	180.541	-7
4	0	-25.513	180.541	-7
4	41.301	-22.729	-93.619	4
5	0	-20.409	-93.619	5
5	41.298	-19.346	-398.43	21
6	0	-19.346	-398.43	21
6	41.298	-20.409	-93.619	5
7	0	-22.729	-93.619	4
7	41.301	-25.513	180.541	-7

member	station (in)	axial force (k)	moment (in-k)	eccentricity (in)
8	0	-27.16	180.541	-7
8	41.295	-30.601	294.027	-10
9	0	-30.484	294.027	-10
9	41.301	-33.269	108.285	-3
10	0	-30.47	108.285	-4
10	41.298	-31.533	-461.591	15

## 2.4 Application of Rigid-Plastic Analysis Methods

The rigid-plastic methods, described in Section 2.2, will be applied to the arch illustrated in Figure 8. For this loading, the relationship between bending moment and axial force can be represented as a parabolic line of thrust. The line of thrust represents the shape of a structure that can resist the given loads by axial force alone or, alternatively, can be seen to represent the eccentricity  $e = M/P$  of the axial thrust in the arch. By a suitable choice of the horizontal thrust component, the line of thrust can be established such that  $|e| = |M|/P < t/2$ , satisfying the yield condition without compression cap, given in Figure 3 and in Section 2.2. Figure 12 shows the maximum and minimum permissible values of horizontal thrust for the case of uniformly distributed loading, which are calculated as  $H_{max} = 13.2$  k and  $H_{min} = 10.8$  k.

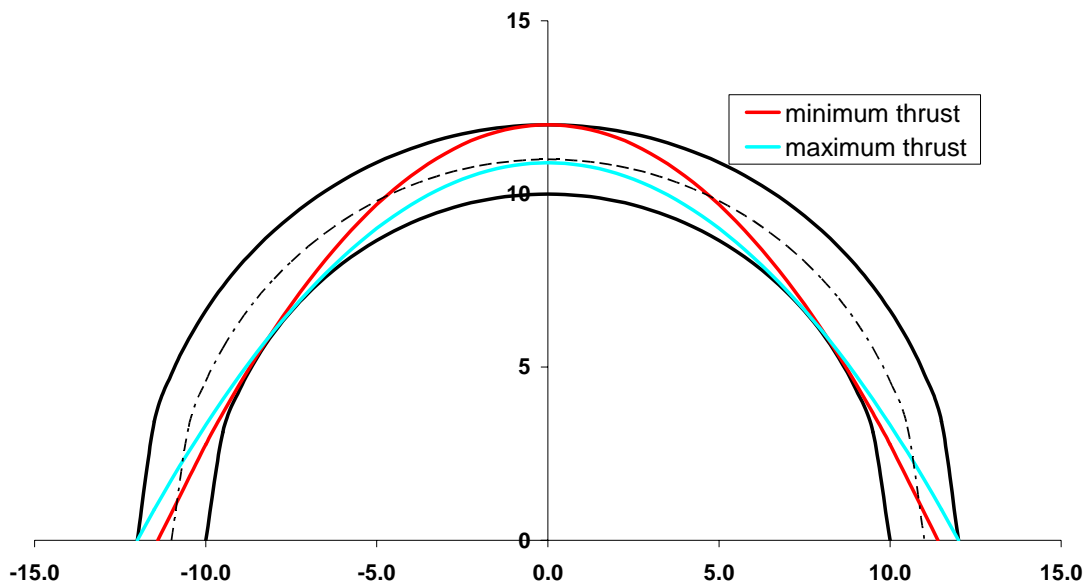


Figure 12: Maximum and Minimum Horizontal Thrust

The upper bound theorem can be used to determine the maximum concentrated load to be applied to the crown to disturb the stable state of this arch. A mechanism results from the formation of hinges at the base of the arch, at the crown of the arch, and at the haunches, as illustrated in Figure 13. The angle of the hinge from the horizontal is designated as  $\alpha$ , and the three hinges on the half of the arch are designated a, b, c. The virtual work can be assessed by recognizing that hinge c moves vertically under the action of the concentrated load, that the portion of the arch between hinges a and b rotates about hinge a, and that the remaining portion of the half-arch rotates about the instantaneous center, designated I.C. in the figure. This allows a relationship to be established between the displacement at the load point  $\Delta$  and the rotation of the segments of the arch.

From the figure, segment 1 of the arch can be seen to rotate about hinge a in the base. The displacement of segment 2 can be analyzed by establishing an instantaneous center of rotation, based on the displacements at hinges b and c. The instantaneous center must be perpendicular to the displacement at b, thus on a straight line from a to b, and must also be perpendicular to the displacement  $\Delta$  at the load point, thus on a horizontal from c. Further inspection of the geometry of the figures allows the following relationships to be established.

$$\beta = \tan^{-1} \left( \frac{10' \sin \alpha}{12' - 10' \cos \alpha} \right)$$
$$x_{ic} = 12'(1 - \cot \beta)$$
$$\theta_1 = \frac{\Delta}{x_{ic}}$$
$$\theta_2 = \left( \frac{12' - 10' \sin \alpha}{10' \sin \alpha} \right) \theta_1$$

It can be noted that the center of gravity (estimated to be at the average x-coordinate of the extrados) of each of the load segments supported by segment 1 and 2 moves upwards as the load at the crown moves downwards. The magnitude of this upwards movement is equal to the distance of the centroid of each segment from the center of rotation ( $x = 12$  ft for segment 1;  $x = x_{ic}$  for segment 2). The positive work of lifting these loads is set equal to the negative work  $P\Delta$  to find the crown load  $P$  associated with this mechanism. The implementation of these relationships in a spreadsheet permits the calculation of the upper bound collapse load for



differing values of the angle  $\alpha$ , as shown in Table 3. The least upper bound for the crown load is then 13.9 kips, associated with an angle  $\alpha$  of  $34^\circ$ .

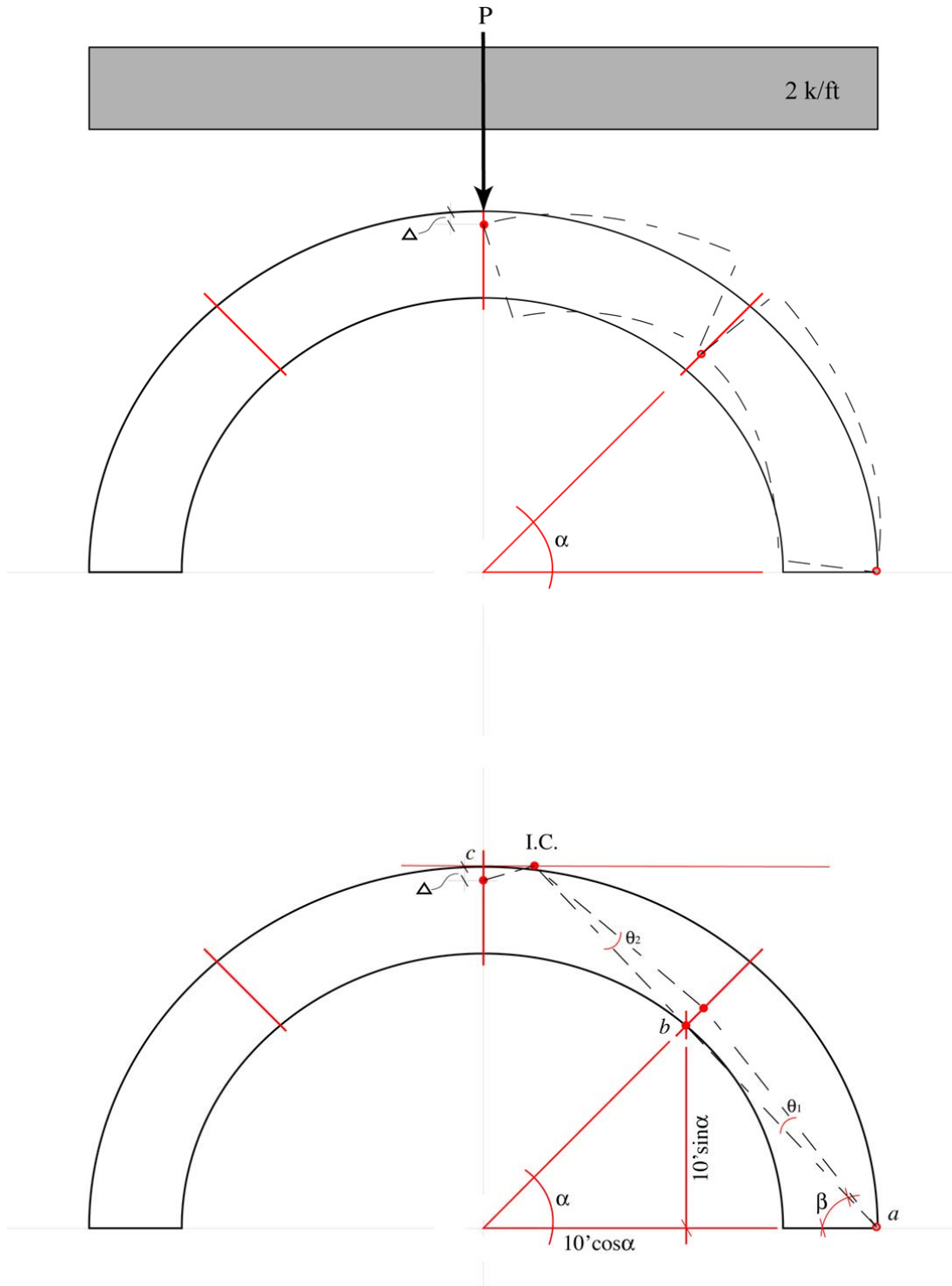


Figure 13: Collapse Mechanism for Crown Loading

Table 3: Virtual Work Summary for Crown Loading

$\alpha$	$\beta$	$x_{ic}$	L1: horiz. length seg. 1	L2: horiz. length seg. 2	$\theta_1$	$\theta_2$	seg. 1 uplift	seg. 2 uplift	P
20	52.73	2.87	0.72	11.28	0.69	0.35	0.25	0.97	44.32
25	55.20	3.66	1.12	10.88	0.59	0.27	0.33	0.49	22.61
30	56.26	3.98	1.61	10.39	0.57	0.25	0.46	0.30	15.57
32	56.41	4.03	1.82	10.18	0.56	0.25	0.51	0.26	14.43
34	56.44	4.04	2.05	9.95	0.56	0.25	0.58	0.23	13.95
36	56.37	4.02	2.29	9.71	0.56	0.25	0.65	0.21	14.01
38	56.21	3.97	2.54	9.46	0.57	0.25	0.72	0.19	14.57
40	55.98	3.90	2.81	9.19	0.57	0.26	0.80	0.18	15.61
50	53.97	3.27	4.29	7.71	0.63	0.31	1.35	0.18	28.74
60	51.05	2.30	6.00	6.00	0.80	0.43	2.40	0.30	64.94

## 2.5 Non-linear Analysis Using Frame Analysis Programs

Although the foregoing methods are sufficient in most cases for the assessment of plane arches and represent much simpler inputs and outputs, it is sometimes necessary to use the non-linear capabilities of frame analysis programs to assess the capacity of an arch. The following section will discuss, through means of an example, the considerations that are brought into the analysis of an arch in a realistic case. The example that will be followed, illustrated in Figure 14, consists of an arch supporting a diaphragm wall 18 inches thick, which supports a triforium above. The diaphragm wall subjects the arch to a distributed load, while the columns of the triforium cause a concentrated load at the top of the diaphragm wall. For the loading of the arch, however, the loading from the triforium columns is distributed through the diaphragm wall. The cross-sectional dimensions of the voussoirs are 18"×24". The intrados span of the arch is 21 feet or 23 feet center/center. The arch is pointed in a 'tiers-point' style, that is, the radius of the intrados is 2/3 of the span, so that the intrados radius is 14 feet, while the centerline radius is 15 feet.

The analysis program to be used in the case is SAP, although many of the considerations in this case can be applied through other analysis programs as outlined in Section 3.10. The geometry of the arch is entered into the frame analysis program through a series of x and z coordinates (it is significantly easier to deal with gravity loading correctly using the z-coordinate

as upwards in SAP). The x and z coordinates are shown in Table 4. The nodes are joined by a series of 10 frame elements, with the section properties of an 18"× 24" voussoir.

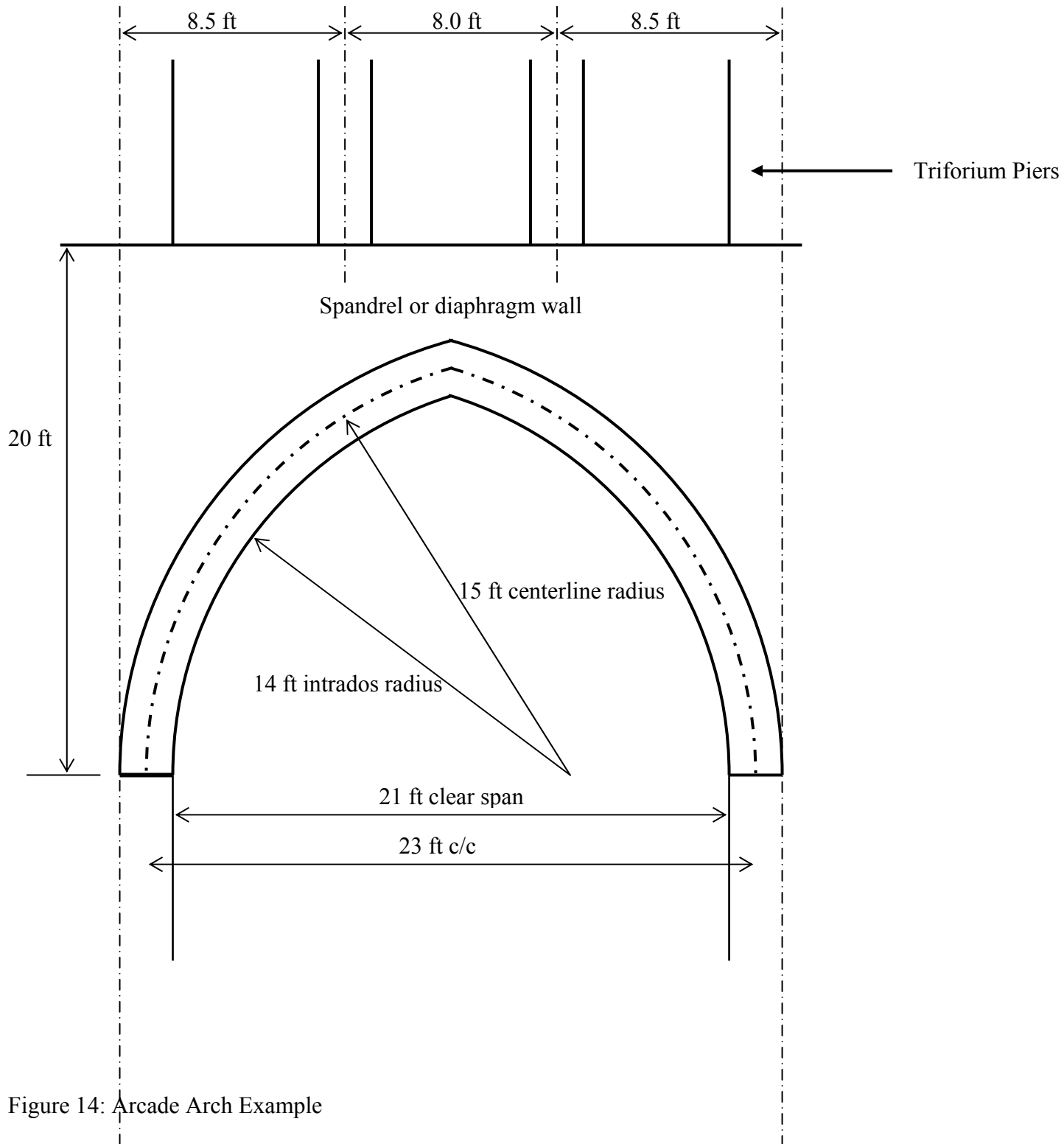


Figure 14: Arcade Arch Example

Table 4: Nodal Coordinates For Arch Analysis

Node	x (feet)	z (feet)	diaphragm wall depth (feet)	nodal load (k/ft)
1	11.50	0.00	20.00	4.80
2	10.77	4.64	15.36	3.69
3	8.64	8.82	11.18	2.68
4	5.32	12.14	7.86	1.89
5	1.14	14.27	5.73	1.38
6	0.00	14.59	5.41	1.30
7	-1.14	14.27	5.73	1.38
8	-5.32	12.14	7.86	1.89
9	-8.64	8.82	11.18	2.68
10	-10.77	4.64	15.36	3.69
11	-11.50	0.00	20.00	4.80

Two basic types of loading are present on the frame elements: gravity due to self-weight of the voussoirs and the diaphragm wall, and loads from the triforium piers above. The example investigation will focus on the maximum sustainable loading from the triforium piers, which will be characterized as a 'live load.' The self-weight of the voussoirs is entered simply as a gravity load constant, based on the cross-sectional area of the voussoirs and a unit weight of 160 lbs/ft<sup>3</sup>. The gravity load due to the diaphragm wall is entered as a linearly varying load, depending on the depth of the diaphragm wall at the two end nodes of each element.

The load from the triforium piers is entered as a variable live load and factored upwards to obtain an estimate of the capacity of the arch. Because of the low resistance of any arch to concentrated load the pier loads are considered to be dispersed through the diaphragm wall at a slope of 1 horizontal to 2 vertical. The arch is fixed at the supporting piers.

### 2.5.1 Linear Analysis

A linear analysis of the arch is accomplished by entering linearly elastic material properties of  $E = 1500 \text{ k/in}^2$ ;  $\nu = 0.2$ . The masonry is considered to have a compressive capacity of 2000 psi and a tensile capacity of 100 psi. This analysis is completed following the procedure identified in Section 2.3 and includes the application of the self-weight of the arch, the dead load

due to the spandrel wall above the arch, and a large factored load. The arch model in SAP is shown in Figure 15.

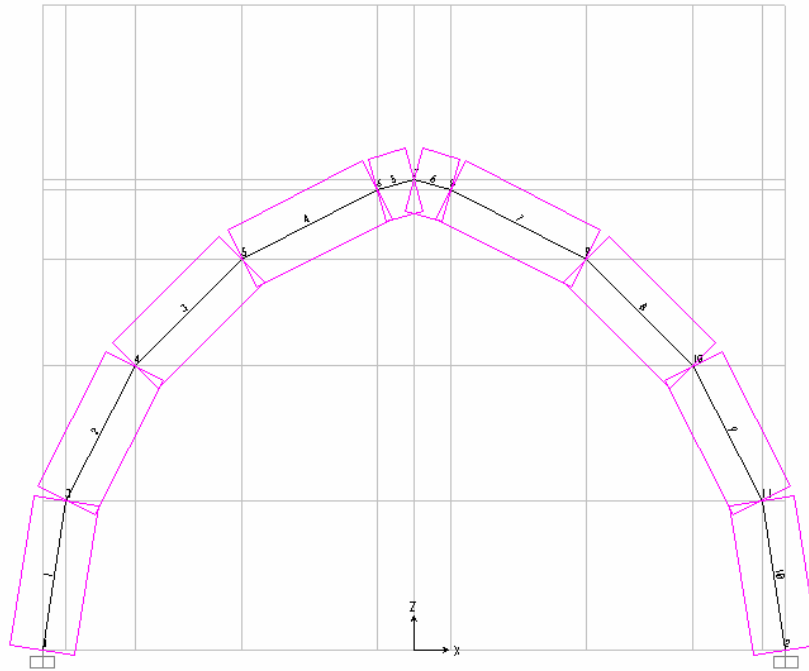


Figure 15: SAP Model of Arcade Arch

The concentrated forces of the triforium piers, applied to the top of the diaphragm, are not applied to the arch as concentrated loads, but are significantly dispersed through the diaphragm. Two alternative procedures can be used for the modeling of the effect of the concentrated loads of the triforium piers on the arch. It is possible to model the diaphragm region as shell elements, subjected to membrane stresses only, and to apply the load from the triforium piers directly to the top of the diaphragm. This process presents additional complications in modeling and interferes with the ability to obtain non-linear results, because the shell elements constrain the frame elements of the pier. It is also not clear that this procedure results in accurate distributions of the concentrated forces to the arch. Instead, it is recommended that a reasonable assumption about the distribution of concentrated forces through the diaphragm be adopted and applied to the determination of the linearly varying loads applied to the top of the arch. In this case, it is assumed that the concentrated loads applied at the top of the diaphragm are dispersed through the diaphragm at a slope of 1 horizontal to 2 vertical. Thus,

for instance, a 6.67 kip load at the level of the top of the wall ( $z=20$  feet) produces a pressure of 0.84 k/ft at node 4 ( $z=12.14$  ft). The view in Figure 16 displays the live load pressures used in the analysis of this structure. The loads are symmetric about the  $x=0$  axis through the crown of the arch.

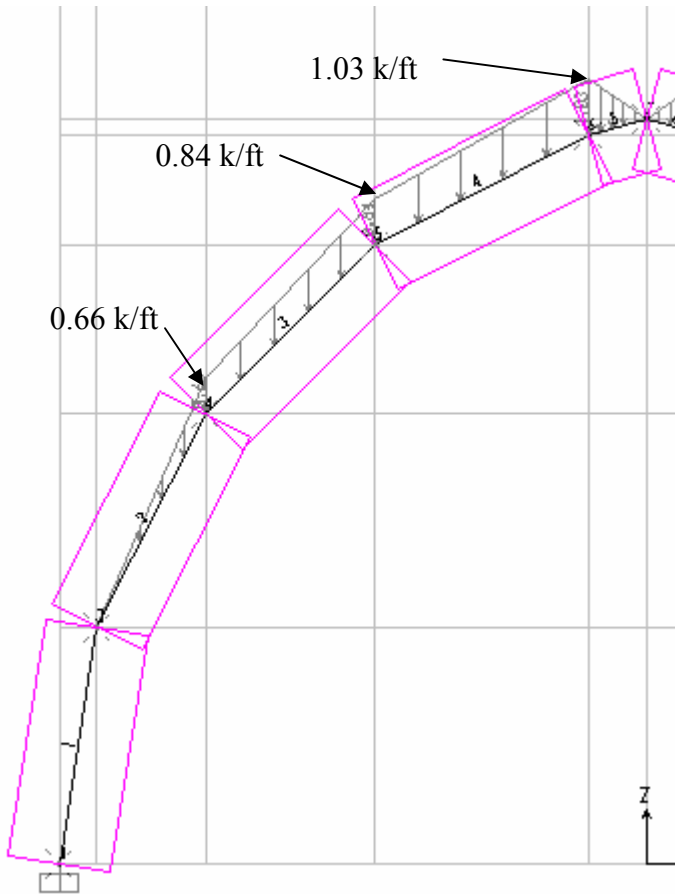


Figure 16: Live Load Pressure Resulting from Triforium Piers

A live load factor of 19, representing a load of 127 kips in each pier, is applied to the loading from the triforium piers, along with a dead load factor of 1. This is the live load that induces failure of the system in the non-linear model described in the following section. The internal bending moment and axial force results are shown in Table 5. The table also shows the required capacity of the masonry calculated by the equation presented in Section 2.1.

$$f_c = \frac{P}{bd} \left( \frac{d}{d - 2e} \right)$$

The symmetry of the problem is noted, so that only the members to the left of the  $x=0$  axis are tabulated. The eccentricities are generally acceptable, being less than 12", however, the compressive strength of the masonry, supposed to be 2000 psi, is exceeded at the supports in the linear model.

Table 5: Linear Axial Force and Bending Moment Results, Arcade Arch

Member	P	M	eccentricity	required capacity
	kips	Kip-in	in	k/in <sup>2</sup>
1	-269	2435	-9.04	2.53
	-258	543	-2.11	0.72
	-247	-1397	5.65	1.08
2	-257	-1397	5.44	1.09
	-242	-1203	4.97	0.96
	-215	-1307	6.07	1.01
3	-208	-1307	6.28	1.01
	-181	-105	0.58	0.44
	-152	301	-1.98	0.42
4	-144	301	-2.08	0.40
	-124	1055	-8.51	0.99
	-102	639	-6.26	0.49
5	-107	639	-5.96	0.49
	-105	490	-4.68	0.40
	-104	294	-2.83	0.31

### 2.5.2 Non-Linear Analysis

The structure under consideration is an acceptable under the above analysis which uses a simple linear analysis. It may be considered useful to obtain additional information from a non-linear analysis. The non-linear features of frame analysis programs can be advantageous in completing such an analysis. It must be noted that the non-linearity in this problem, as with most masonry structures, are material non-linearity. The changes in loading that result from gross deformation can be investigated through the application of geometric non-linearity. Many conventional frame analysis programs permit the input of a wide range of material non-linearity. However, the use of the non-linear material properties is usually confined to frame elements. The properties are used to create hinges on the basis of the material properties. It is not possible to insert material non-linearity into other sorts of elements, such as shell or solid elements. This is a further reason for the strategy of investigating the action of the arch as a frame, as discussed

in Section 0. The material stress-strain law shown in Figure 18 and it is used as a representative masonry property.

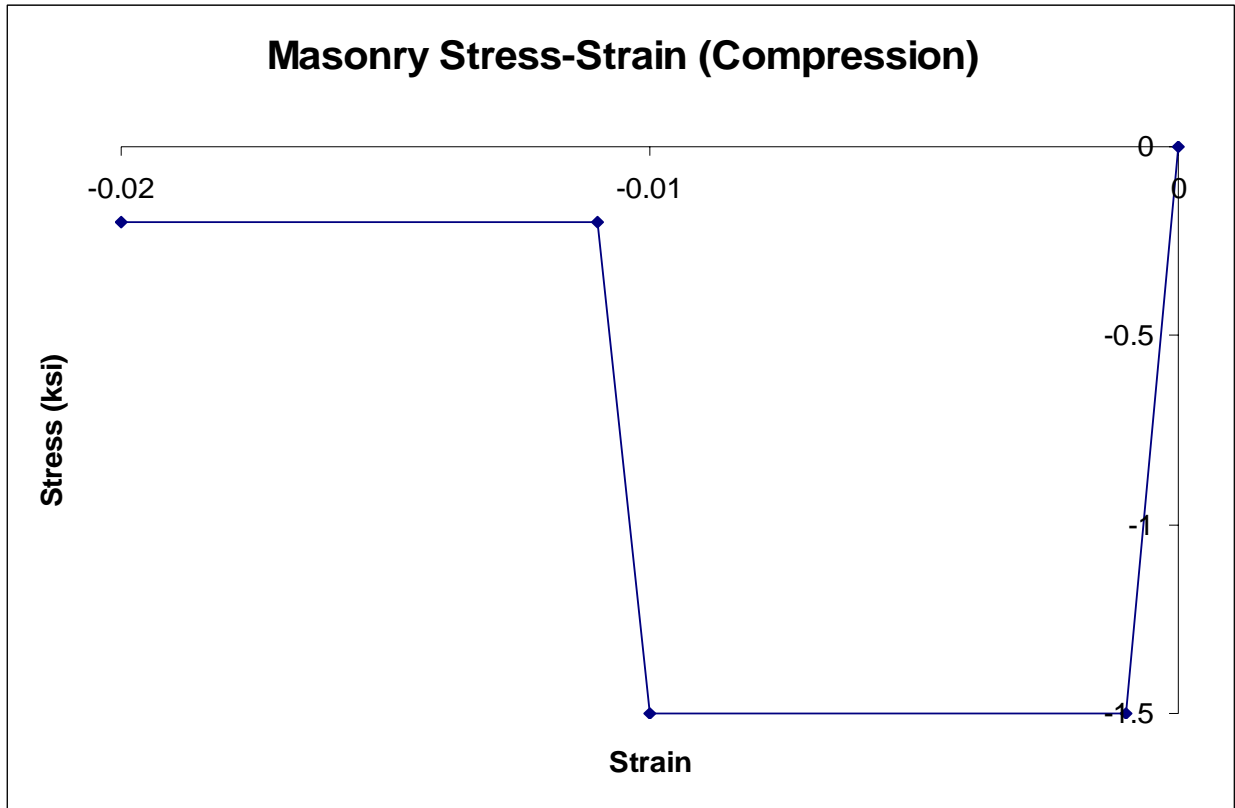


Figure 17 Masonry Stress-Strain Law for Compression

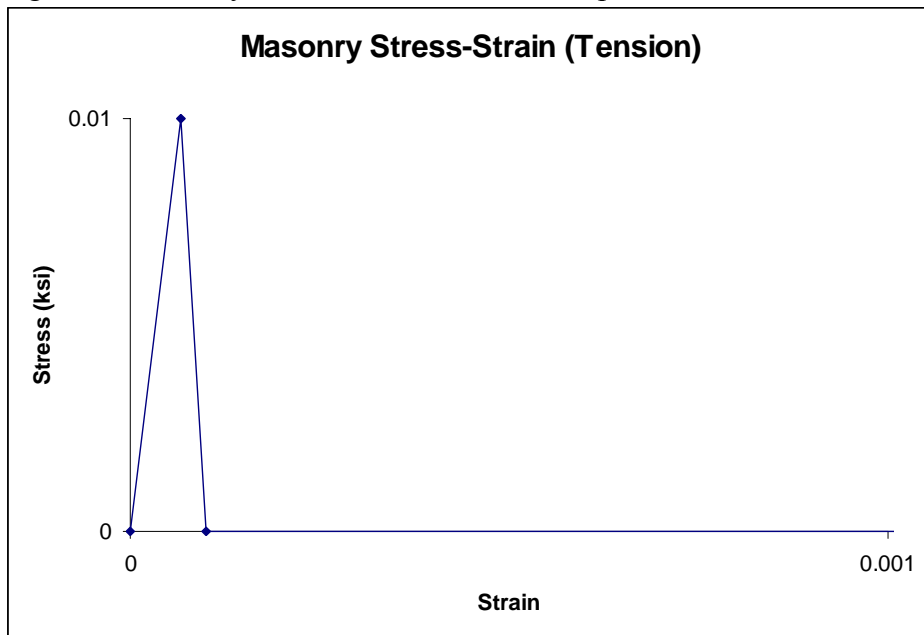


Figure 18: Masonry Stress-Strain Law for tension



The use of a frame hinge with non-linear properties can be illustrated by means of an example of the pushover analysis for a fictitious pier, 24"  $\times$  24" in cross section, with a height of 120", illustrated in Figure 19. The pier has a unit weight of 160 lbs/ft<sup>3</sup> or a total weight of 6 kips. The simple overturning moment on the pier is then 0.6 kips, applied as a lateral force to the top of the pier. The cross-section is divided into eight sections, as illustrated in Figure 20. The area properties of each of these sections, 72 in<sup>2</sup>, are lumped at eight points, endowed with the material stress-strain curves in Figure 18. This defines a frame hinge, which is located at the base of the frame element used to represent the pier.

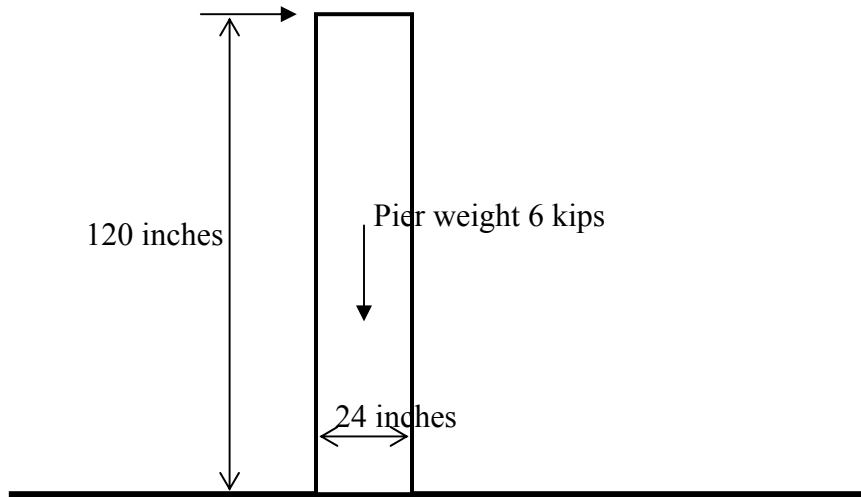


Figure 19: Pier for pushover analysis

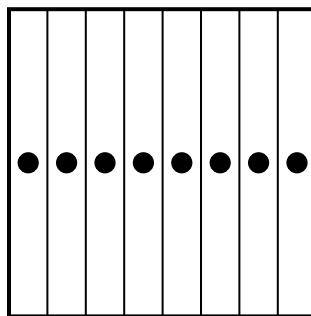


Figure 20: Fiber hinge for pushover analysis

The load on the pier is divided into two cases: the dead load and the lateral load at the top. The dead load, due to self-weight, is applied first, followed by the lateral load. The lateral load is applied in very small steps, and the results are recorded for each of the steps. The

pushover analysis shows the development of small non-linear load-displacement relations at a load of over 0.5 kips, followed by a distinct softening of the system response, with total collapse at 0.563 kips, just below the simple overturning force of 0.6 kips.

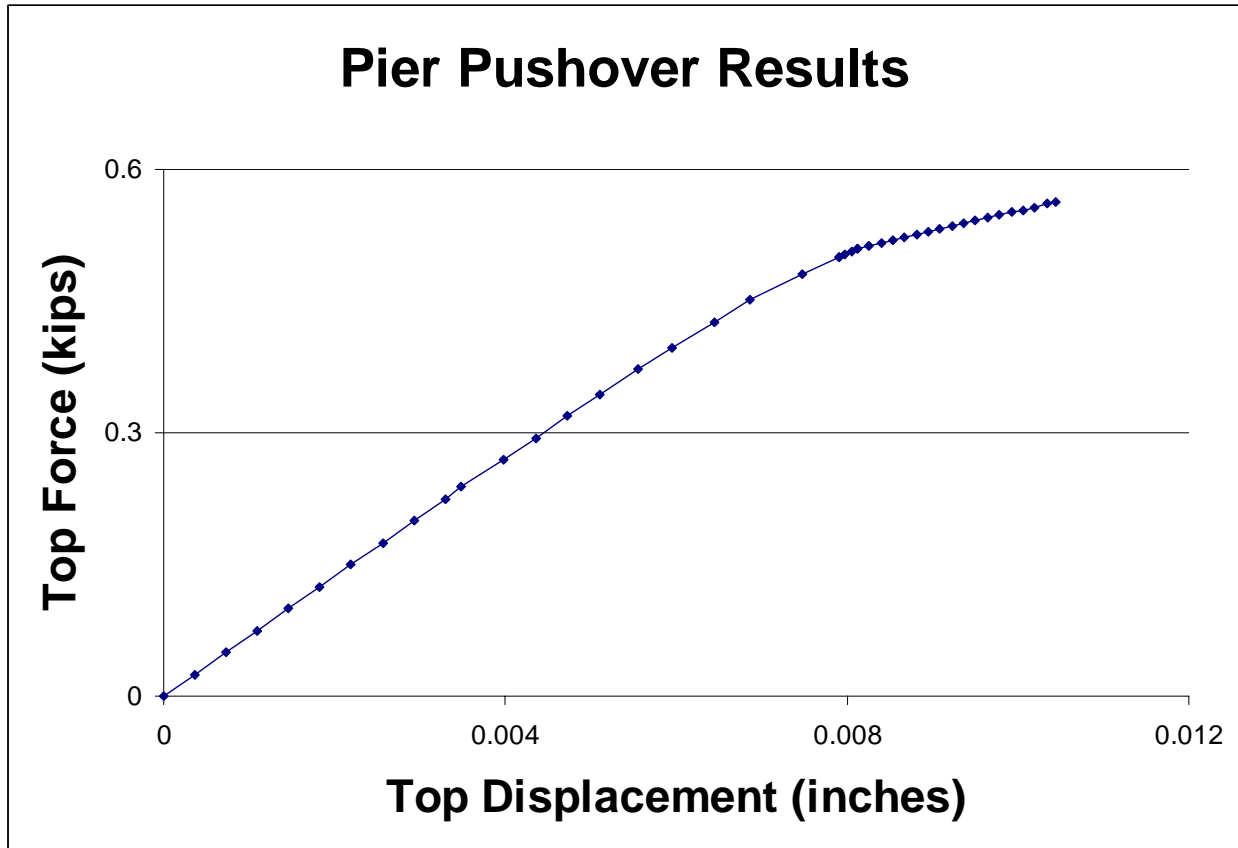


Figure 21: Pier pushover analysis load-displacement results

Returning to the arch example, the material non-linearity is invoked by insertion of hinges within a frame element. The non-linear properties are applied at the specific hinge location, while the remainder of the frame element remains linearly elastic. The simplest form of a plastic hinge, a moment-only hinge, is not appropriate for masonry, as the plastic deformations depend on combinations of axial force and deformation. In SAP, the properties of such a hinge can be input either by input of a  $P-M$  curve or by use of a 'fiber hinge,' in which the cross-section properties are lumped in a given number of fibers. The program checks the state of stress and strain at each load cycle and verifies the consistency between stress and strain, according to the non-linear material properties input. In this way, an appropriate  $P-M$  plastic hinge is obtained.

The difference between tensile strength and compressive strength is also modeled automatically by selection of this hinge type. In this example, the properties of the section are lumped into six fibers, each having an area of  $36 \text{ in}^2$  and centroids at 2, 6, and 10 inches from the centroid of the cross-section. A hinge is located at each end of each frame element, as shown in Figure 22.

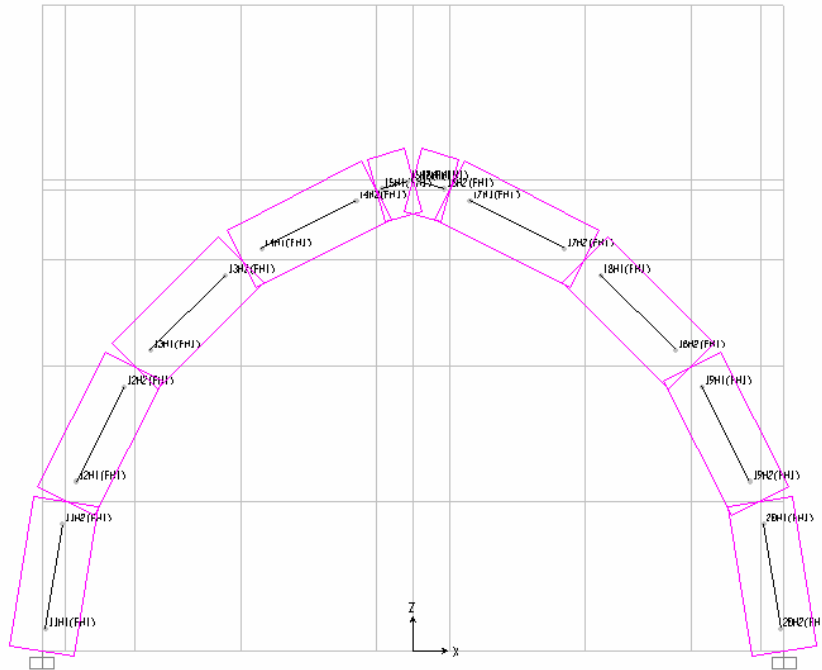


Figure 22: Frame Hinge Locations

An analysis case is defined using both dead loads and triforium pier loads as non-linear loads. Loads are applied to the non-linear model in two stages. The first stage is the application of the dead loads, and the second stage is the application of factored live loads. In the second stage, it is necessary to save multiple results set in addition to the final results. The maximum load is found by a process of trial and error. A load factor that is too great will cause non-convergence of the solution, while a load factor that is too small converges readily. In practice, the load factor is increased slightly until the solution fails to converge, and the model is finally run at the greatest load factor for which convergence is achieved. Figure 23 shows the hinge status in the model at various load factors. As the loads increase, a number of partial hinges develop along the arch barrel (State A to B), representing the initial non-linear part of the stress-

strain curve. At the final load state, the hinges at the supports are in a state of instability, and the solution no longer converges.

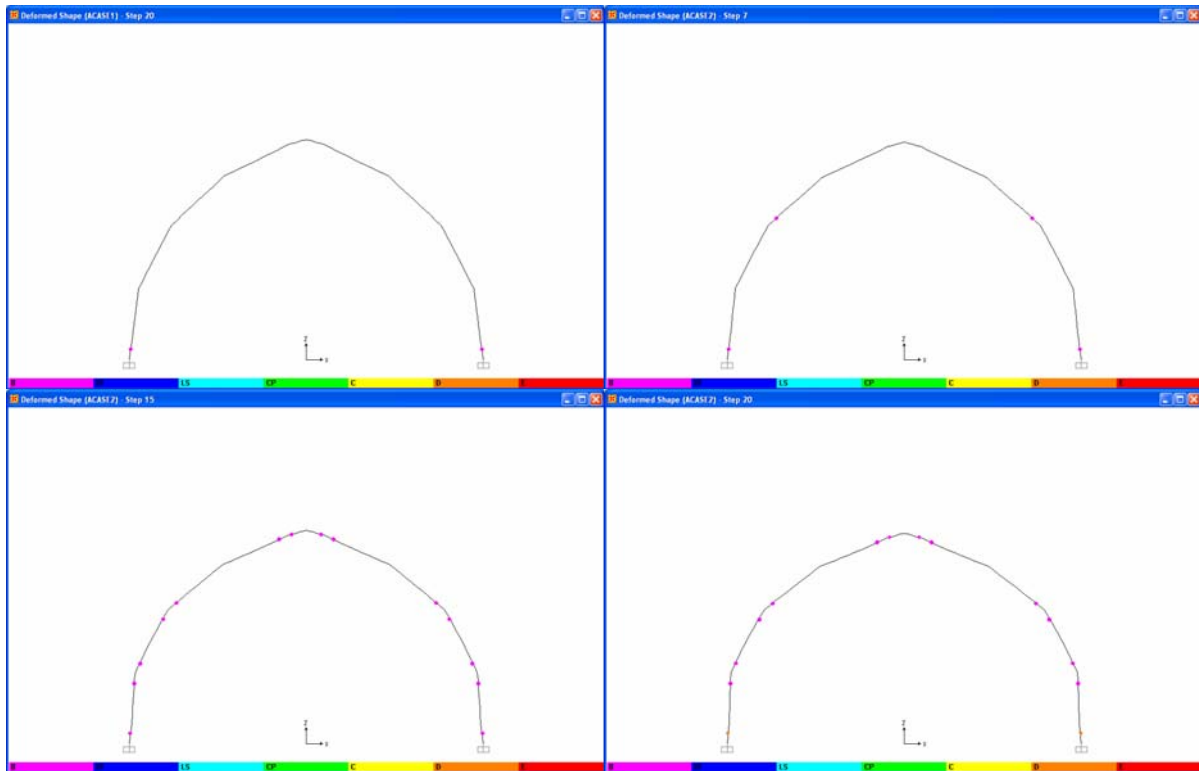


Figure 23: Hinge Status at Various Load Factors

Upper Left: 33.3 k at each pier.

Upper Right: 66.7 kips at each pier.

Lower Left: 100 kips at each pier

Lower Right: Final state, 126 kips at each pier

Although it generally involves a considerable effort to set up a non-linear analysis and especially to adjust the model to the point where it will run and give meaningful results, such an analysis can return more realistic results. From the discussion in Section 2.2, the arch does not fail immediately as a result of developing a hinge at the supports, as supposed in the linear analysis for this structure in Section 0. Instead, the arch has significant capacity to redistribute excess bending moments from hinge locations to the remainder of the arch and can develop residual capacity beyond the formation of hinges. This is illustrated very clearly in Figure 23. A further illustration of the potential value of non-linear analysis is provided by the comparison of linear and non-linear analysis for this arch at the same maximum load. Figure 24 illustrates the bending moment diagram for this structure for the linear and for the non-linear analysis. It is clear from this diagram that the excess bending moments at the supports, present in the linear

analysis, have been re-distributed to the remainder of the arch in the non-linear analysis; this is as a result of the decreasing stiffness of the frame hinges at the supports. The diagram of the eccentricity in Figure 25 especially shows a significant balancing of the eccentricity in the arch, which results in a general increase in the capacity.

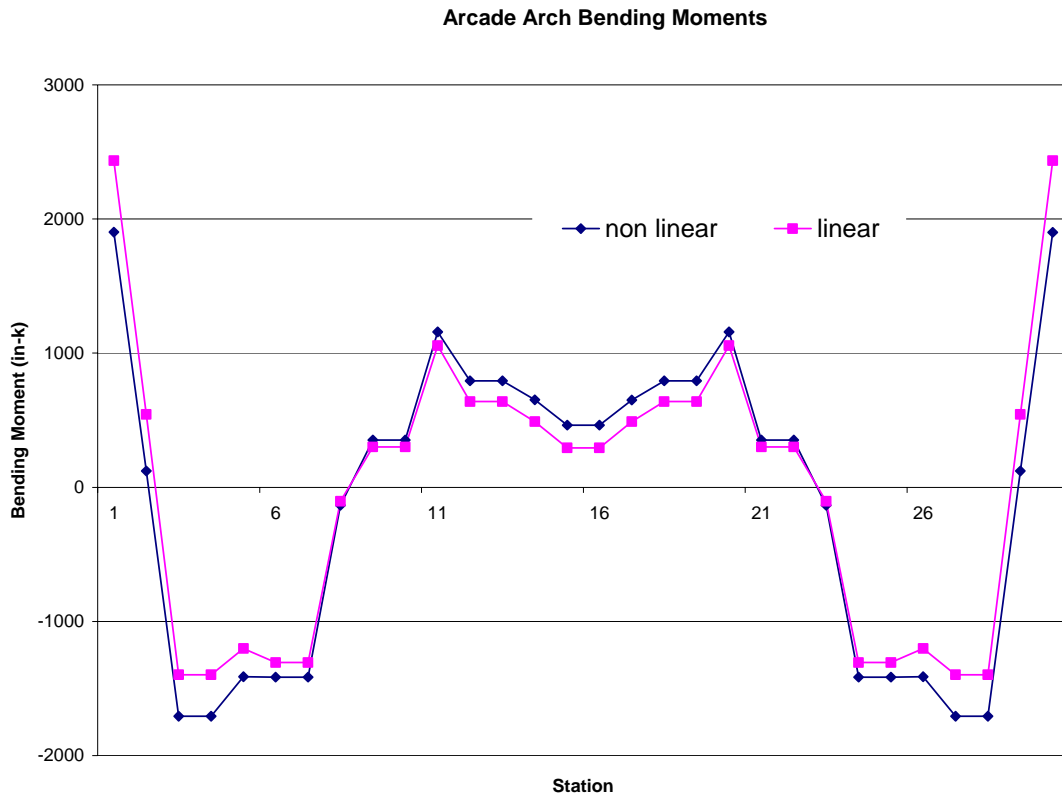


Figure 24: Bending Moment Diagram for Arcade Arch

In conclusion, it is reasonable to model a two-dimensional arch as a frame structure. Material and geometric properties of the arch can be input with relative ease into a standard frame analysis program. In rare cases, some advantage may be gained by invoking the non-linear material properties available in frame analysis programs, but this procedure should be used judiciously and based on knowledge of the actual non-linear features of the program at hand.

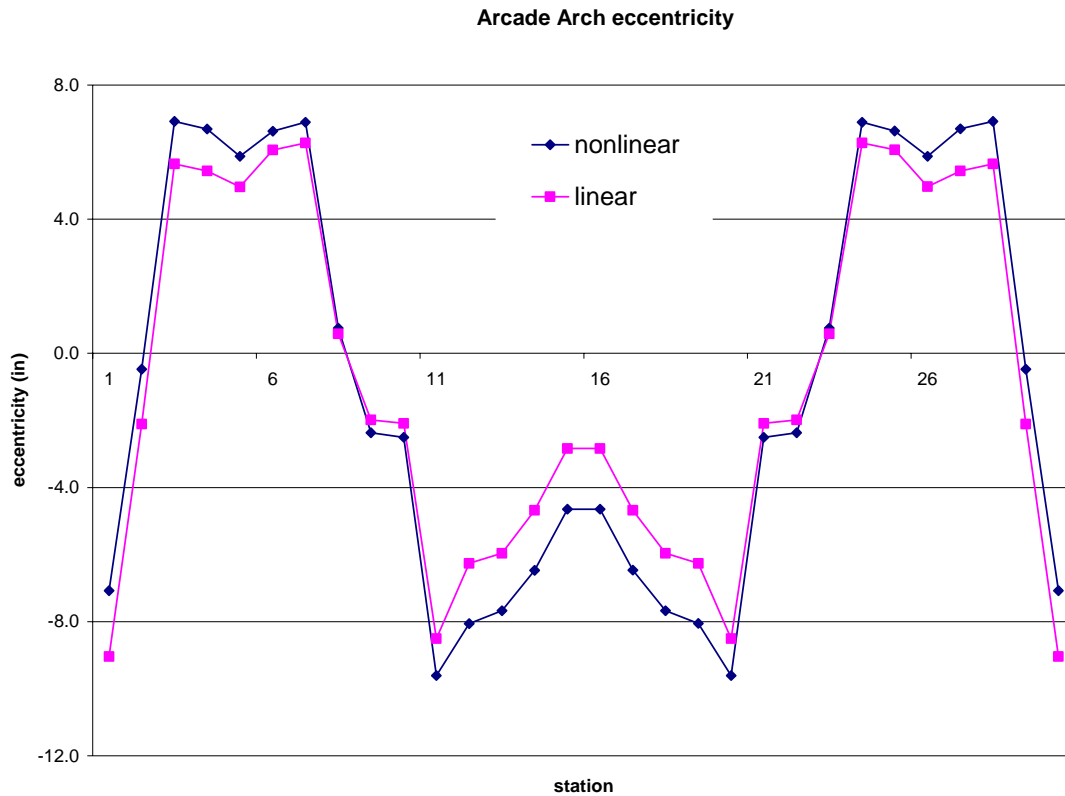


Figure 25: Eccentricity Diagram for Arcade Arch

### 3 Three-Dimensional Masonry Vault Assessment

#### 3.1 Building a Model

- The process of developing an analytical model of any three-dimensional structure consists of
  - Development of a geometric model of the structure.
  - Development of a solid model of the structure.
  - Identification and selection of element types.
  - Meshing the solid model, using the selected element types.
  - Identification of material properties, and applying to the elements.
  - Application of loading conditions.
  - Application of boundary conditions
  - Solution of model.

The process must continue beyond the solution of the initial model. The solution must always be tested against known information on the structure, such as the results of testing or the location of cracks or other damage. Following the initial solution, the model may be refined, the boundary conditions may be altered, material properties may be adjusted, and the model is re-run. This process is generally known as tuning or calibration of the model. It is also prudent to identify which parameters have the greatest influence on the outcome of the model, by varying all of the major parameters, such as material strength or stiffness, and examining the influence on the results. This process is known as sensitivity analysis. Each of these steps, including calibration and sensitivity analysis, will be discussed in detail below, and the examples in Section 4, 5, 6 will illustrate the application of these procedures.

### **3.2 Geometric Model**

The geometric model is initiated by identifying an underlying point grid. Although the grid can be automatically generated by most computer software programs for a plane frame, the location of the points in space for a three-dimensional vaulted structure must be entered manually. Building survey measurements can be used to locate the points in a three-dimensional coordinate system. Connections between the points take the form of straight lines, arcs, or splined curves.

In general, it is necessary to determine the physical dimensions of a masonry assembly in order to develop an accurate structural model. Although a higher level of detail may be desirable in some instances, the analysis of load-bearing masonry structures does not require an extraordinary level of detail in the determination of the physical dimensions of the structure. The thickness of piers or walls supporting the structure should be determined at the base and at any important (>10-20 %) changes in thickness. The key dimensions for a load-bearing arch are span, rise, and thickness as shown in Figure 4. A significant proportion of required analytical work on an arch can be completed with these dimensions, along with a knowledge of the general arch profile, whether segmental (circular), two-centered, or four centered. These dimensions are illustrated below. The profile of load-bearing arches, unless seriously distorted due to loading or settlement effects, can be adequately characterized by span/rise and 1/4 point rise. If feasible, a smaller measurement interval may offer additional precision, but this is not strictly necessary.

Figure 23 shows the types of arches that have the same span, rise and thickness and the importance of the 1/4 point measurement in determining the arch type.

Arches are often provided with filling or diaphragm walls, either at the supports or along the entire span of the arch. Where such walls are present, rudimentary measurements of the height and thickness of the wall are necessary.

The dimensions of rib vaults can be adequately determined on the basis of the bordering arches of the vault, based on the discussion above: span, rise, and 1/4 point rise. Arch ribs generally have a constant thickness; so any means of determining the dimensions of an arch rib, whether by remote measurement, consulting plans, or hand's-length measurement, is sufficient. When these have been determined, the actual shape of the vault between ribs makes very little difference in the adequacy of the vault. Domes are almost always sections of a sphere, and a satisfactory model of a dome can be created using a very limited set of span, rise, and thickness measurements (see example in Section 6). Groin vaults require the simple measurement of arch parameters in the direction of the two intersecting barrel vaults. Vaults are often provided with filling from the supports up to the haunches, and the height and general composition of the filling also need to be surveyed. The thickness of vault webs and domes may be difficult to determine unless there are holes in the vault. The use of impact-echo or other non-invasive tools for this determination is described in a following section.

One of the greatest difficulties in obtaining physical dimensions of a masonry assembly consists in identifying the inner structure of relatively thick masonry elements. Where a wall or vault webbing has a thickness of one or two wythes of masonry, it is relatively simple to infer gross cross-section properties. However, large piers and thick walls invariably have a carefully constructed outer facing and a rough core, often consisting of rubble or a large void. Certain non-destructive or semi-destructive methods can be effective in determining the nature of the inner core. A borescope investigation can determine the existence of a large void. Among the methods listed in the *Guideline for Structural Condition Assessment of Existing Buildings* (ASCE 1999), ultrasonic pulsed velocity measurements can assist in the location of interior interfaces. Other methods that have been investigated include impact-echo testing and tomography. The latter method is particularly appropriate to elements having access to all sides, such as isolated piers or interior bearing walls.



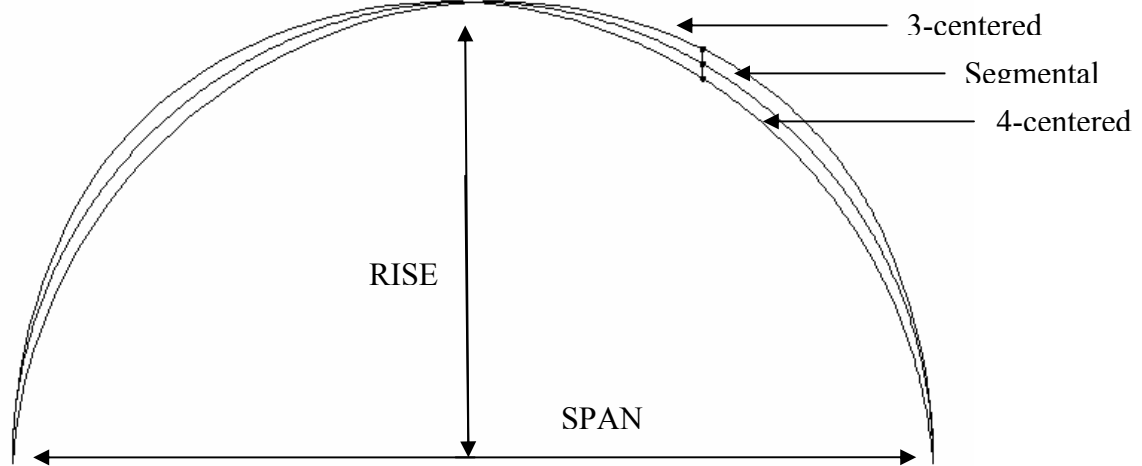


Figure 26: Arch profile related to 1/4 point rise. The three arches have the same span and rise, but are differentiated by the 1/4 point rise.

In complex structures, such as rib vaults or piers having multiple colonnettes, it is important to determine the level of simplification that will preserve realistic results in advance of the modeling effort. Complex molding profiles on vault ribs or arch ribs are practically impossible to model accurately in finite element analysis (FEA), and the excessive effort spent on attempting to model these shapes is not justified by the increased accuracy of the results obtained. In general, it is preferable to reduce complex cross-sectional shapes to a simpler rectangular shape of approximately the same cross-sectional area and of a slightly reduced structural depth. Examples of such reductions from the authors' studies of the National Cathedral are illustrated in Figure 27. As discussed in Section 5, these reductions had a large impact on the effort involved in modeling the structure and did not have a substantial impact on the fidelity of the modeling results.

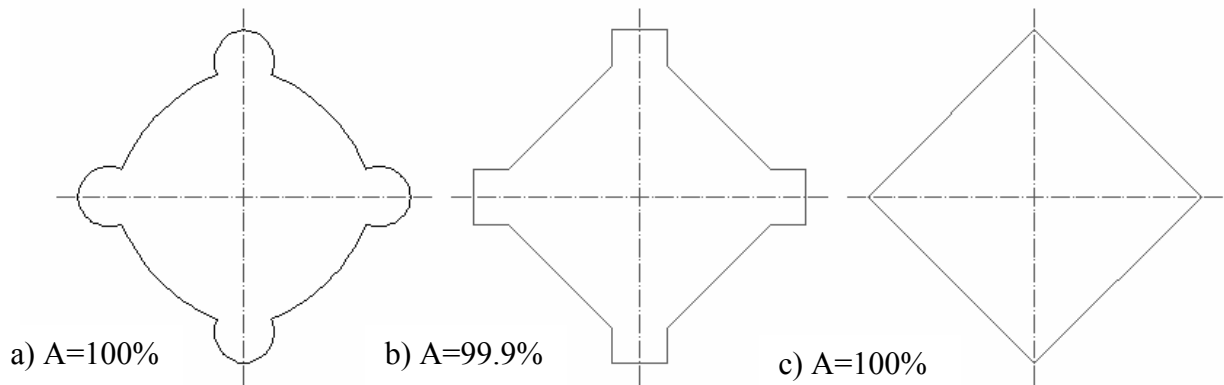


Figure 27: Geometric simplification of the center pier cross section with constant area.

### 3.3 Solid Model

Solid models can be generated on many computer platforms, including CAD programs, or using modeling utilities in the structural analysis software. There are significant interactions between the development of the solid model and the choice of elements for use in structural analysis. For instance, if shell elements are used for vault webs, then the model of the structure will represent the thickness of the vault by a reference surface, usually the middle surface. Where solid elements are used, the solid model must include three-dimensional objects. The intersection of elements such as vault ribs creates significant challenges in the development of the solid model, and the ability to mesh the final product must always be borne in mind. Figure 28 illustrates a typical intersection of vault ribs. The model of the ribs, in keeping with the discussion in Section 3.2, consists of equivalent rectangular sections. The intersection of these sections is illustrated in Figure 29. Meshing of the small, poorly shaped areas between ribs is critical to the proper performance of the model and needs to be considered carefully.



Figure 28: Vault Rib Intersection at Springing

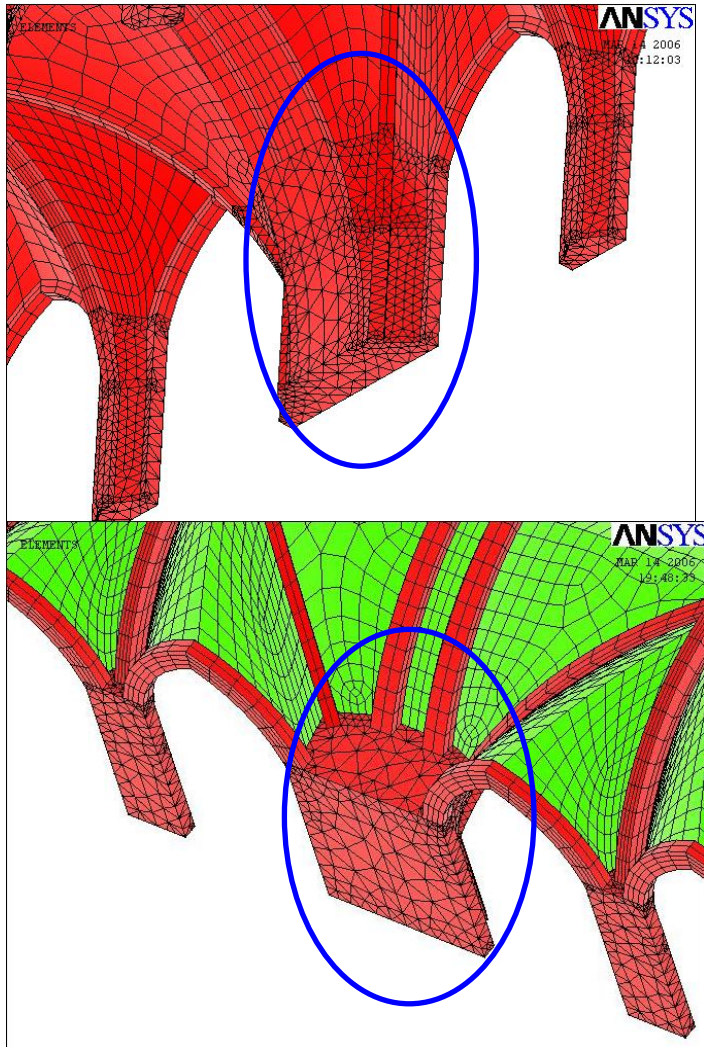


Figure 29: Model of Vault Rib Intersection

### 3.4 Element Types

#### 3.4.1 Frame

Frame elements represent a beam or bar by a single line, usually along the centroid of the member. The element may be straight or curved. A spatial frame element has up to six degrees of freedom (three displacement and three rotation) at each end, while a frame element in a plane has only three degrees of freedom at each end. The stiffnesses of a spatial element include bending about two axes, torsion, axial force, and relative displacement in two directions. Although frame elements are widely used in modeling framed structures, such as reinforced concrete or steel frames, they have little use in modeling unreinforced masonry structures. The

only exceptions are for the occasional incidental modeling of lintels or the modeling of steel or concrete members supporting a masonry structure.

### **3.4.2 Shell**

Shell elements are well suited to model singly curved or doubly curved surfaces of varying thickness. For homogenous materials, the shell is represented by the middle surface, or reference surface, that is half the thickness away from exterior faces. Although the developers of this element did not provide a clear definition of 'thin,' generally a shell is accepted to be thin if the thickness is less than one-tenth of the radius of curvature of the reference surface.

Shell elements can be three or four cornered node elements. All shell elements have nodes at the corners, while more refined elements may have mid-side nodes. The nodes each have six degrees of freedom: three translational and three rotational. The shell element has bending, torsional, membrane and shear stiffnesses. The size and complexity of a problem can be significantly reduced by considering membrane (in-plane) forces only, suppressing the bending and torsional stiffnesses, or by omitting the membrane stiffnesses and considering only bending, torsional and shear stiffnesses. The former strategy is appropriate for shells with relatively low bending stiffness, such as very thin shells, while the latter may apply better to thick shells.

Shell elements are particularly well-suited to the modeling of vault webbing, as they are economical compared to solid elements and include all of the load effects that characterize vault webbing, including the interactions between membrane forces and bending moments. Output is generally in the form of nodal moments and stresses that computer software automatically converts to membrane forces and bending/twisting moments at the edge of the shell element. In some programs, the user has a choice of where the reference surface is located within the thickness of the shell; this can be very convenient for modeling relationships between ribs and webbing in a rib vault structure.

### **3.4.3 Solid**

Solid elements have three dimensions and hence a greater number of nodes than frame or shell elements. Tetrahedral solid elements with four nodes exist, but problems are encountered

in stress calculations due to geometric problems and the lower accuracy of this type of element. A so-called brick element has a minimum of eight nodes, while refined versions of this element, including one mid-side node, has twenty nodes. Nodal degrees of freedom include translations only. The element stiffnesses include only the stiffness in response to normal and shear forces. Rotations of the overall element are modeled by relative displacements of nodes within an element and among elements, while the determination bending and twisting moments requires the use of several solid elements through the thickness of a member.

Because solid elements are particularly useful in modeling mass structures, they can also be easily used for the modeling of unreinforced masonry. However, they are uneconomical, consuming large numbers of nodes. The requirement of at least three elements through the thickness of any significant structural member imposes limitations on the use of solid elements. For instance, modeling a 6" vault web using solid elements requires three solid elements through the thickness. Limitations on the aspect ratio of elements requires that the other dimensions be no greater than 6" to 8", resulting in an unnecessarily fine mesh. Therefore, the ideal choice in this situation would be to use shell elements. Vault ribs, on the other hand, may be effectively modeled as solid elements, but require at least a nine-element cross section. Walls may be modeled using either solid elements or shell elements, depending on the scale and the situation. Because of the irregular shape of surcharge volumes, tetrahedral solid elements are virtually necessary for these features. The principal limitation of tetrahedral solid elements is that stress results are unreliable for this element type. However, the precise determination of stresses in the surcharge is usually unnecessary.

### **3.5 Meshing**

On completion of the solid model and selection of the element types, the solid model is broken down into individual elements according to a systematic procedure known as meshing the model. The shape and size of the elements has important impacts on the solution. A mesh that is too coarse can produce inaccurate solutions, while a mesh that is too fine will result in problems with program limits on the number of nodes or elements or will result in excessive run times. The aspect ratio of the elements (ratios between key dimensions, such as length, width, thickness) must also remain within reasonable limits: an aspect ratio of less than two is desirable,

while a ratio of greater than four is unacceptable. Similarly, the angles of corners can be neither too acute nor too obtuse. Most programs give warning prompts when aspect ratio or corner angle limits are exceeded.

When solid elements are used, the requirements of the aspect ratio give some guidance on the required fineness of the mesh. Given, for instance, a vault rib of dimensions 100 cm × 100 cm and given the requirement of three elements through the thickness in any direction, the length of the elements along the vault rib can be no more than approximately 100 cm. Where it is impossible to observe these limitations, consideration should be given to using other element types, such as shell or frame elements: a frame element has no limitations on aspect ratio, while a shell element does not have a limitation on the thickness.

Beyond this, experience indicates that, at the scale of most monumental masonry structures, an element dimension of approximately 10-30 cm results in an appropriate level of mesh refinement (Atamturktur 2006). Particularly difficult problems in meshing are present at the intersections of vault webbing and ribs and at the springing of vaults. At these locations, multiple ribs are closely spaced, and the webbing between the ribs has to be meshed with shell elements. Moreover, the vault web is very narrow at these locations, making it virtually impossible to observe aspect ratio limitations, especially given that the shell elements need to share nodes with the solid arch rib elements. This type of situation is illustrated in Figure 28 above. It has been found that omitting the vault webbing in the very narrow parts is often the best way to manage this modeling problem. It is also important to ensure that the length of the rib elements is approximately the same on each of the intersecting ribs. The vault webbing can be resumed at the location where the distance between ribs is approximately 10-20 cm.

### **3.6 Material Properties**

The real behavior of masonry is non-linear, in the sense that the stress-strain law, even for elastic compression behavior in compression, may show softening. The behavior in tension at low stress levels is inelastic due to the influence of cracking. The behavior in compression at higher stress levels is also inelastic due to irreversible softening effects. Due to the orientation of the mortar joints, the material is anisotropic and inhomogeneous.

Although it is by far simplest to work with linearly elastic, homogeneous, isotropic material properties, it is necessary to exercise caution in adopting this viewpoint of masonry behavior. On the other hand, significant progress in the assessment of a masonry structure can be made using this simple form of constitutive law. The behavior of a structure under self-weight can be determined quite accurately using linear elastic material properties, and the service load behavior can also be predicted very accurately, as long as the tensile stresses in the structure are low. At the very least, the initial analysis for any masonry structure should include a linearly elastic analysis; this can be completed quickly, without the convergence problems associated with non-linear analysis. The presence and magnitude of tensile stresses in the masonry is determined and analyzed as a result of the initial linear analysis. The assessment of the need for a non-linear analysis is made on the basis of the initial linear analysis. Factors that would indicate the need for a non-linear analysis include tensile stresses exceeding the rupture strength of the masonry in a large zone, the presence of large foundation settlement, or the presence of large cracks of unexplained origin in the structure.

Alternative material formulations are available in some widely-distributed frame analysis programs. Using frame elements only, SAP allows the input of a stress-strain property table for the materials, which can be solved by invoking non-linear analysis. This table may include softening behavior such as is experienced in masonry after cracking. An example of the application of such material properties is previously provided in Section 2.5.2.

STAAD includes support conditions and member formulations that resist compression-only, which can be useful in the analysis of unreinforced masonry. However, these are not material properties and can only be used at the member level of analysis. When a compression-only member is invoked, the member is neglected if it is in tension. This feature has limited application to masonry structures. The support conditions can be very useful at the supports for a pier or a buttress.

Material properties can be obtained by consulting reference material, by conducting tests on specimens of material extracted from the structure, and by methods of non-destructive evaluation. The principal material properties required for structural modeling are the compressive strength, tensile strength, density and modulus of elasticity of the masonry assembly. Poisson's ratio input is required for analysis programs, but is of secondary



importance. A generic value of 0.10 to 0.20 is satisfactory. It is tempting to think that the most reliable procedure for obtaining the stiffness and compressive strength properties of the masonry units is to extract a specimen of masonry from the structure. However, it is impossible to keep a mortar joint intact during the extraction process, and a direct measurement of strength and stiffness properties is impossible on specimens directly extracted from the structure, particularly when considering tension-controlled properties, such as flexural bond strength. On the other hand, re-fabrication of prisms using mortar of similar properties to the original mortar allows an intelligent estimate of tensile properties. The determination of the properties of in-situ mortar can be made on the basis of historical records, or testing according to ASTM C1324, and can be supplemented by the use of petrographic testing of samples of the mortar. Compressive strength may be relatively unaffected by the breaking of mortar joints during specimen extraction. As a result, it is possible that compressive strength and compressive modulus of elasticity tests may be able to be conducted on such specimens. The extraction of masonry prisms follows the procedure of ASTM C1587. Prisms are tested for compressive strength properties according to ASTM C1314, while stiffness properties may be determined by the application of ASTM E111. Flexural bond strength may be tested according to ASTM E518.

According to ASTM C1197 and ASTM C1196, flat-jack testing can be used for either the determination of elastic stiffness properties of solid masonry, or for the estimation of in-situ compressive stresses in solid masonry. Other non-destructive methods have been used with limited success in masonry structures, although they are not described in an ASTM standard specific to masonry and are not listed as masonry evaluation methods in ASCE Standard 11-99. These include generally acoustically-based methods of imaging the internal conditions in a masonry wall to determine general construction parameters, such as thickness of wythes, existence of internal voids, composition of facing and rubble core, etc. Due to the thickness of load-bearing masonry elements and to the uncertainties of their construction, uni-directional ultrasonic imaging has been found effective only for the determination of gross parameters such as very large voids or abrupt changes in construction. However, where access to both sides of a wall or three or more sides of a pier is available, the automated imaging of cross sections on the basis of multi-axial ultrasonic probing has been found to be much more effective (Schuller, *et al.* 1997) (Binda, Saisi, and Zanzi 2003).

### **3.7 Loading**

Loads can be applied to nodes as thermal, inertial, concentrated or distributed forces in the form of nodal displacement or nodal force. The arrangement of loading conditions depends on analysis type. In static analysis, defining the gravitational acceleration as well as existing external loads is necessary. In modal analysis, the results are independent from force input, and the only possible loading condition is a zero displacement constraint, in other words, a boundary condition. However, transient and harmonic analysis options require a user-defined time dependent loading in addition to the provided boundary conditions.

### **3.8 Boundary Conditions**

Boundary conditions, also called support conditions, have great influence on the computed results. For true representation of the structural behavior of the actual system in the FE model, boundary conditions must be represented as closely as possible to the actual conditions of the structure. In general, it is expedient to model only a portion of the structure, and it is very difficult to assign correct boundary conditions as that portion of the structure modeled is supported elastically. The estimation of boundary conditions is difficult in masonry, compared to other engineering materials. The boundary conditions are dependent on physical properties and configuration of the material, rather than intentionally designed 'pins' or 'points of fixity,' as in a steel structure. In many cases the choices are imposed by the analyst's intuition and the technology/capacity of the FE software.

Because boundary conditions are applicable to the degrees of freedom at the nodes, rather than to the elements, the prescription of boundary conditions is related to the selection of element types. In most commercially available FE software, physical constraints are invoked by zero displacements and/or rotations at the user-defined nodes. For situations of partial restraints, an elastic foundation, which is usually simulated by a series of springs, can be utilized.

It is crucial to start with physically reasonable boundary conditions in the initial FE model. If empirical data are available, the initial model can be calibrated with successive iterations so that the FE solutions correlate to the experimentally obtained data. The summary of the results of the case studies described in Section 4.3 and Section 5.2 presents a reasonable set of boundary conditions for most of the elements in a monumental structure.

In the subsequent discussion, the longitudinal axis of the nave will be described as the  $x$ -axis, the transverse axis of the nave will be designated the  $y$ -axis, and the vertical axis will be the  $z$ -axis. The recommended boundary conditions vary, depending on the nature of the study being conducted. If the purpose of the study is to determine the thrusts of the vaults on the supporting structure, then the vault is modeled from the springing point upwards. In such cases, the boundary conditions include restraint in the  $x$ ,  $y$ , and  $z$  directions at the pier tops. The edges of the vault are subject to symmetry boundary conditions. Generally, the nave wall above the level of the springing of the vault should be modeled. This wall is subject to restraint in the  $x$  direction for the full height of any buttressing, including wall buttresses. The wall should also be restrained at the bearing point of any roof trusses. This point is discussed in more detail in the case study in Section 5.2.

In another type of model, the full height of a bay, or 1/4 bay, may be modeled. In this case, the base of the pier and the exterior wall is restrained in the  $x$ ,  $y$ , and  $z$  directions. If a 1/4 bay is modeled, symmetry boundary conditions are imposed along the centerlines of the bay along the longitudinal axis,  $x$ -translation, and rotation about the  $x$  and  $y$ -axes, and along the transverse axis,  $y$ -translation and rotation about the  $x$  and  $y$ -axes. When a full bay is modeled, similar conditions are applied to represent the effect of the adjacent bays.

### **3.9 Solution**

Depending on the goals of the study, two main analysis types are available in most FE software: static and dynamic analysis. Static analysis slows the forces being applied so that no inertia or dissipative resistance is activated, while dynamic analysis examines how the external loads are balanced with inertial, dissipative and elastic resistance of the system within the discretized time domain. Static solutions may be linear or non-linear, depending on the material, geometric, and constraint properties selected.

### **3.10 Software Specific Suggestions**

The following section outlines some of the considerations involved in adapting some widely distributed software to the analysis of unreinforced load-bearing masonry structures. In general, it is not cost-effective to undertake a non-linear analysis, and the difficulties of such an

analysis compromise the potential results. At the very least, it is critical to complete a linear analysis on any structure, for which a non-linear analysis is proposed, for comparison of results and to determine the need for conducting a non-linear analysis. Excessive tension in the linear model, excessive deflections in the linear model, excessive deflections in the prototype not explained by a linear model, or unexplained cracking in the prototype are all indications that a non-linear analysis may be warranted.

### **3.10.1 ANSYS**

ANSYS is a very large general-purpose finite element program and can be adapted to the solution of virtually any engineering problem. This adaptability makes it very difficult to use in conventional engineering analysis, as a very large number of basic decisions have to be made in the application of this program, including the element types, procedures for dealing with material and geometric non-linearity, modeling of geometric objects, and other issues. The specific application of ANSYS to three example structures is described in Sections 4, 5, and 6. In Sections 4 and 6, a much simpler model is developed using SAP for comparison.

### **3.10.2 SAP**

SAP 9.0 is essentially a frame analysis program, with additional shell and solid element capabilities. It is best suited to completing frame analysis of plane arches or vault ribs. Input of frame section properties is greatly facilitated by the user interface, and the output from this type of element is easily understood and can be displayed in stress or force units. For the analysis of more complex structures, diaphragm walls above arches, or vault webbing, can be entered as shell elements and, when analyzing entire vault systems, it is possible to enter surcharge as solid elements (an example of the analysis of such a structure is furnished in Chapter 4). The program has limited but useful capabilities for modeling non-linear behavior of materials, which can be incorporated into the analysis of masonry structures. Non-linear behavior is primarily entered through the use of link elements, which may be used to connect frame elements, and given non-linear properties. Another option is through the use of frame hinges, which are inserted into elastic frame elements. Support conditions may also be made non-linear, either through the use of link elements or through the use of tension-only or compression-only supports. The use of

non-linear material properties is generally limited to frame members. Such properties cannot be used in conjunction with shell elements. Particular attention should be paid when combining shell and frame members, if non-linear inputs are desired, as the shell elements will confine the attached frame elements and suppress non-linear behavior.

### **3.10.3 STAAD**

STAAD is a frame analysis program similar to SAP, but lacking most of the non-linear features of SAP. It is perfectly well suited to the development of linear solutions to problems in the assessment of load-bearing masonry. It has shell and solid elements available and a similar graphical interface for the development of structural models. STAAD includes support conditions and member formulations that resist compression-only, which can be useful in the analysis of unreinforced masonry. However, these are not material properties and can only be used at the member level of analysis. When a compression-only member is invoked, the member is neglected if it is in tension. This feature has limited application to masonry structures. The support conditions can be very useful at the supports for a pier or a buttress.

## **3.11 Validating a Model**

### **3.11.1 Validation by Dynamic Analysis**

Experimental modal analysis (EMA), a powerful interdisciplinary technique, is utilized to understand the dynamic behavior of a system. It will be used in this study as a validation method for analytical models of masonry domes. In modal analysis, by the use of response transducers and signal processing techniques, the structure can be described in terms of its dynamic characteristics, such as damping ratios, natural frequencies and mode shapes.

When a system is subjected to a time dependent force, its response will be dynamic. The dynamic behavior of the system shows differences from the static behavior since it invokes the effects of inertia and damping forces. The mass and stiffness are the main parameters to determine the natural frequencies and mode shapes of a structure. Consider a simple system of mass and spring loaded by a time dependent sinusoidal force with a constant magnitude. If the rate of oscillation of the force is swept in a frequency range, the frequency response function (FRF) graph displays an asymptotic behavior at both low and high frequencies. When forcing

frequency is much lower than the natural frequency, the system stiffness dominates the response. When excitation frequency draws near the natural frequency, the response of the structure displays a sharp maximum. At much higher excitation frequencies, the FRF is determined by the mass of the system.

A full knowledge of theoretical foundations of modal analysis and post-processing techniques is essential to obtain good quality data. Although the theory behind the experiments is of particular importance, it is available in various references (Ewins 2000, Hatch 2000, Maia et. al 1997). The emphasis of the following section is the practical aspects of modal testing particular to this study.

In this study the structures are excited with an impact hammer under controlled conditions, and the response of the vaults is captured by accelerometers directly mounted on the vault shell. With the help of data acquisition and signal processing devices, the data is analyzed, and natural frequencies and corresponding mode shapes are revealed.

The preliminary FE model of the vaults is then solved for model analysis in order to obtain the dynamic characteristics. The calibration of the FE model is done manually by comparisons of the natural frequencies, mode shapes and the sequence of mode shapes. The obtained mode shapes provide a basis for the possible boundary conditions. Iteratively the initial boundary conditions are modified until the overall agreement is achieved between experimental and analytical data.

As in most FE programs, the field solution in ANSYS is based on nodal displacement, and strains as well as stresses are calculated from this outcome. Therefore, the analyst should be aware of obtaining less accurate results for stress while displacement values are reasonably correct. Therefore the mesh should be further refined for regions where stress distribution is important. If a validation study will be held, it is recommended to start with an initially refined mesh to overcome the problems of transition from a dynamic FE model to a static FE model.

## 4 Case Study 1: Cathedral of Saint John the Divine; New York, NY

The architectural design and the construction of the Cathedral of St. John the Divine were progressed in four phases over the course of a century. The firm of Heins & Lafarge, which was contracted through a competition, created the Romanesque-Byzantine design of the cathedral. The original construction was initiated in 1892. Two years after the Guastavino Company built the main crossing dome in 1909, Heins & Lafarge, Cram, an architectural firm specializing in gothic architecture, was hired to complete the design. They modified the original design to an English Gothic style. In 1941, the 601-foot-long nave was completed and opened to public. However, construction had to stop due to World War II. It was not until the 1980's that work on the North and South Towers started to progress. As of today, the Cathedral of St. John the Divine is only two-thirds complete and is in service.

An assessment study was completed on the vaults of the Cathedral of St. John the Divine. The masonry vaults, which cover a square bay, are sexpartite rib vaults. In the Cathedral of St. John the Divine, there are four nave vaults in which the intersecting stone ribs are filled with Guastavino tile.



Figure 30: Nave Vaults of Cathedral of St. John the Divine

---

This study focuses on the third choir vault from the crossing dome. It begins with the development of the preliminary finite element model in ANSYS and is followed by experimental studies on the existing masonry vaults. This preliminary ANSYS model is tuned according to the experimental results. The validation of the model is done based on this dynamic analysis. Subsequently, the FE models of the vaults were created in the more widely-used SAP 9.0 software. The validated ANSYS model is then used as a base for the verification of the SAP 9.0 model. The SAP 9.0 model is validated based on the comparisons of the static behavior of the vaults estimated by SAP 9.0 with those of the validated ANSYS model.

#### **4.1 Building the FE model in ANSYS**

The preliminary physical model was created according to the construction dimensions from the architectural drawings. As the onsite measurements showed different values than the drawings, the FE model was modified according to the site survey.

The three-dimensional geometry of the groin-vaults is complex and composed of multiple arches. In ANSYS, an arc is defined with three nodal points. Hence, an AutoCAD drawing was developed to precisely obtain the coordinates of the nodes [Figure 31].

Although the decorations on the ribs are actually part of the structural behavior, it is prudent to simplify the complex formed moldings into rectangular cross-sections. The simplified geometry is selected such that the equivalent cross-sectional area and moments of inertia are almost identical.

The solid model is created by inputting the nodal coordinates and defining the connecting line elements. The web surface is defined with area while the ribs and surcharge volume is defined with volume.

The stone ribs are modeled with the brick element SOLID95. This element has 20 nodes including one mid-side node at each edge. Nodal degrees of freedom include translations only. Therefore, in order to obtain a reasonable approximation of the bending affects, the mesh is refined to have 16 elements ( $4 \times 4$ ) within the rib cross-section. The Guastavino tile webbing of the vaults falls under the definition of the ‘thin shell theory.’ The element SHELL93, which has an improved ability to fit curved surfaces, is utilized to represent the vault shell in the ANSYS



model. The irregularly shaped surcharge volume is defined with the tetrahedral solid element, SOLID92, which has 10 nodes and quadratic displacement behavior.

---

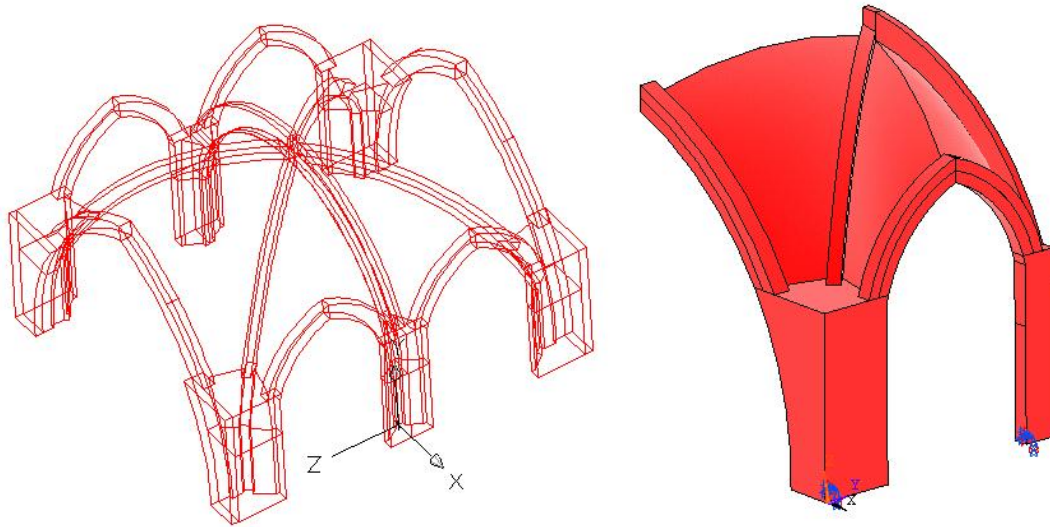


Figure 31: a) The AutoCAD drawing of the nave vaults b) the solid model in ANSYS

---

On completion of the element type selection, the solid model is meshed with the described elements. For this purpose, the automatic mesh generation feature of the ANSYS program is utilized. As discussed earlier, elements of approximately 20 cm give the best accuracy when modeling masonry stone buildings; hence, the mesh refinement is adjusted accordingly in this study.

As usual, in the Cathedral of St. John the Divine, the rib, webbing and surcharge intersections cause odd geometries, which require the use of degenerate elements. Previous studies have shown that the quadrilateral and triangular elements yield parallel results. The choice between the two depends on the quality of the elements they provide at these critical mesh points. In order to reach elements with reasonable aspect ratios, it might be necessary to repeat the meshing process several times.

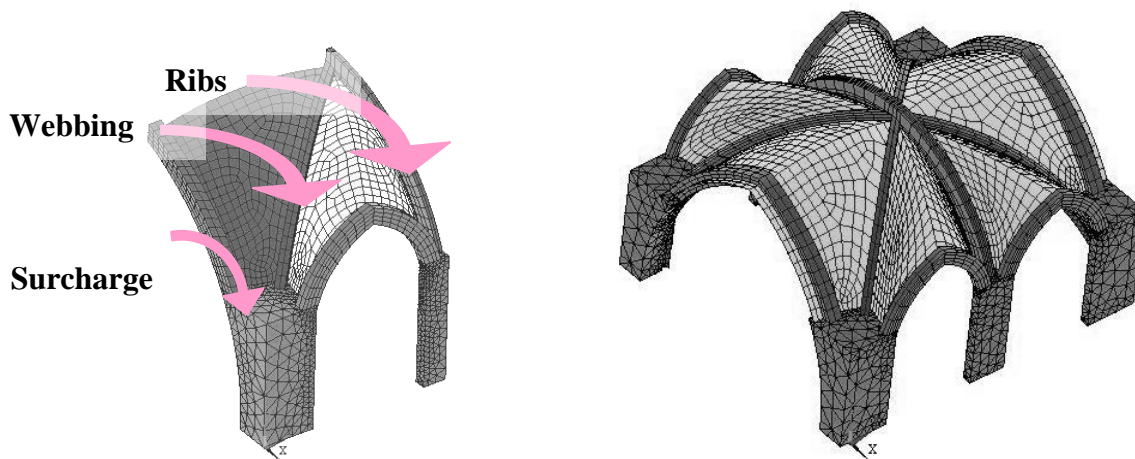


Figure 32: The quarter and full vault model of the Cathedral of St. John the Divine in ANSYS

The development of the preliminary ANSYS model begins with the quarter model, which is reflected to form the full vault as seen in Figure 32. This modeling approach ignores the construction imperfections and existing asymmetry in the physical dimensions. However, these imperfections are not influential to the results.

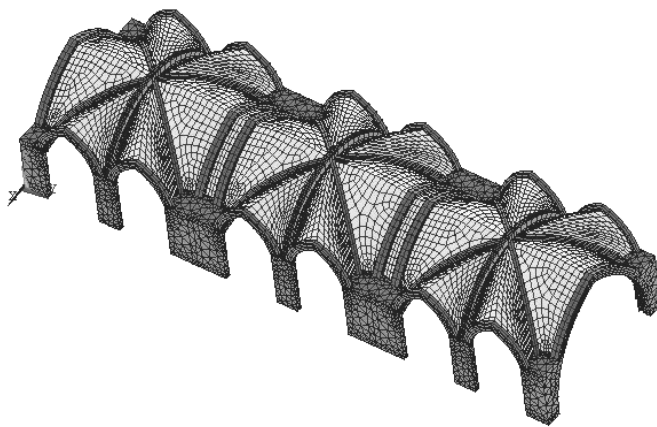


Figure 33: The three-vault model of the Cathedral of St. John the Divine in ANSYS

As discussed earlier, the entire system participating in the dynamic behavior needs to be created in the FE model. The techniques of experimental model analysis can be utilized to

determine the dynamic interaction between the important components of the system. Because the response of the vaults extends only to the neighboring bays, the accurate estimation of the dynamic properties of the vaults requires the inclusion of the two adjacent bays, as shown Figure 33.

The ANSYS model requires Young's modulus and density input entry for each material type. The material properties of the stone ribs, concrete surcharge and Guastavino tile webbing are found in literature. Table 6 presents the material properties assigned to the main components of the finite element model.

Creating an accurate representation of the boundary conditions is the most significant challenge in the modeling of masonry vaults in FEA. A set of initial boundary conditions, based on the previous experiences and an on-site condition survey, is assigned for the preliminary model. However, a calibration process is necessary to obtain better representation of the actual behavior of the system. The next section discusses the application of experimental modal analysis and the iterative tuning of the boundary conditions based on experimental data.

Table 6: Material Properties used in Vault Models

St. John the Divine		Vault Ribs	Vault Webbing	Surcharge
Density	kg/m <sup>3</sup>	2100	1500	2100
	lb/ft <sup>3</sup>	131	94	131
Young's Modulus	GPa	12	6.5	4.5
	k/in <sup>2</sup>	1740	942	652

## 4.2 Application of Experimental Modal Analysis

When testing on masonry vaults, developing a preliminary FE model is crucial to determining the fundamental mode shapes and the upper frequency range of interest. The excitation points and the accelerometer placement are determined to capture as many lower modes as possible. Based on the knowledge gained from the preliminary FE model, a testing plan involving seven accelerometers was developed. The accelerometer mounting points were placed to define the geometry of the vaults and leveled with wax at major points. The vault system was excited under controlled conditions by a Piezotronics Inc. PCB model 086D20 instrumented impulse hammer. The response of the structures, due to the impact, is captured by

model 393A03 accelerometers, manufactured by PCB Piezotronics, Inc., with a calibration value of approximately 1 V/g. The FFT based data acquisition and signal-processing system, SIGLAB, was utilized to plot the ratio of the system response to the excitation force in the frequency domain, also known as the frequency response function (FRF). The structure is excited at three different points, as illustrated in Figure 34. Figure 35 presents the driving point frequency response functions for point two and point three. As seen, the system response amplifies and attenuates at certain frequencies. Using manual and automatic techniques of system identification, several mode shapes have been detected after post-processing the experimental data.

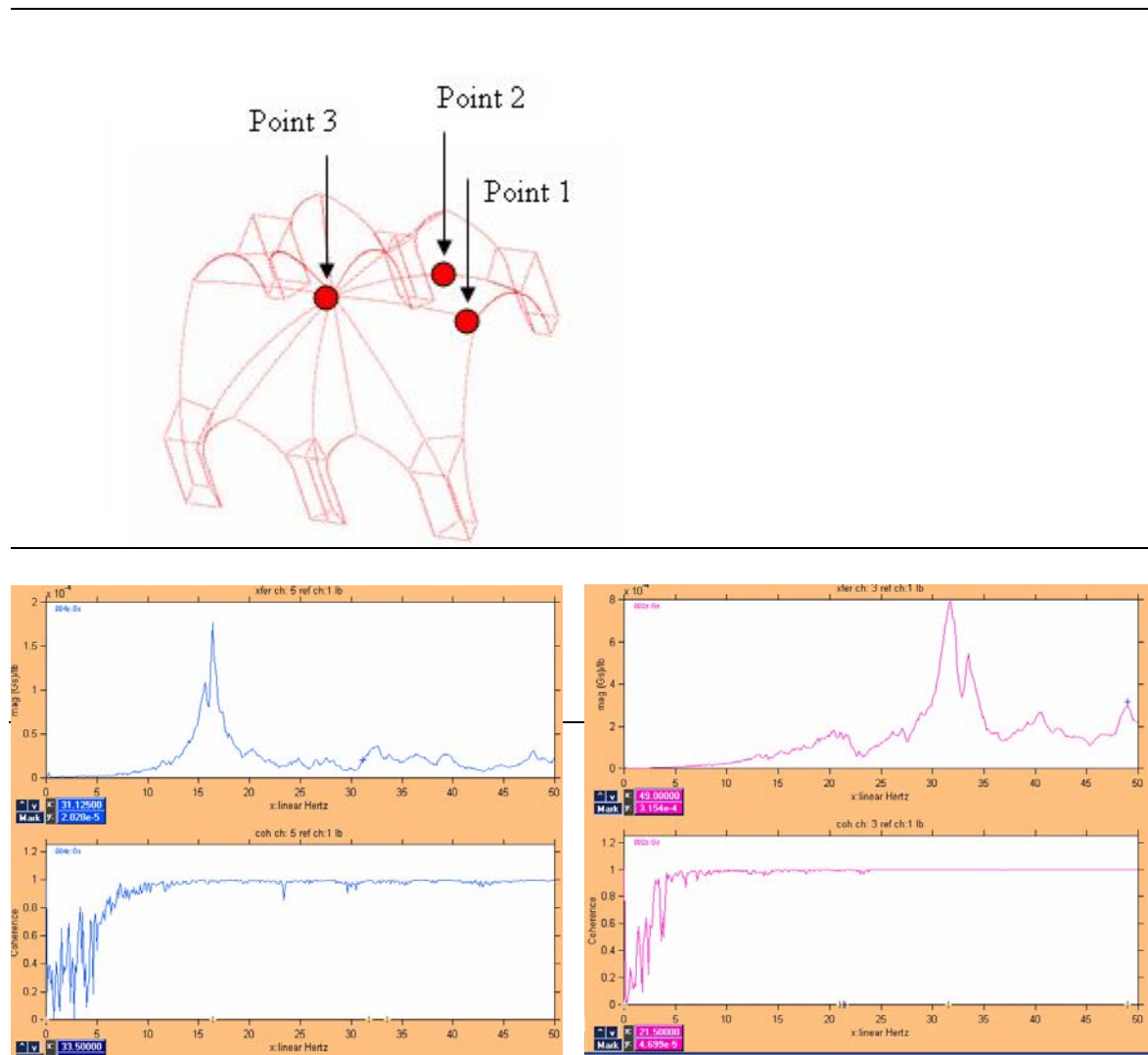


Figure 35: The FRF and coherence graphs at the driving point #2 and #3

### 4.3 Validation of ANSYS Model Based on Dynamic Analysis

Experimentally obtained mode shapes provide a basis for the initial set of boundary condition assumptions. The calibration of the boundary conditions of the preliminary FE model was completed according to the numerical comparison of natural frequencies and the visual comparison of mode shapes until an acceptable accuracy was reached. Along with the overall correlation of natural frequencies and mode shapes, an accurate match of the mode shape order is

---

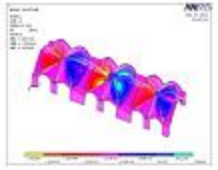
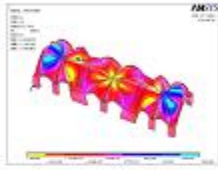
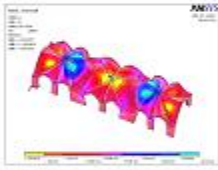
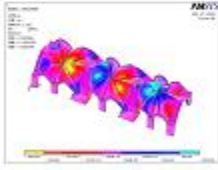
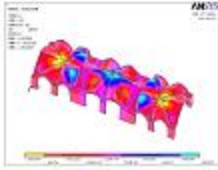
<b>Mode Shape</b>	<b>Experimental</b>	<b>Analytical</b>
	13.61 Hz	12.31 Hz
	15.84 Hz	15.71 Hz
	16.27 Hz	16.68 Hz
	17.70 Hz	17.13 Hz
	20.24 Hz	20.51 Hz

Figure 36: The comparison of the results obtained from experimental and analytical methods.

---

also an important factor for the validation.

The calibration process yields the final boundary conditions, which are presented in Figure 37. The base of the ribs and the surcharge volume are restrained in all directions to represent lower sections of the structural system, which are excluded from the model. Longitudinal and vertical restraints are assigned to the end arches to account for the effect of adjacent components. The vertical lines, as shown in Figure 37, are restrained in the transverse direction to replicate the contribution of buttresses, which can also be seen in the same figure.

---

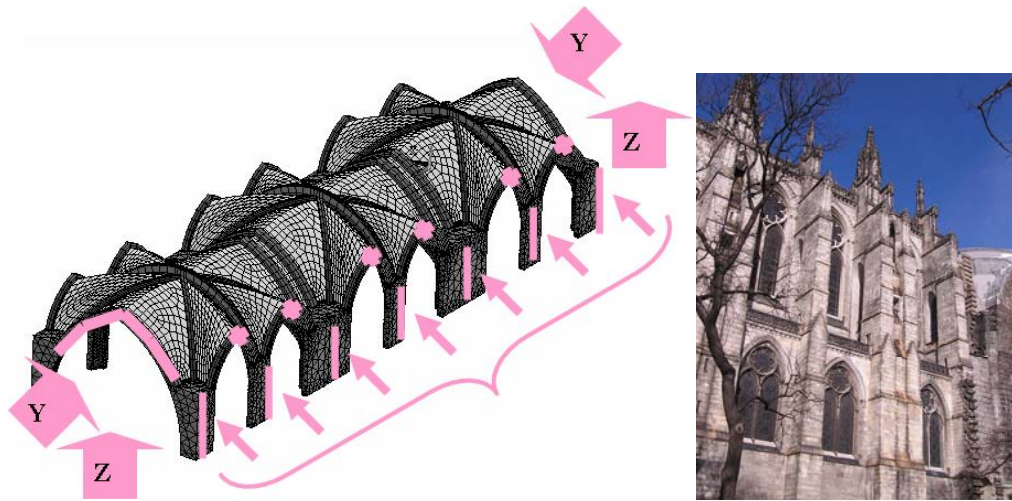


Figure 37: The final boundary conditions and the Nave of Cathedral of St. John the Divine, New York, NY, viewed from south

---

#### 4.4 Static Analysis with ANSYS Model

Once the three-vault FE model is validated, static analysis can be held on a single vault model to obtain the reaction forces, maximum stress formations, or displacements at desired locations. The transformation from a three-vault model built for dynamic analysis to a single-vault model used for static analysis is done by focusing on the intermediate vaults and providing the symmetry boundary conditions on the two edges. Since the planes of symmetry are vertical, it leads to in-plane displacements (translation at  $x$  and  $z$  axes) as well as the rotation about the axis normal to the symmetry plane (rotation about  $y$  axis). The developed single-vault model can then be used to obtain the reaction forces at supports, maximum stress formations, etc.

Furthermore, the sensitivity of the FE model to the main input entry is investigated. When a parameter is subjected to an insignificant variation and results in significant alteration in the outcomes, the FE model is then considered to be sensitive to that parameter. In these instances, the parameter needs to be determined with more accuracy.

The sensitivity analysis for variations on the material properties –mass and stiffness and Poisson’s ratio– is completed to investigate the level of required precision for the input entry.

Table 7,

Table 8 and Table 9 present the influence of 1%, 5% and 10% variation in the mass and stiffness values on the selected parameter, which is displayed in Figure 38.

Table 7: Sensitivity Analysis on Tile Mass Variation

VARIATION IN TILE MASS (Vault Webbing)					
Change in Parameter	Validated Single-vault Model	1% Variation		5% Variation	
Crown Displacement A (m)	-8.31E-04	-0.00083155	0.09%	-8.34E-04	0.44%
Horizontal Thrust at B (N)	-24672	-24701	0.12%	-24816	0.58%
Horizontal Thrust at C (N)	5291.9	5298.2	0.12%	5323.6	0.60%
Horizontal Thrust at D (N)	-24665	-24694	0.12%	-24809	0.58%
Vertical Reaction at center node (N)	224	224.18	0.08%	224.9	0.40%
Max Principal al Tensile Stress (Gpa)	5.55E+06	5.56E+07	-901.80%	5.58E+06	-0.54%

Table 8: Sensitivity Analysis on Tile Stiffness Variation

VARIATION IN TILE STIFFNESS (Vault Webbing)					
Change in Parameter	Validated S-vault Model	1% Variation		5% Variation	
Crown Displacement A (m)	-8.31E-04	-8.31E-04	0.01%	-8.30E-04	0.04%
Horizontal Thrust at B (N)	-24672	-24750	0.32%	-25055	1.55%
Horizontal Thrust at C (N)	5291.9	5298.8	0.13%	5326	0.64%
Horizontal Thrust at D (N)	-24665	-24744	0.32%	-25048	1.55%
Vertical Reaction at center node (N)	224	223.98	0.01%	223.9	0.04%
Max Principal Tensile Stress (pa)	5.55E+06	5.56E+06	-0.18%	5.57E+06	-0.36%

Table 9: Sensitivity Analysis on Poisson's Ratio Variation

VARIATION IN TILE Poisson's Ratio (Vault Webbing)					
Change in Parameter	Validated S-vault Model	10% Variation		25% Variation	
Crown Displacement A (m)	-8.31E-04	-8.31E-04	0.02%	-8.30E-04	0.04%
Horizontal Thrust at B (N)	-24672	-24588	0.34%	-24463	0.85%
Horizontal Thrust at C (N)	5291.9	5284.4	0.14%	5273.4	0.35%
Horizontal Thrust at D (N)	-24665	-24581	0.34%	-24456	0.85%
Vertical Reaction at center node (N)	224	224.02	-0.01%	224.06	-0.03%
Max Principal Tensile Stress (Pa)	5.55E+06	5.55E+06	0.00%	5.50E+06	0.90%



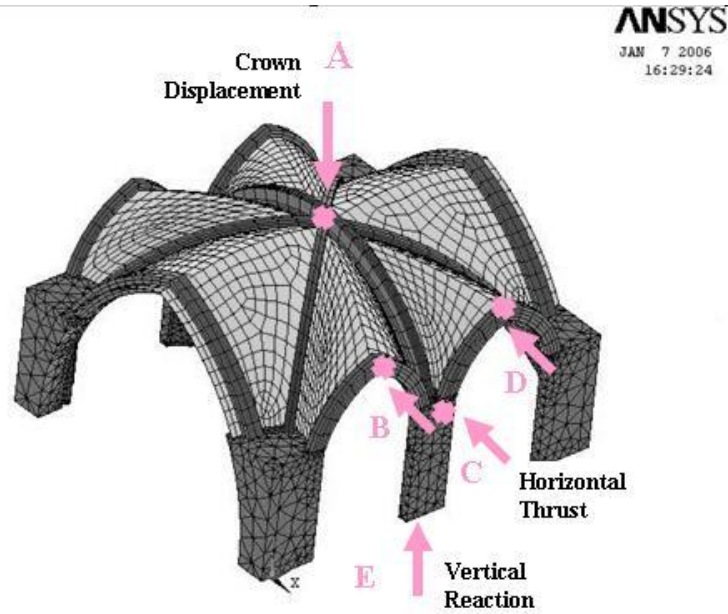


Figure 38: The quarter and full vault model of the Cathedral of St. John the Divine in ANSYS

In most cases, meshing and mesh refinement are dependent on the program mesh generator and the available maximum node number. The sensitivity of the static results to the mesh size and mesh refinement is investigated to determine the required optimum mesh size while modeling masonry vaults. Table 10 presents the change in outcome due to the refinement in the mesh size.

Table 10: Sensitivity Analysis on Mesh Refinement

VARIATION IN MESH REFINEMENT			
Change in Parameter	Validated S-vault Model	Size Refinement (webbing)	
Crown Displacement A (m)	-8.31E-04	-8.31E-04	-0.03%
Horizontal Thrust at B (N)	-24672	-24775	-0.42%
Horizontal Thrust at C (N)	5291.9	1918	63.76%
Horizontal Thrust at D (N)	-24665	-24763	-0.40%
Vertical Reaction at center node (N)	224	224.01	0.00%
Max Principle Tensile Stress (pa)	5.55E+06	5.56E+06	-0.18%

## **4.5 Building the FE Model in SAP 9.0 Nonlinear**

The previous work done on the masonry vaults of the Cathedral of St. John the Divine is used as a reference while modeling the vaults in the finite element software SAP 9.0 Nonlinear.

The solid modeling in SAP 9.0 requires further simplification of the physical geometry of the vault system. The three-dimensional simplified geometry is developed in AutoCAD. The intention in developing the AutoCAD drawing is to facilitate importing the model geometry into the SAP 9.0 software. It is also optional to develop the mesh in the AutoCAD drawing. This is preferable as it allows justification of the element sizes and aspect ratios by the analyst. Again, symmetry conditions are invoked, and the quarter model is copied multiple times to achieve the full model. Although this assumption overlooks possible construction imperfections, reasonable accuracy is still reached.

The vault ribs are best simplified as frame elements, using the general three-dimensional beam formulation including the effects of biaxial bending, torsion, axial deformation, and biaxial shear deformation. Frames are modeled in a straight line connecting two nodal joints. Since SAP 9.0 does not provide curved frame elements, the curved objects must be divided into multiple straight lines and represented by several frame elements. Each individual frame element can be assigned different section properties, which facilitates the representation of non-prismatic members. If necessary, non-prismatic cross-sections can also be defined within each element. Gravity, concentrated, distributed, strain, and temperature loads may be applied to the frame elements. The internal forces are calculated at member ends and at the user defined locations within the element.

The vault webbing is most accurately defined with three or four node shell elements, which combine membrane and plate bending behaviors. In SAP, translational in-plane stiffness and rotational stiffness normal to the plane surface define the membrane behavior, while out of plane rotational stiffness and translational stiffness normal to the plane surface define the plate bending. Each shell element can be defined as a pure membrane, pure plate or full shell. It is recommended to use full shell elements unless the entire structure is planar. SAP 9.0 evaluates the internal forces and stresses at Gauss integration points and extrapolates to the nodal points. Therefore two adjacent elements sharing a common joint usually display different results, which help in identifying the scale of approximation error and the desired mesh refinement.

The eight-node solid elements are utilized for the surcharge volume as presented in Figure 42. In SAP, the solid elements include optional compatible modes which significantly improve the bending behavior. Gravity, surface pressure, pore pressure and temperature loads are allowed for solid elements. Like shell elements, two-point Gaussian integration is adopted for solid elements, and the stresses are extrapolated from the Gauss points to the nodal joints. Again, the analyst can use the discrepancy between two solid elements sharing a common node as a means to define the approximation errors and the corresponding required mesh refinement.

For quadrilateral elements, the best results are obtained when all the corners are closest to 90°. When deformed shell elements are necessary because of the desired form, it is crucial to keep all the angles between 45° to 135°. The quadrilateral elements are not forced to be coplanar. Up to 30° twisting between the corners is accounted for by the SAP 9.0 software.

The three-node and four-node shell elements need to be arranged as two-dimensional surface elements in the .dxf file. The thickness variation within individual elements is not possible. However, if required, it is possible to provide different section properties for each element in the FE software. The continuity of the lines is again important; the 'merge' comment in SAP 9.0 might be helpful for small discontinuities. The consistency of units between SAP 9.0 and AutoCAD is crucial.

Perhaps the most critical aspect at this stage is the meshing of the vault webbing, since it is done manually. The quality of the meshing depends on the analyst's intuition. Providing an acceptable aspect ratio for each element is particularly important. SAP 9.0 allows both four-node and three-node elements. The ratio of the longest side to the shortest side in a triangular element is called aspect ratio. For a quadrilateral element, this ratio is the distance between the midpoints of opposite sides. Keeping the aspect ratio as close as possible to unity gives the most accurate results. For severe geometric conditions, the aspect ratio may be increased to four.

At this stage, the analyst must follow a particular procedure to import the AutoCAD model into SAP 9.0. The origin of the drawing is automatically imported as the origin of the FE model. Each of the elements –shells, solids, and nodes– need to be defined in separate layers in the drawing file. A layer can only be used for one element type. The link, beam and frame elements are defined as lines in the .dwg format. SAP 9.0 recognizes the three-dimensional faces

in .dwg format as shell elements and the three-dimensional solids and meshed polylines in .dwg format as solid brick elements.

---

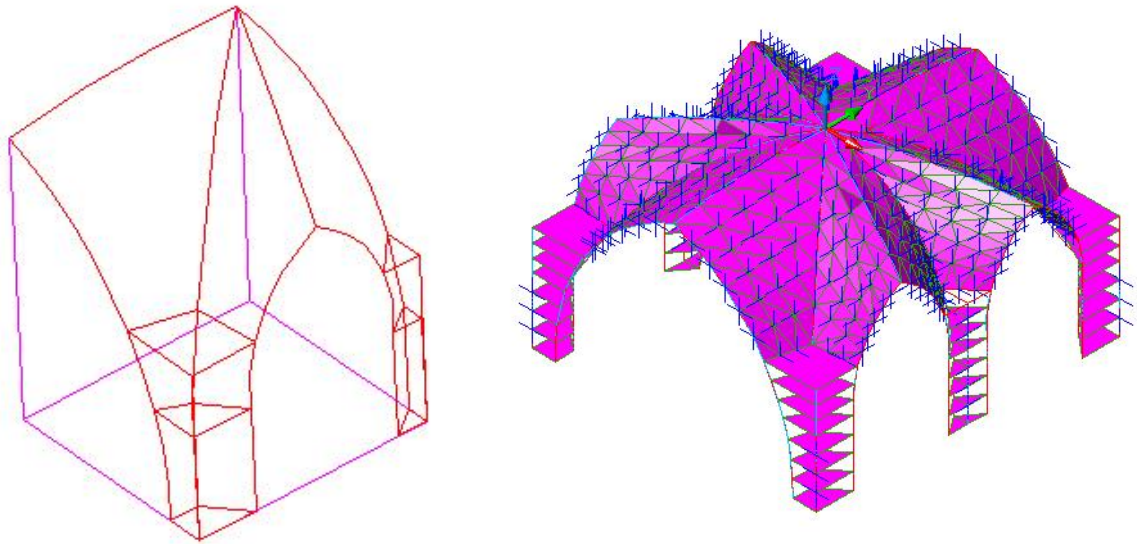


Figure 39: The simplified geometric models of the masonry vaults of the Cathedral of St. John the Divine in AutoCAD

---

The nodal points –if desired within the finite element program– need to be defined as individual ‘points’ with a separate layer in the AutoCAD drawing. It is necessary to convert the AutoCAD drawing (.dwg) into .dxf extension to be compatible with SAP 9.0 before importing. The procedure to import an AutoCAD file into SAP 9.0 is paraphrased from SAP 9.0 manual:

- 1** Start a new model or open an existing model. You cannot import a .dxf file if you do not have a model or coordinate system defined first.
- 2** From the File menu, click Import and then .dxf. This will display the Import .dxf File dialog box.
- 3** Choose the file from the list box and press the Open button.
- 4** From the Import Data dialog box select the Global Up direction of the dxf file elements being imported and the units that the file was drawn in.
- 5** Press the OK button in the Import Data dialog box to see the .dxf Import dialog.

- 6 Select from the dropdown list boxes the layer to import from the .dxf file for each SAP2000 element type. A layer can only be used for one element type.
- 7 If there is no data to be imported for a given element type, then the corresponding list box should read NONE.
- 8 Click the OK button to import the .dxf data.

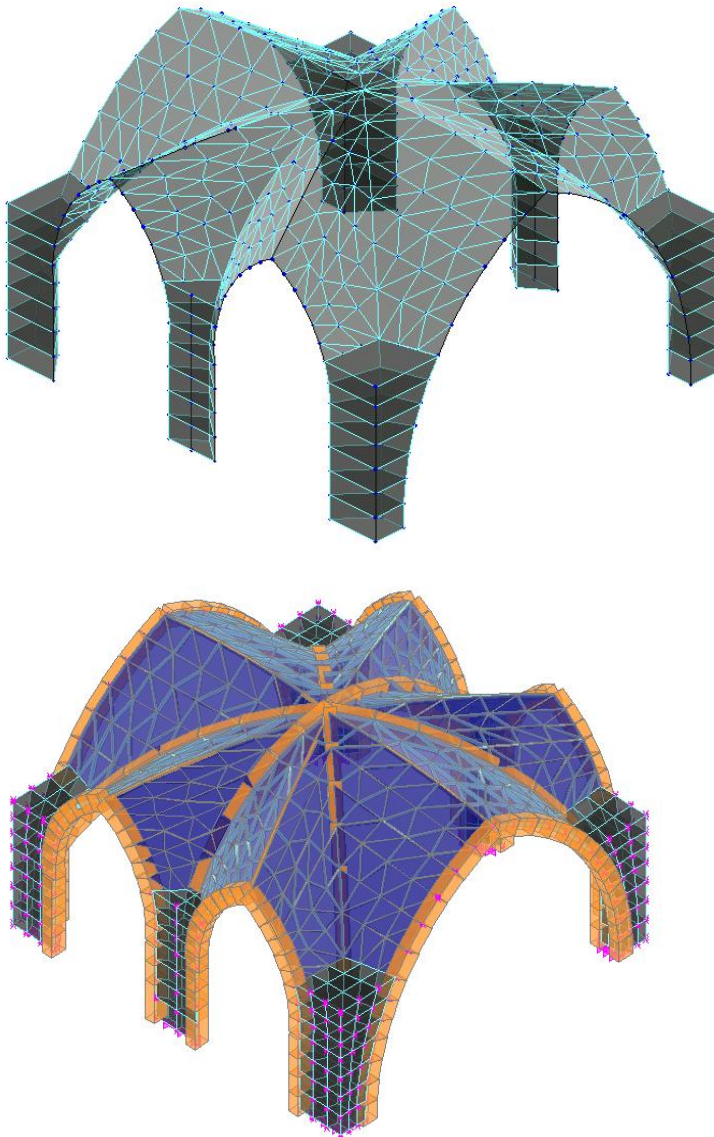


Figure 40: The SAP 9.0 model of the vaults of the Cathedral of St. John the Divine in AutoCAD

Once the meshed solid model is imported into SAP 9.0 [Figure 40], the modeling proceeds with the material property and the boundary condition definitions. SAP 9.0 allows for the assignment of different material properties to each individual element. For this, one must first define the necessary material types. Both isotropic and orthotropic material behavior can be assigned. Unit mass, Young's modulus and Poisson's ratio entries are necessary while defining a material type. For thermal analysis, the thermal coefficient of the material is also required. At this stage, material damping properties or the non-linear stress-strain relationship can be invoked as well.

The boundary conditions can be defined as displacement restraints at joints. The definition of boundary conditions can be to restrict/allow translation and/or rotation. For intermediate cases where the physical configuration of the material creates a certain amount of restriction in movement, translational or rotational spring elements can be defined.

The material properties and boundary conditions of the validated ANSYS model are adapted into the SAP 9.0 model, which is then solved for the static state of the vaults. The next section presents the results obtained through the SAP 9.0 static analysis and compares them with those of the ANSYS model.

#### **4.6 Validation of SAP 9.0 Model Based on Static Analysis**

Through solving a static analysis under gravity loading, the reaction forces at the locations illustrated in Figure 38 are obtained. As seen in Table 11, the results of SAP 9.0 and ANSYS models revealed similar reaction solutions.

Table 11: The Comparison of Reaction Forces for SAP 9.0 and ANSYS

Reaction Forces	Validated ANSYS-vault Model	SAP
Change in Parameter		
Horizontal Thrust at B (N)	-24672	-26230
Horizontal Thrust at C (N)	5291.9	7890
Horizontal Thrust at D (N)	-24665	-26230

## 5 Case Study 2: National Cathedral; Washington, DC

### 5.1 General Information on ANSYS Model

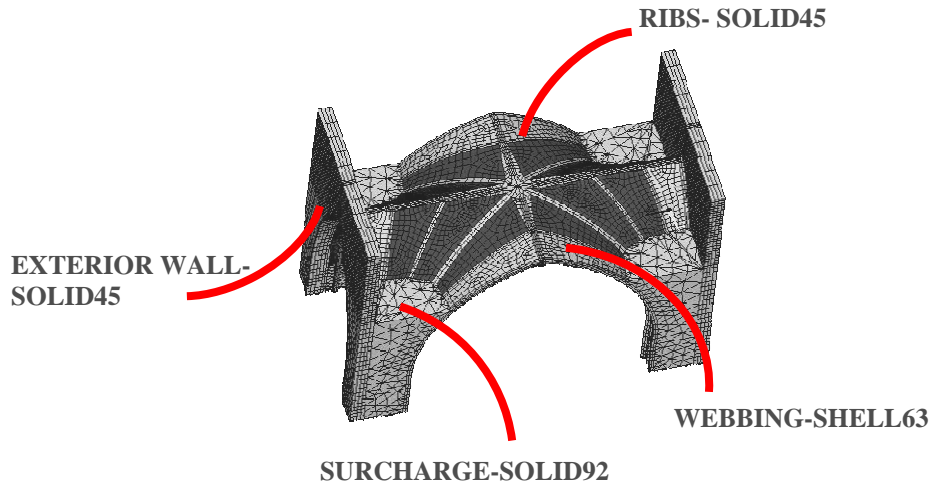


Figure 41: Full-vault model of National Cathedral Choir Bay

A study of the choir vaults of the National Cathedral (NC) was undertaken by Erdogmus (2004). In this study, the third choir vault, counted from the crossing, is modeled, and validation experiments are conducted mainly on this vault. Several models are created for this vaulting system. First, a quarter-vault model is created. Then, by using the “reflect” command in ANSYS, the half and full vaults are generated. Finally, the exterior walls are added, and the full-vault model with walls is achieved (Figure 41). The portion of the structure modeled must be compatible with the portion of the structure active during the experiment and the necessary variables must be selected carefully for a sensible model validation. Although the focus was on the third bay during the experiments, the sensors were located in an area covering three bays. Therefore, the full vault model (with the exterior walls) is tripled, and a three-vault model is created (Figure 42).

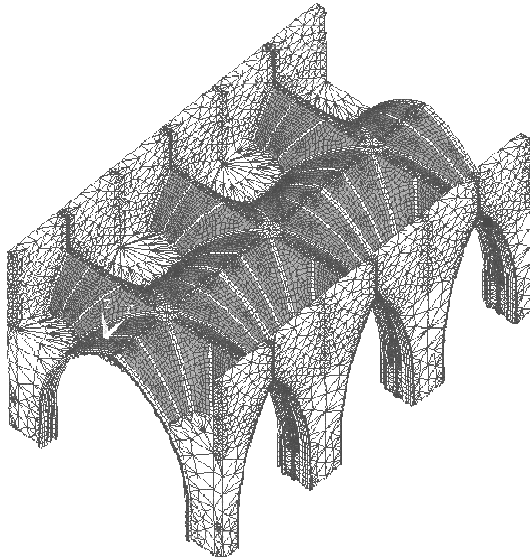


Figure 42: Three-vault model of the NC choir vaults

## 5.2 Boundary Conditions

The boundary conditions depend on how much of the structure is modeled and what kind of an analysis is conducted. For all the NC vault models, the bottom of the pier and the surcharge are restrained in all directions to account for the parts of the structure below that point. For model validation using experiments, the parts of the structure active in the experiments must be included in the model. In the case of the NC, the experiments cover three bays, and there is active response from all the sensors covering the three bays. Therefore, a finite element model with three vaults is created. As the model validation procedure is developed on the NC, a single vault model is also analyzed dynamically to understand the relationship between the three-vault model and the single-vault model. When isolating one or three bays of a multiple bay structure, boundary conditions applied at these edges must reflect the actual behavior with the adjacent bays. This can be done by using the pre-set symmetry boundary conditions. As the planes at the edge of the modeled area are vertical, the symmetry boundary conditions allow only translation in the plane of symmetry and rotations about the axis normal to the plane of symmetry. Another possibility for simulating the boundary conditions at these edges is by adding specific nodal constraints. Accurate representation of the boundary conditions is uncertain at best in finite element modeling, and in this study, a few initial boundary condition assumptions based on the



drawings and in situ observations are made. One example of such initially proposed boundary conditions for a three-vault model is shown in Figure 43. Then, these initial boundary conditions are updated according to the validation by the experimental results.

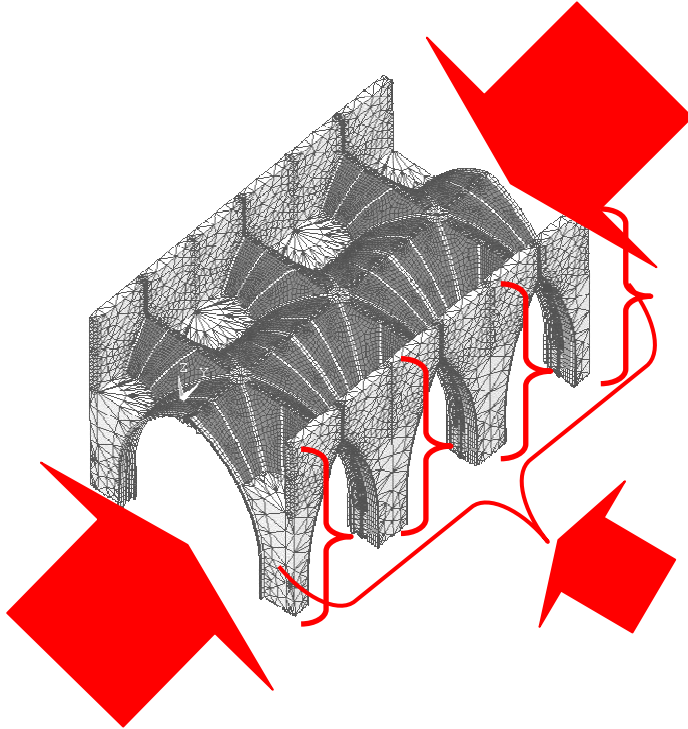


Figure 43: Initially Assumed Boundary Condition Set-1 for the NC. Instead of symmetry boundary conditions, horizontal restraints due to the adjacent bays are applied on all the side edge nodes

### 5.3 Material Properties

The vaults at the NC are known to be made of Indiana limestone, the material properties of which are published as listed in Table 12 (<http://www.langstone.com/indiana.htm>), and the surcharge is concrete. A sample of the stone used in the vaults was available for laboratory testing. This sample was tested in order to accurately determine the Modulus of Elasticity, Poisson's ratio and the density of the material. The results of the laboratory tests are given in Table 13.

Table 12: Material Properties for Analysis of National Cathedral Vault

<b>Material Property</b>	<i>Modulus of Elasticity (E)</i> (MPa)	<i>Density (d)</i> (2300 kg/m <sup>3</sup> )
<b>Indiana limestone</b>	22,750 – 37,250	2300
<b>Concrete Surcharge</b>	24,000	2100

Table 13: Test Results: Stone Used in National Cathedral Construction

<b>Indiana Limestone Stone Sample Properties</b>	<i>Modulus of Elasticity (E)</i> (MPa)	<b>Poisson's Ratio</b>	<b>Density ( kg/m<sup>3</sup>)</b>
	31,000	0.23	2100

Since the material stiffness entered to the finite element analysis program is for the mortar-masonry assembly rather than the stone alone, an effective stiffness is calculated according to the following equation

$$E_{eff} = \left( \frac{(l_m / l)}{E_m} + \frac{(l_u / l)}{E_u} \right)^{-1}$$

where  $E_{eff}$  is the effective stiffness of the stone mortar assembly

$l_m$  is the length of the mortar joint, which is reported as varied between ¼ inch to 3/8 inch;

$l$  is the total length of the stone units and the mortar joints;

$E_m$  is the modulus of elasticity of the mortar alone. Type O mortar value ranging between 0.31-1.4 GPa (McNary & Abrams, 1985);

$l_u$  is the length of the stone unit;

$E_u$  is the modulus of elasticity of the stone unit alone. The value of 31,000 MPa obtained from the laboratory tests are use.

Depending on the stiffness of the mortar and the thickness of the mortar joint, the effective stiffness of the assembly varies. Table 14 summarizes the possible modulus of elasticity ranges for masonry assembly with type O mortar and Indiana limestone. The mortar joint thicknesses vary between 10 mm and 6 mm (3/8" - 1/4").

Table 14: Assembly Material Properties

<i>Mortar (E in GPa)</i>		<i>Joint Thickness mm- (in)</i>	<i>Masonry (E in GPa)</i>	<i>E<sub>eff</sub> (GPa)</i>
<i>Max</i>	<i>1.4</i>	<i>6 (1/4)</i>	<i>31</i>	<i>21</i>
	<i>1.4</i>	<i>10 (3/8)</i>	<i>31</i>	<i>18</i>
<i>Average</i>	<i>0.85</i>	<i>6 (1/4)</i>	<i>31</i>	<i>18</i>
	<i>0.85</i>	<i>10 (3/8)</i>	<i>31</i>	<i>15</i>
<i>Min</i>	<i>0.31</i>	<i>6 (1/4)</i>	<i>31</i>	<i>10</i>
	<i>0.31</i>	<i>10 (3/8)</i>	<i>31</i>	<i>8</i>

According to the information given in Table 14, the modulus of elasticity for the masonry-mortar assembly for the finite element model ranges between 8 GPa and 21 GPa, depending on the condition and thickness of the mortar joints. When the model is updated according to the correlation of the experimental results and the modal analysis results, the most probable value for the masonry assembly stiffness will be found.

## 5.4 Model Validation

The vault models at the NC were validated by experimental modal analysis. The dynamic experiments performed on the choir vaults of the NC are explained, and the results are presented in this section. Seven accelerometers are used in these experiments with two main configurations as shown in Figure 44 and Figure 45. The principal setups are a longitudinal arrangement covering multiple bays (column) and an arrangement where the sensors are on the transverse rib passing through the crown of the third bay in the choir, counted from the crossing (row). In both setups, point A is the driving point (i.e. the point where the excitation occurs), and this point corresponds to the intersection of the fourth column and the fourth row.

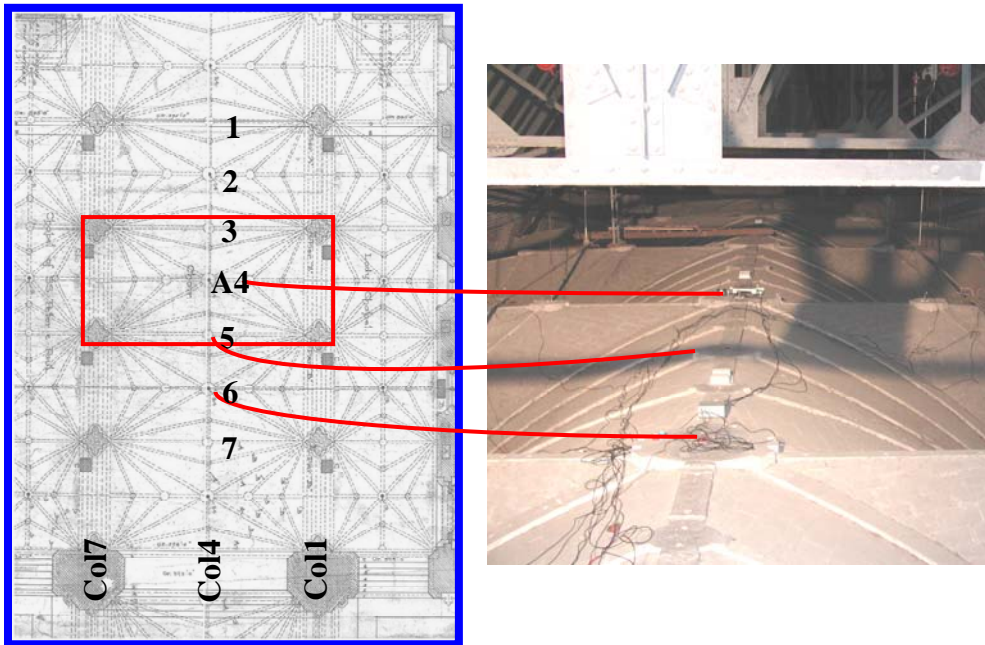


Figure 44: Experimental Setup Column above the National Cathedral Vaults  
The photo on the right shows the actual locations noted on the partial floor plan  
The impact was applied at point 4.

The setups, shown in Figure 44 and Figure 45, enable the collection of data for the determination of an approximate deformed shape for the top horizontal ribs. Additional points to collect acceleration data improve the definition of the deflected shape at the observed mode. However, the curved surfaces on the structure make sensor placement at other points difficult. Therefore, the accelerometer locations, which form a grid of data points, are limited to the flat surfaces of the bosses which exist at the intersection of the ribs.

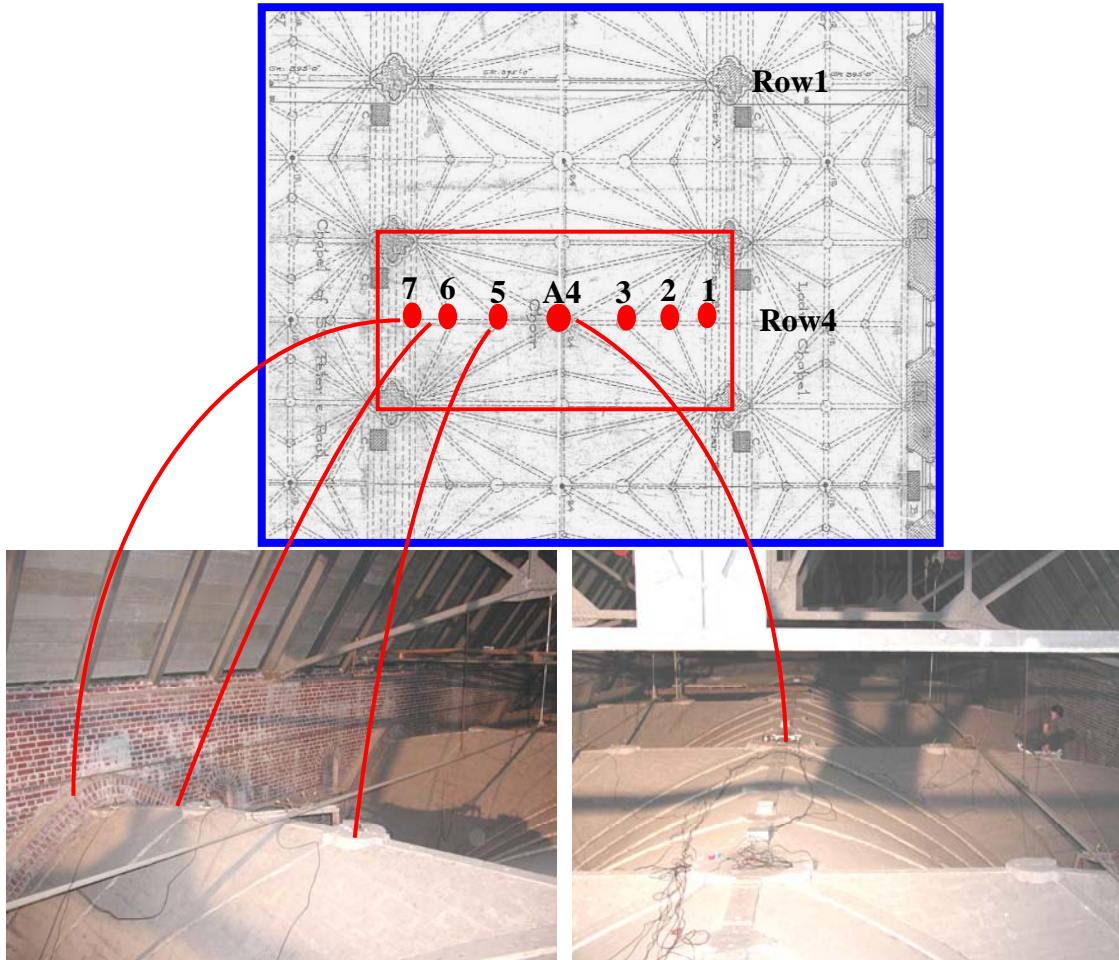


Figure 45: Experimental Setup Row above the National Cathedral Vaults.

Two primary means of applying the excitation are used in these experiments: heel drops on a force plate and impulse hammer. The results of some of these experiments are presented here and are used in the parameter extraction. All excitations are performed on force plates, and the FRF is collected in each case. Figure 46 illustrates the FRF from the heel drops performed on point A4 while the accelerometers are arranged in the column setup. This plot illustrates the response of all the accelerometers in this setup.

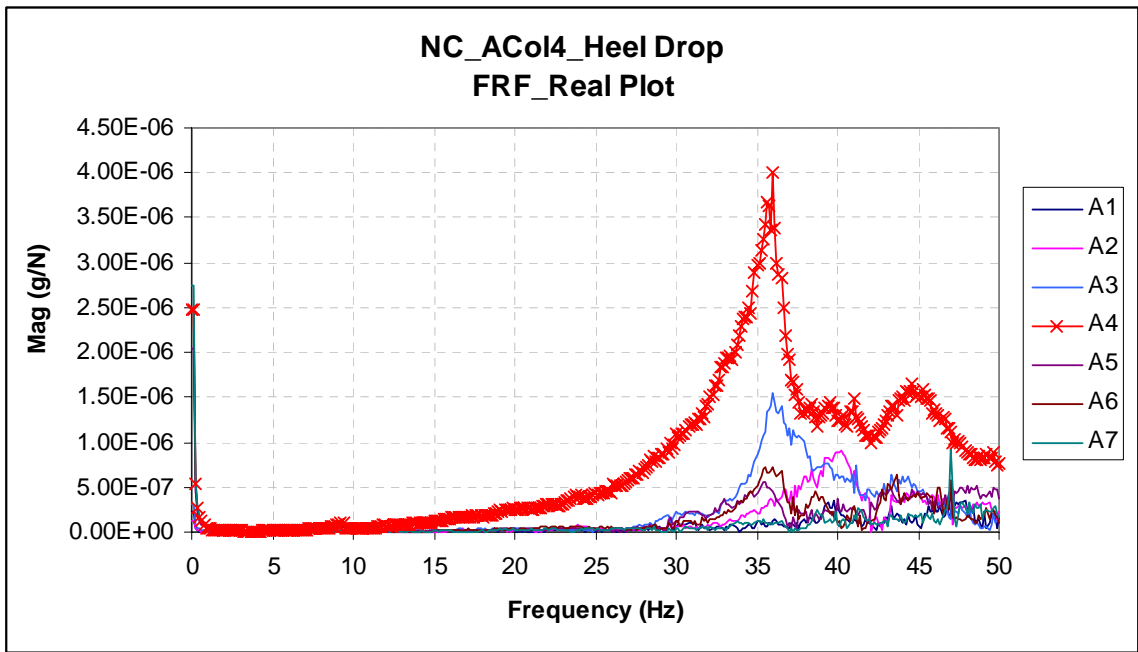


Figure 46: National Cathedral FRF plot for all the accelerometers in Column Setup

There is a dominant resonant peak at approximately 36 Hz, according to the response of almost all the accelerometers. Moreover, the natural frequency for the observed mode can be gathered from the phase plot, since at this frequency there must be a phase shift of  $90^\circ$ . Figure 47 presents the phase plot for accelerometer 4, which is located immediately adjacent to the driving point. The phase angle of  $-90^\circ$  around 36 Hz shows that there is a natural frequency at this point. Figure 48 shows the FRF and the coherence (COH) plots for accelerometer 4 only, and the COH close to unity around the resonant frequency of 36 Hz demonstrate that the data are consistent and reliable.

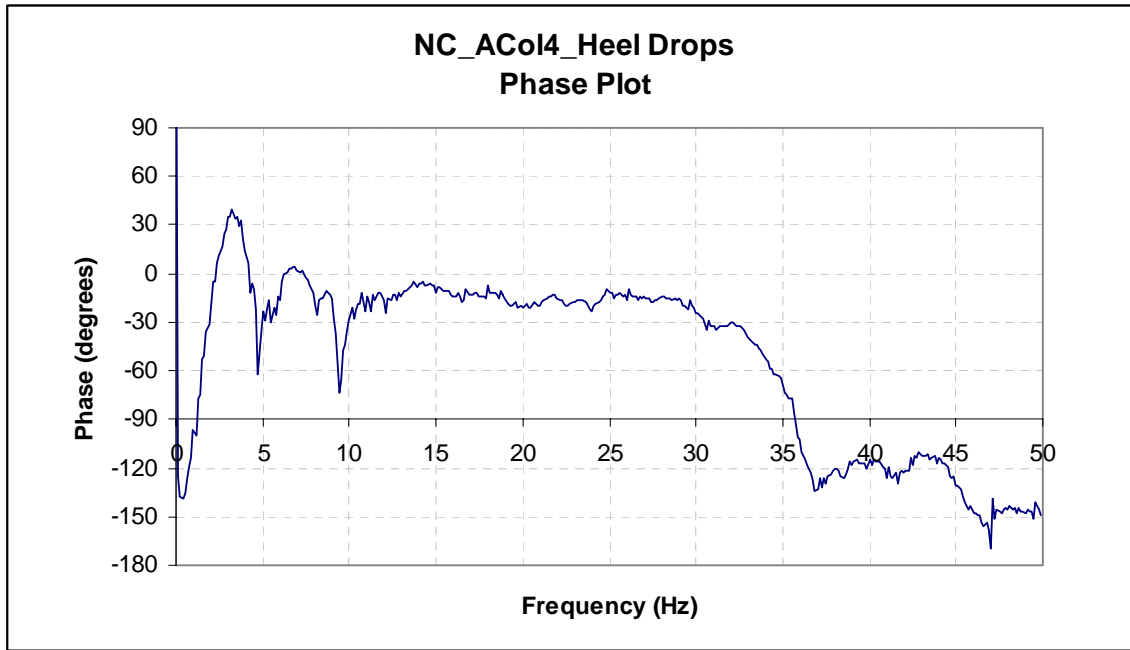


Figure 47: Phase Plot for Accelerometer 4 on Column Setup - Heel Drop at Point A

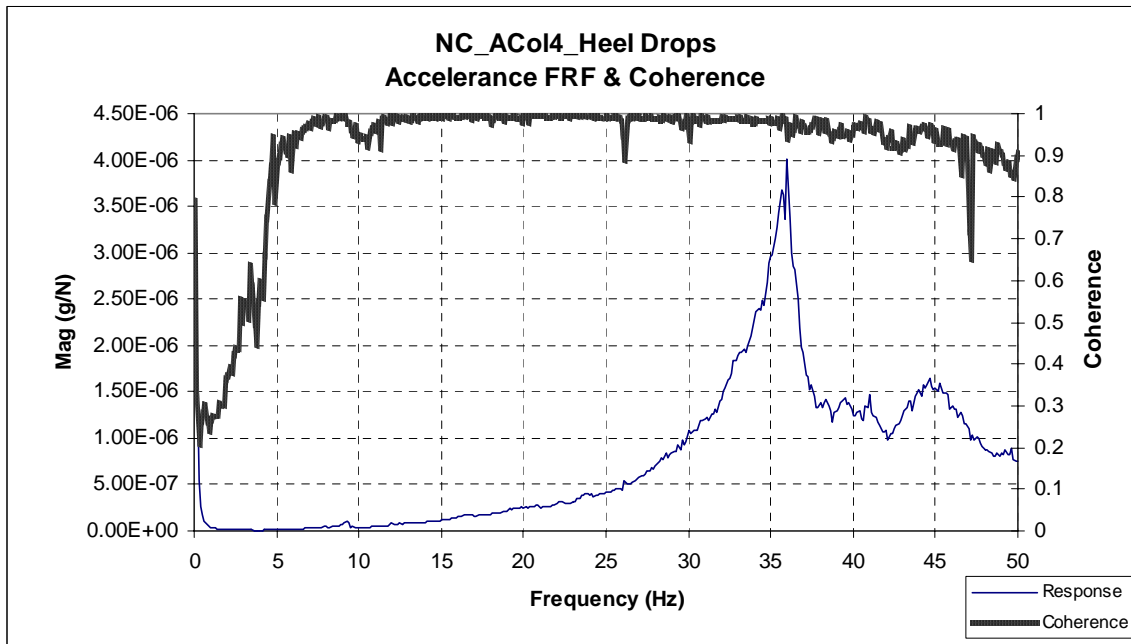


Figure 48: Accelerance FRF and Coherence Plots for Accelerometer 4 on Column Setup-Heel Drop at Point A

Next, the deformed shape for this mode is determined. The previous plots of the FRF present the magnitude of the FRF in absolute value. The imaginary plot of the FRF, which includes the sense of the acceleration, reveals information about the deformed shape of the structure. Figure 49 illustrates the imaginary plot for the experiment discussed above.

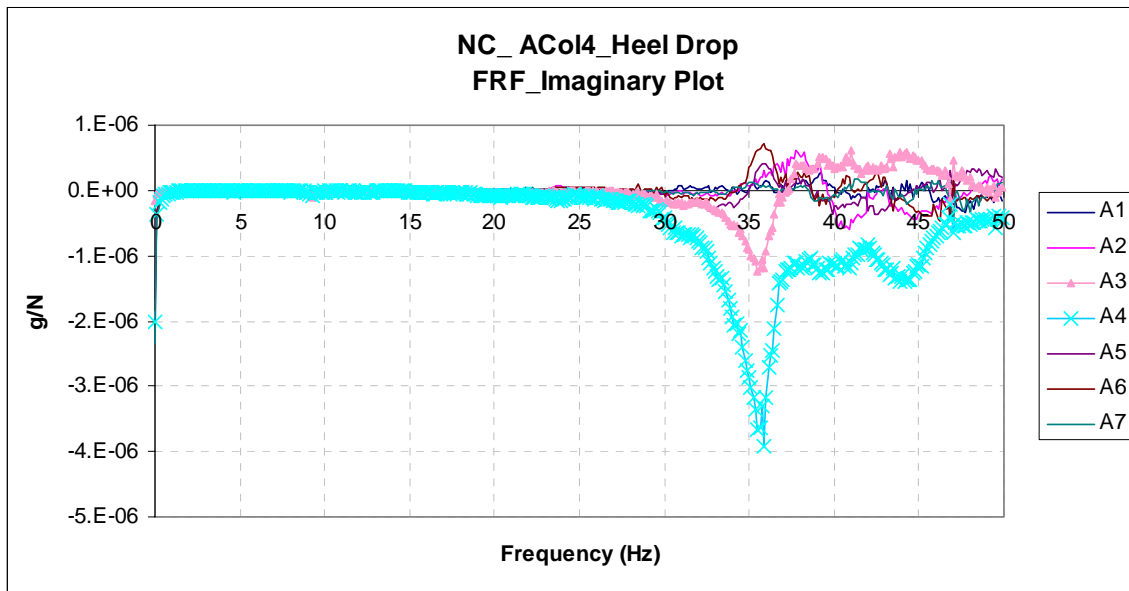


Figure 49: Imaginary Plot for the FRF for Column Heel Drop Excitation

When a similar plot is assembled for a “Row” setup for excitation at the same point, then the mode shape for the top ribs is established. Using the column setup above, combined with similar data from the row setup, a schematic deformed shape for the top ribs is shown in

Figure 50. Consequently, a mode shape, with similar behavior on these top ribs with a natural frequency around 36 Hz, is the target for the analytical model analysis results.



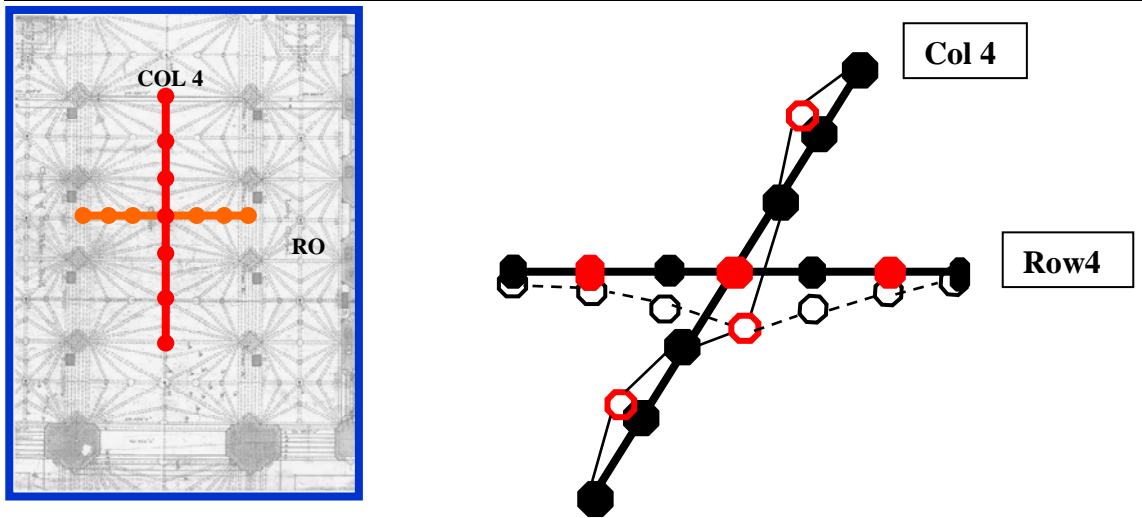
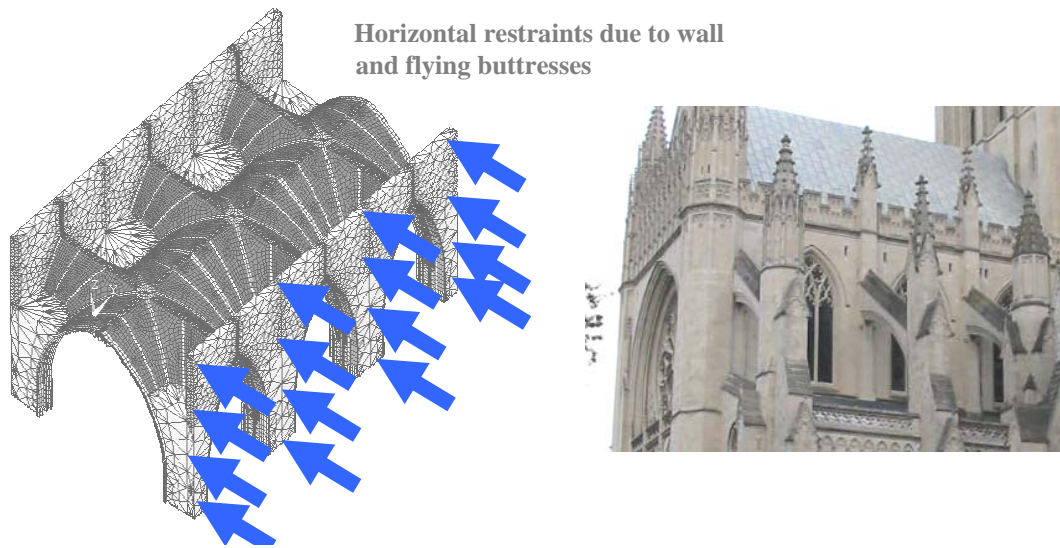
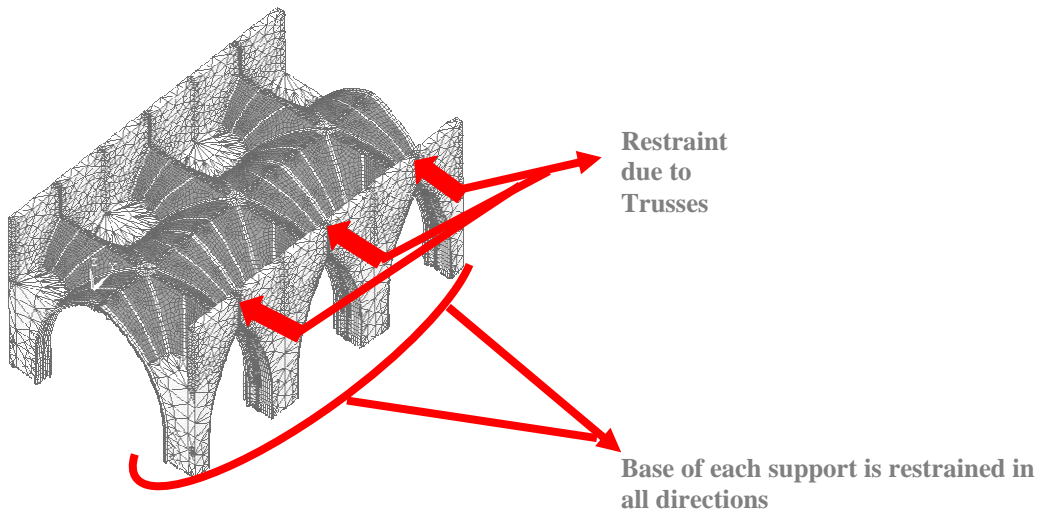


Figure 50: Schematic for the deformed shape of the top ribs in the NC

The model analysis results, for these two different boundary conditions, suggest that the symmetry boundary condition at the outer edges do not yield the experimentally observed mode shape. Thus, the best boundary condition set is the second set with the addition of some vertical restraints along the transverse arch at the edges, to account for the partial vertical movement limiting effects due to the adjacent vault. Once the model updating is concluded, the boundary conditions in Figure 51 and the material properties in Table 15 result in the natural frequencies in Table 16 for the first ten modes of vibration.

Table 15: Final Material Properties for National Cathedral Finite Element Model

	<b>Modulus of Elasticity (GPa)</b>	<b>Poisson's Ratio</b>	<b>Density (kg/m<sup>3</sup>)</b>
<b>Masonry Assembly</b>	12	0.2	2100
<b>Concrete Surcharge</b>	24	0.15	2100



Vertical restraint at the crown of the outer transverse arches for the motion limitations due to adjacent vaults

Figure 51: Final Boundary Conditions for the NC Triple-Vault Model

Table 16: Natural frequencies for the NC three-vault model

Mode #	1	2	3	4	5	6	7	8	9	10
Freq (Hz)	28.9	29.1	29.2	33.1	35.5	36.9	37.4	38.9	39.7	40.2

The first mode with significant vertical movement at the points where the sensors are located (Setup 1 and 2) is mode 5, with a natural frequency of 35.5 Hz. Figure 52 demonstrates the deformed shape for this mode on the full model and for top ribs only. This analytical mode shape agrees with the experimentally observed mode shape demonstrated in Figure 50.

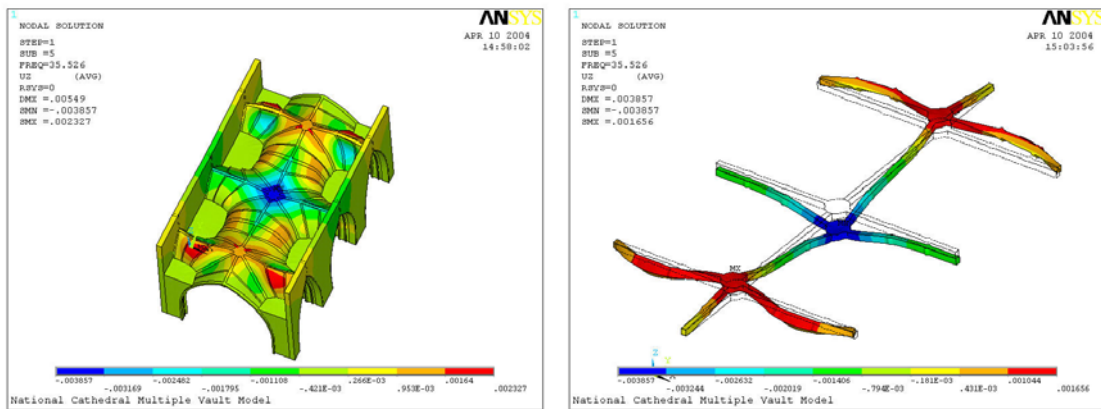


Figure 52: The NC Triple Vault Model: UZ displacements plot- Mode 5 Entire model (left) and only top beams (right)

As a result, with the selected boundary conditions and the material properties, the analytically observed deformed shape is in excellent agreement with the experimental results.

## 5.5 Building the FE Model in SAP 9.0 Nonlinear

The finite element of the choir vault of National Cathedral is accomplished as described previously in Section 4.5. The AutoCAD drawings are built based on the available construction drawings and onsite measurements (Figure 53).

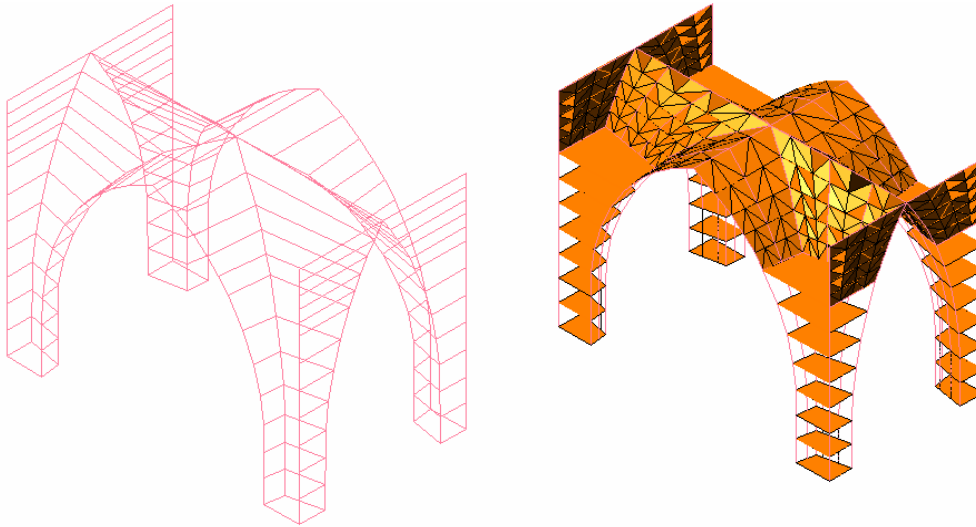


Figure 53: The AutoCAD drawings of National Cathedral.

The stone rib elements are modeled with frame elements while the concrete surcharge volume is represented with solid brick elements. The vault webbing is meshed with triangular elements, which are recognized as thin shell elements in SAP program. The dxf file is imported into SAP 9.0. The boundary condition and material property input is adopted from the validated ANSYS model (Figure 54).

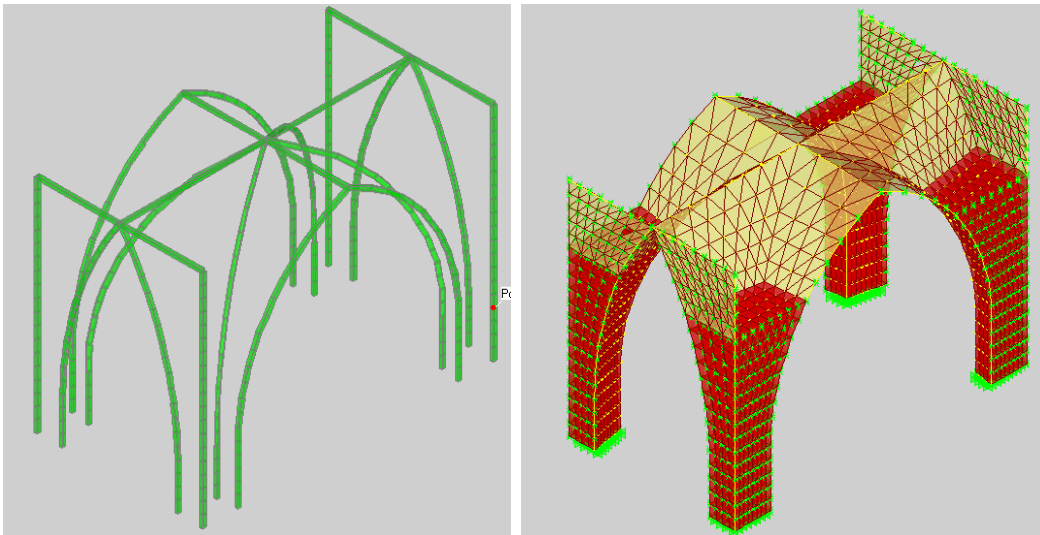


Figure 54: The SAP model of a single choir vault.

Once the modeling is complete, the finite element model is used to obtain information on the stress distribution within the vault. Illustrates the mean stress resultant on the vault web.

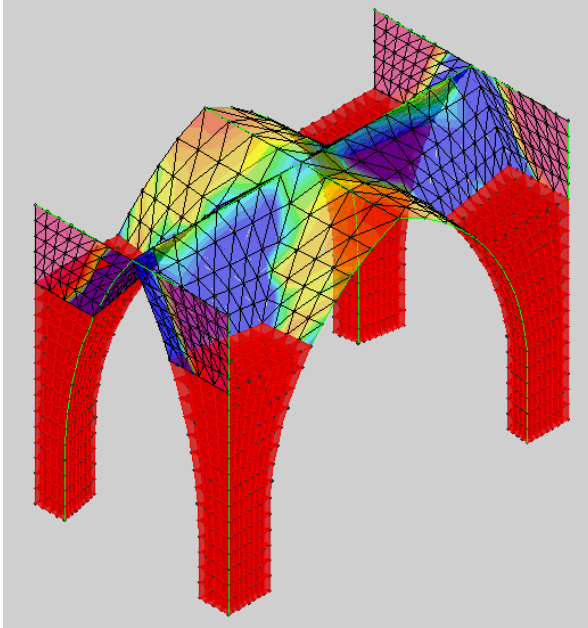


Figure 55: Solution of SAP model for stress resultant.

## 6 Case Study 3: State Education Building; Albany, NY

The structural system of study in the State Education Building is arranged with twelve side-by-side domes filling a three by four grid. This arrangement creates a repetitive circular system reminiscent of Labrouste's Bibliothèque Nationale in Paris. In the SEB, slender iron columns support the repeated system of Guastavino tile domes of 6.7 m radius. The transformation from a circular plan to a square bay is accomplished by means of pendentives and slender ribbed arches. Each dome is configured from a segment of a sphere over a square plan form supported by pendentives. This study focuses on a center dome, which is symmetrically surrounded by nine identical domes at his peripheries.



Figure 56: The view of rib and dome construction.

Initial observations inside the attic space reveal that the unreinforced masonry domes are not load bearing. The steel trusses, which touch the dome shell periphery every 45°, carry the upper floor loads to the columns. At these contact locations, small tile blocks of 40 cm by 150 cm plan dimension connect the steel frame to the dome shell. These buttresses introduce restraint to the dome structures.

## 6.1 Building the FE model in ANSYS



Figure 57: View of the back of the domes.

For the SEB, the architectural drawings of the masonry assembly are available to determine the physical dimensions of the dome. Survey data obtained during the site visit are also used to verify the geometric accuracy of the model. Ignoring construction imperfections, an exact spherical segmental dome is modeled in ANSYS.

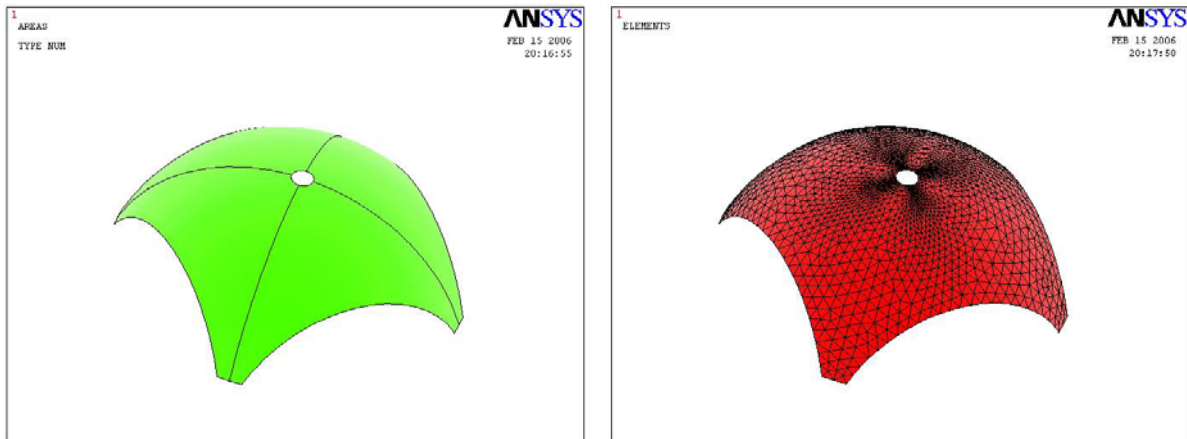


Figure 58: FEM model of the single dome.

There are, however no specifications of the webbing thickness on the available drawings. Further studies based on the impact-echo technique (Sansalone 1997) to non-destructively determine the shell thickness reveal a thickness of 13.5 cm, and this value is approximated as a uniform and constant quantity in the FE solid model.

Since the arches and ribs are slender, the interaction between the side-by-side domes under dynamic loading is not clear. Moreover the complex composition of the different structural members -steel trusses, tile domes, tile buttresses, and rubble-stone surcharge—presents challenges for the assessment of the dynamic characteristics of the system. The structure of interest was subject to dynamic testing in order to identify the integration of structural members with the center tile dome, which is selected to be the focus of the study (see Section 6.2). The steel truss members do not exhibit a noticeable dynamic contribution in the frequency range of interest. Adjacent domes are similarly found to be structurally independent, based on the experimental data.

It is considered that the volume and material of the surcharge have a limited effect on the dome behavior, and thus the surcharge volume is excluded from the solid model. In this formulation, the analysis of the whole vault system is reduced to a single dome model, which is

determined adequate for the FE calibration and validation procedure. Consequently, the influence of the adjacent structural members—surcharge, steel frame, buttresses, adjacent domes—is represented by boundary condition definitions. The experimental procedure, describe in following sections, is utilized to reduce the uncertainties in the boundary condition definitions.

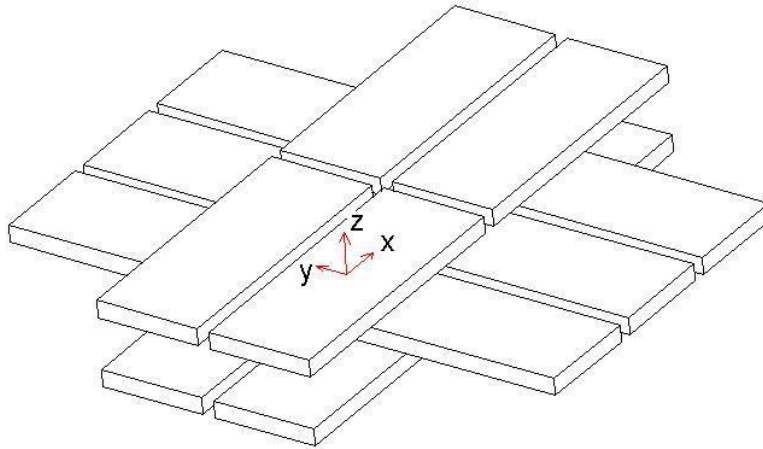


Figure 59: The composite nature of tile and mortar assembly.

When attempting to analyze a tile masonry structure, the fundamental material stiffness property is an effective modulus of elasticity representing the combined effect of tile masonry units, mortar, joints and voids. To achieve an accurate material input entry laboratory tests are conducted on both mortar and tile samples obtained from site (Figure 60). The initial values obtained through these tests are presented in Table 1Table 17. The tile units were oriented in both directions in the construction of the domes. A homogenization study is necessary to find a Young's modulus value for the combined effect of the mortar and tile units that compensates anisotropic characteristics in two directions. The homogenized values are presented in Table 18. These values will later be tuned based on the experimental data.





Figure 60: The hydraulic displacement controlled testing of tile and mortar unit.

Table 17: The experimentally obtained material properties for tile and mortar.

<b>Tile Longitudinal Young's Modulus (E)</b>	<b>13.2 10<sup>9</sup></b>	<b>N/m<sup>2</sup></b>
<b>Tile Transverse Young's Modulus (E)</b>	<b>15.4 10<sup>9</sup></b>	<b>N/m<sup>2</sup></b>
<b>Tile Longitudinal Poisson's ratio (<math>\nu</math>)</b>	<b>0.182</b>	<b>-</b>
<b>Tile Transverse Poisson's ratio (<math>\nu</math>)</b>	<b>0.194</b>	<b>-</b>
<b>Tile Density (d)</b>	<b>1800.000</b>	<b>Kg/m<sup>3</sup></b>
<b>Mortar Young's Modulus (E)</b>	<b>2.97 10<sup>9</sup></b>	<b>N/m<sup>2</sup></b>
<b>Mortar Longitudinal Poisson's ratio (<math>\nu</math>)</b>	<b>0.320</b>	<b>-</b>

Table 18: The material properties of tile and mortar assembly input for the preliminary FE model.

<b>Young's Modulus (E)</b>	<b>7.58×10<sup>9</sup></b>	<b>N/m<sup>2</sup></b>
<b>Poisson's Ratio (<math>\nu</math>)</b>	<b>0.26</b>	<b>-</b>
<b>Density (d)</b>	<b>1800</b>	<b>Kg/m<sup>3</sup></b>

## 6.2 Application of Experimental Modal Analysis

To confirm the validity of the analytical data a final experiment plan is developed. The primary purpose of the testing plan is having an improved the resolution by increasing the number of data points along the meridians as well as investigating the dynamic interaction between different parts of the structure.

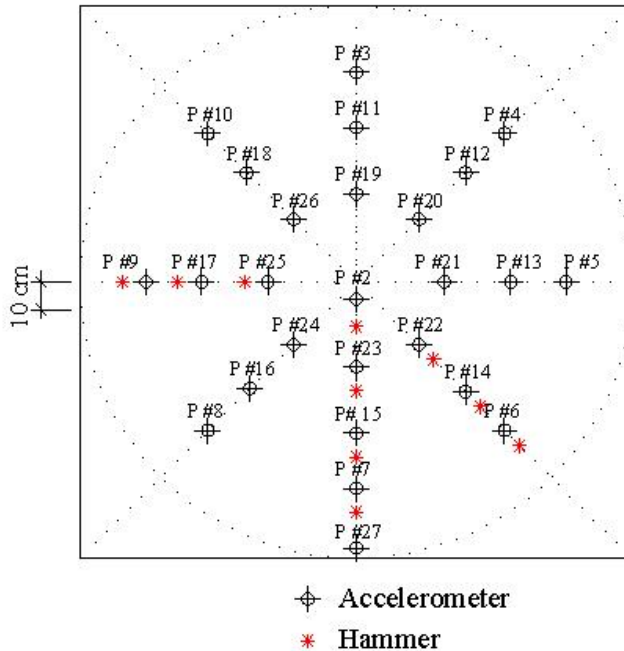


Figure 61: The dynamic testing plan.

The testing procedure is initiated with a test plan including 26 data points and utilizing the same equipment as in the previous test. Capturing the higher order, axisymmetric modes enables a comparison between experimental and analytical result. This is the intention in improving the meridional resolution. Three Siglab units are combined and 11 data points are measured simultaneously. In each step, the accelerometers at each ring level are relocated while the accelerometer at point #2 and #27 are held stationary. This multi-run test plan is executed in three steps. Identical equipments as in National Cathedral are utilized for response and impulse transducers. A sample FRF graph is presented in Figure 62.

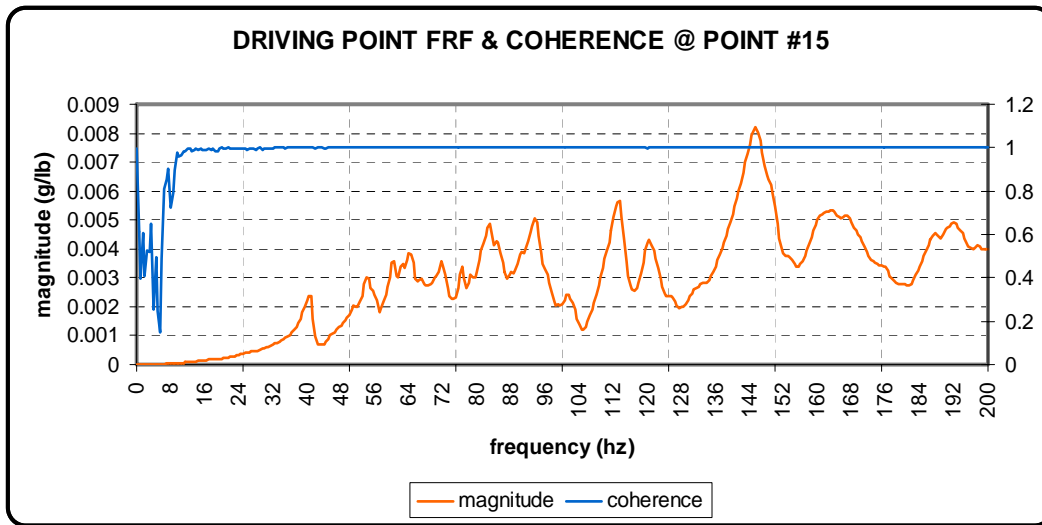


Figure 62: The FRF and coherence plot at Point 15.

### 6.3 Validation of ANSYS Model Based on Dynamic Analysis

In order to reach accurate results, the boundary conditions are of particular interest. Because boundary conditions are applicable to the degrees of freedom at the nodal points rather than to the elements, at the points where a constraint is desired a keypoint must be defined during the geometric model creation.

Since the physical configuration of masonry assemblies places further challenges on the identification of boundary conditions, it is crucial to adjust them through a calibration procedure. An extensive experimental data set is available for the SEB, which gives information on the possible boundary conditions to work with during the calibration process. It is useful to start with physically reasonable boundary conditions in the initial FE model.

The peripheral edges of the dome are restrained from a horizontal movement perpendicular to the plane of symmetry. At the base line where the dome webbing meets the supports, translation in all three axes is restricted. The tile buttresses between the adjacent domes provide vertical restraint while the diagonal buttresses allow vertical movements. The different behavior of the buttresses is determined via the experimental studies. The calibration of boundary conditions reveals that the steel I girders, contacting the dome surface along the pendentive edges at four corners, restrict rotation. The boundary conditions obtained through the fine-tuning process are presented in Figure 63.

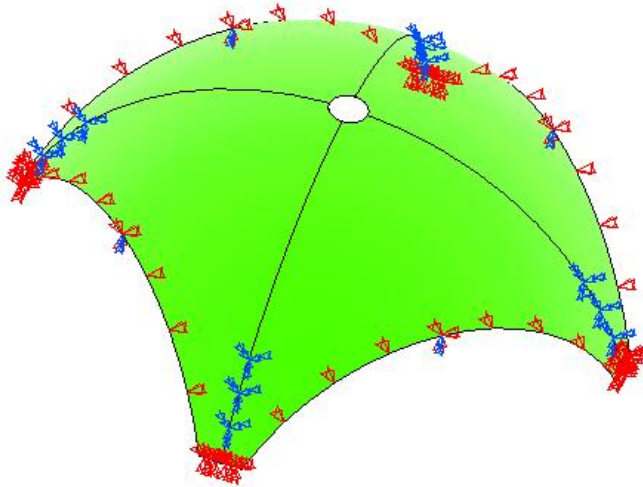


Figure 63: The calibrated boundary conditions.

The preliminary material properties of the assembly are fine-tuned based on the experimentally obtained natural frequencies, which are assumed to represent the actual behavior of the structure. Since only one type of material is modeled in this analysis, the natural frequencies from the FE model are dependent on the material properties. The material properties obtained through the fine-tuning process are presented in

Table 19: The material properties of tile and mortar assembly derived from FE model calibration process.

<b>Young's Modulus (E)</b>	<b><math>7.40 \times 10^9</math></b>	<b>N/m<sup>2</sup></b>
<b>Poisson's Ratio (<math>\nu</math>)</b>	<b>0.26</b>	<b>-</b>
<b>Density (d)</b>	<b>1800</b>	<b>Kg/m<sup>3</sup></b>

The iterative calibration process, manual tuning of boundary conditions and material properties, is completed when an overall agreement between experimental and analytical data is reached. The mode shapes used for comparison with the experimental data are listed in Figure 64 while the comparison of natural frequencies is illustrated in Table 20.

Table 20: Comparison of natural frequencies.

	Experimental Modal Analysis	Finite Element Method
1	41.0 Hz	40.91 Hz
2	×	41.47 Hz
3	48.33 Hz	50.19 Hz
4	52.04 Hz	51.47 Hz
5	58.50 Hz	53.53 Hz
6	×	57.35 Hz
7	64.50 Hz	60.19 Hz
8	73.00 Hz	64.6 Hz

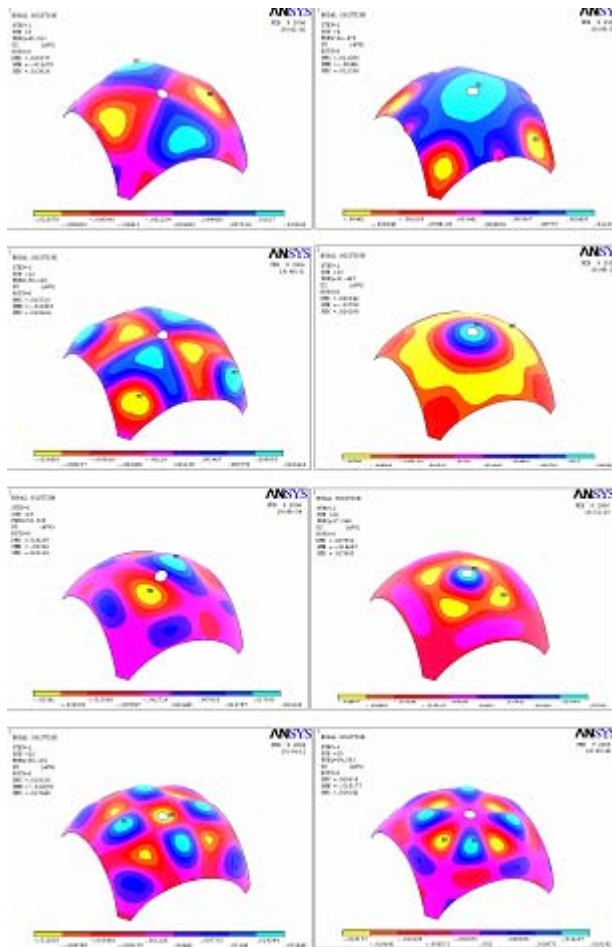


Figure 64: The analytically obtained mode shapes.

## 6.4 Static Analysis with ANSYS Model

Subsequently, reaction forces at boundary locations—illustrated in Figure 65—are obtained under gravity loading. The results show that the steel girder contacting the dome shell at the tile buttresses between adjacent domes contributes significantly to the vertical load transfer of the total dome weight of 10.6 tons. Approximately 15.7 kN is carried by the steel truss at the buttress locations between the domes, while approximately 10.9 kN is transferred through the surcharge volume.

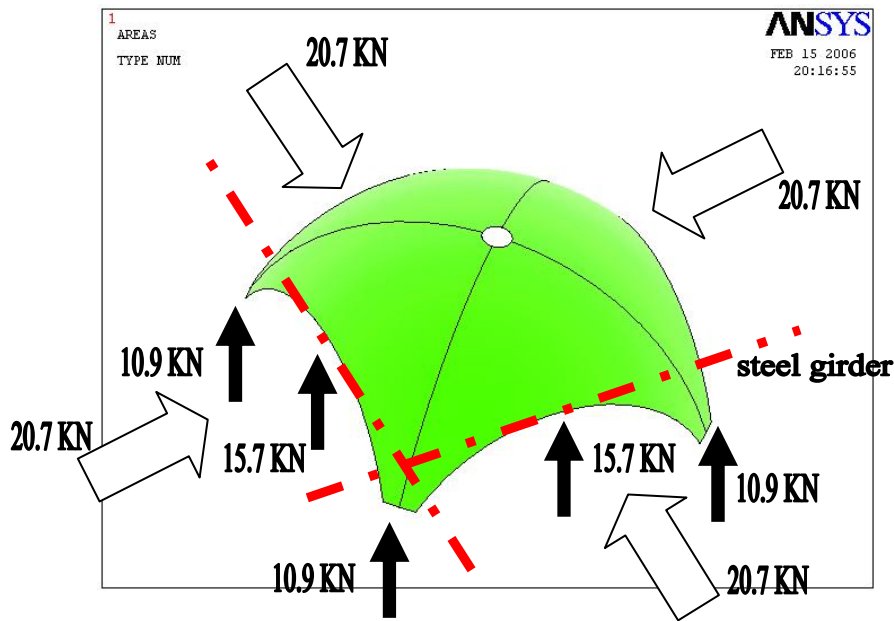


Figure 65: The reaction forces at the validated support conditions.

The horizontal reaction force counterbalanced by the adjacent domes is calculated to be 20.7 kN in total along one side of the pendentive dome. On the other hand, in the x and y directions, the horizontal reaction forces where the dome web meets the surcharge is observed to be limited to 3.4 kN.

The buttress locations between the domes have a minimal reaction force, 0.007 kN, in the direction parallel to the symmetry plane. Although the preceding analysis maintains that support restraint, the necessity of such a restraint is doubtful.

## 6.5 Building the FE Model in SAP 9.0 Nonlinear

Although some of the commercially available finite element programs have special features to built spherical segmental domes of user-defined radius and angle of embrace, it is nuisance to model the deviations from the pure dome geometry, as in the case of a pendentive dome. Accordingly, the same approach described previously for two case studies is employed. First the AutoCAD drawings of the dome is generated. At this stage the manual meshing of the dome is completed as well (Figure 66).

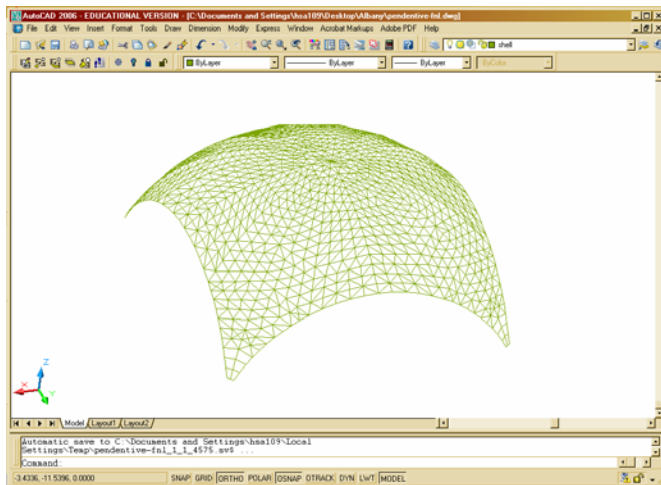


Figure 66: The AutoCAD drawing of the State Education Building dome.

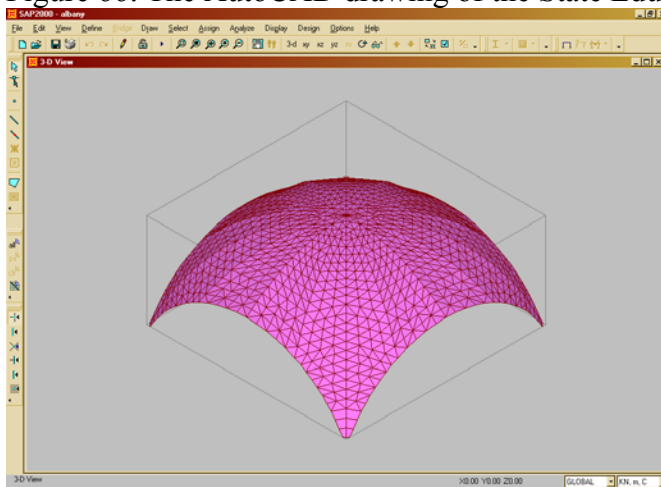


Figure 67: The solid model in SAP.

Subsequently the .dxf file is imported into SAP 9.0. The modeling is completed by inputting the boundary conditions, shell cross section and the material properties based on the validated ANSYS model.

## 6.6 Validation of SAP 9.0 Model Based on Static Analysis

The verification of the accuracy of the solution of the SAP model is accomplished by comparing the static state results of validated ANSYS model with those of SAP model. The comparison of the reaction forces displayed in Figure 65 is presented in y.

Table 21: The comparison of ANSYS and SAP model solutions.

	validated ANSYS model	SAP model
Lateral Thrust	20.7 KN	20.3 KN
Vertical Reaction at Piers	10.9 KN	10.4 KN
Vertical Reaction at Girder	15.7 KN	17.4 KN

## 7 Conclusions

The analysis of historic load-bearing masonry structures must proceed from a fundamental understanding of the premises of the original design, and a fundamental understanding of the mechanical behavior of arched and vaulted masonry systems. The analysis must be based on appropriate limit states. Allowance must be made for non-linear behavior, such as the strength of an arch beyond the appearance of the first crack. Account must be taken of the particular properties of the material used in construction: of the inherent compressive strength of stone masonry, of the limited but finite tensile capacity of masonry assemblies, and of the ductility inherent in high lime content mortars used in historic construction.

Analysis of a two-dimensional arch can be completed conveniently by hand methods using the principles of limit states analysis. An arch collapses only when it develops four hinges, that is, points where the eccentricity of the internal force is approximately half the depth of the arch. The safety of an arch can be assured by finding a statically admissible distribution of internal forces for which the thrust line is contained within the arch. The location of the thrust line can be estimated using simple calculations of plane forces under arch loading due to self-weight, superimposed dead load, and live load. Alternatively, a collapse mechanism can be imposed on the arch, and the load associated with this collapse mechanism can be calculated, recognizing that this load is an upper bound on the collapse load.



The analysis of an arch can be implemented in frame analysis software by developing frame elements endowed with the geometric and material properties of the arch ring, and inputting appropriate load and support conditions. The output is examined for the relationship between axial force and bending moment. Simple results of the eccentricity of internal forces can be inferred, or more complex determinations of the required compressive capacity of the masonry can be made, based on elasticity or plasticity assumptions for the behavior of the masonry.

Some widely distributed frame analysis programs allow inputs appropriate for non-linear analysis of plane arches. The softening behavior under compression, and cracking behavior under tension can be input in the form of stress-strain laws, which can be used to define hinges, based on axial force-moment interaction. These hinges can be located at appropriate intervals within the arch, and can assess the behavior of an arch beyond the elastic limit. Non-linear methods of analysis should be undertaken with caution, only when necessary, and only after completion of an accompanying linear analysis.

The assessment of three-dimensional structures, such as domes and vaults, requires an additional level of sophistication through the implementation of finite elements. The process of building a model involves the steps of the development of a solid model, selection of element types, meshing, application of boundary conditions, application of loads, solution, and post-processing. Several cycles of review of the analysis results, updating of the model, and re-analysis are generally required to develop a satisfactory analytical model. Simplification of the complex geometry of an actual structure is generally necessary to make the size of the model manageable.

In general, walls, buttresses, and vault ribs are modeled using solid elements. At least three elements through the thickness are necessary in order to capture bending moments and rotations. Displacement results are significantly more reliable than stress results and separate substructure modeling may be necessary in order to determine more accurate stress results. Areas of complex geometry for which accurate stress results are not necessary, such as rubble filling, may be modeled with tetrahedral solid elements. Shell elements are appropriate for the modeling of masonry vaults and domes, and simplify many of the modeling issues by working explicitly with internal force and moment resultants.

The use of non-linear analysis is incompatible with finite element modeling of shells and solids in most of the widely available structural analysis and design computer programs. In cases where non-linear modeling is necessary, it is necessary to apply frame elements for arch and vault ribs, in order to be able to insert plastic hinges, as for the two-dimensional arches. If it is absolutely necessary to obtain non-linear shell and solid element results, it is necessary to employ an advanced, general-purpose finite element program.

Varied techniques are available for the modeling of actual structures. The geometry of the structure may be input either through the program interface, or by importing a model from a computer-aided drafting program. Decisions on material properties, element types, meshing, boundary conditions, and loading conditions result from careful review of the structure in the field and of the literature on the particular construction method employed. The results of the analysis need to be interpreted in conjunction with a detailed inspection of the condition of the structure. If possible, a number of additional validation methods are available to increase the confidence in the quality of the structural model. In any event, a sensitivity analysis of the model should be undertaken.

A responsible assessment of a historic load-bearing masonry structure can be undertaken using modern engineering tools, combined with an understanding of the existing structure, and a strong sympathy for the preservation of structures from the past.

## **8 Acknowledgements**

First, the authors gratefully acknowledge the support of the National Center for Preservation Technology and Training, especially Andrew Ferrell for his patience in waiting for the final outcome of this project. The authors also particularly thank the staff of Robert Silman Associates, PC, especially Edmund Meade for their initial guidance in this project. The authors express gratitude to the individuals who assisted them in gaining access to the sites that they studied: Joe Alonso of the National Cathedral, Ray Guyette of the Cathedral of St. John the Divine, and George Webb of the State Education Building.

The authors are indebted to Corinna Fisher for her assistance in editing the manuscript.

## 9 References Cited

- ACI. *Building Code Requirements for Masonry Structures. ACI 530-05.* Detroit, ACI International, 2005.
- ASCE (1999). *Guideline for Structural Condition Assessment of Existing Buildings.* American Society of Civil Engineers, Reston, 1999.
- Atamturktur, H.S. *Structural Assessment of Guastavino Domes.* M.S. Thesis, The Pennsylvania State University, May 2006.
- Binda, Luigia, Saisi, Antonella; Zanzi, Luigi. Sonic tomography and flat-jack tests as complementary investigation procedures for the stone pillars of the temple of S. Nicolo l'Arena. (Italy) *NDT and E International*, v 36, n 4, June, 2003, p 215-227.
- Heyman, J. *The Masonry Arch*, Chichester, Ellis Horwood, 1982.
- Heyman, J. *The Stone Skeleton*, Cambridge, Cambridge University Press, 1995.
- McNary, S. and Abrams, D.P. Mechanics of masonry in compression, *Journal of Structural Engineering*, 111(4), April 1985.
- Roark, R.J. *Roark's Formulas for Stress and Strain*, New York, McGraw-Hill, 1989.
- Sansalone, M. Impact-Echo: The Complete Story, *ACI Structural Journal*, 94(6):777-786, November-December 1997.

Schuller, M., Berra, M., Atkinson, R., Binda, L. Acoustic tomography for evaluation of unreinforced masonry. *Construction and Building Materials*, v 11, n 3, Apr., 1997, p 199-204.